National Aeronautics and Space Administration

Progress in Technology for Exoplanet Missions

An Appendix to the NASA Exoplanet Exploration Program Technology Plan

Dr. Brendan P. Crill
Deputy Program Chief Technologist
NASA Exoplanet Exploration Program
Jet Propulsion Laboratory
California Institute of Technology

www.nasa.gov

JPL document D-108825

Front Cover credit: NASA/JPL-Caltech.

Acknowledgements:

Important contributions and reviews were made to this document by David Ardila, Vanessa Bailey, Eduardo Bendek, Gary Blackwood, Matt Bolcar, Case Bradford, Jennifer Burt, Pin Chen, Tyler Groff, Erika Hamden, Eric Mamajek, Bernard Rauscher, David Redding, Garreth Ruane, Nicholas Sieger, Byoung-Joon Seo, Phil Stahl, Karl Stapelfeldt, John Trauger, Keith Warfield, Feng Zhao, and Neil Zimmerman.

The research was carried out at the Jet Propulsion Laboratory, California Institute of Technology, under a contract with the National Aeronautics and Space Administration (80NM0018D0004). Reference herein to any specific commercial product, process, or service by trade name, trademark, manufacturer, or otherwise, does not constitute or imply its endorsement by the United States Government, or the Jet Propulsion Laboratory, California Institute of Technology.

Approved By:

E-SIGNED by Gary Blackwood
on 2023-01-03 14:05:59 GMT

Dr. Gary Blackwood
Program Manager
Exoplanet Exploration Program
NASA/Jet Propulsion Laboratory
California Institute of Technology

Date

E-SIGNED by Doug Hudgins
on 2023-01-03 17:44:21 GMT

Dr. Douglas Hudgins
Program Scientist for Programs
Exoplanet Exploration Program
Science Mission Directorate
NASA Headquarters

Date

Concurred By:

E-SIGNED by Nicholas Siegler
on 2022-12-17 00:23:33 GMT

Dr. Nicholas Siegler
Program Chief Technologist
Exoplanet Exploration Program
NASA/Jet Propulsion Laboratory
California Institute of Technology

Date

Prepared By:

E-SIGNED by Brendan Crill
on 2022-12-15 17:49:12 GMT

Dr. Brendan Crill
Deputy Program Chief Technologist
Exoplanet Exploration Program
NASA/Jet Propulsion Laboratory
California Institute of Technology

Date

Contents

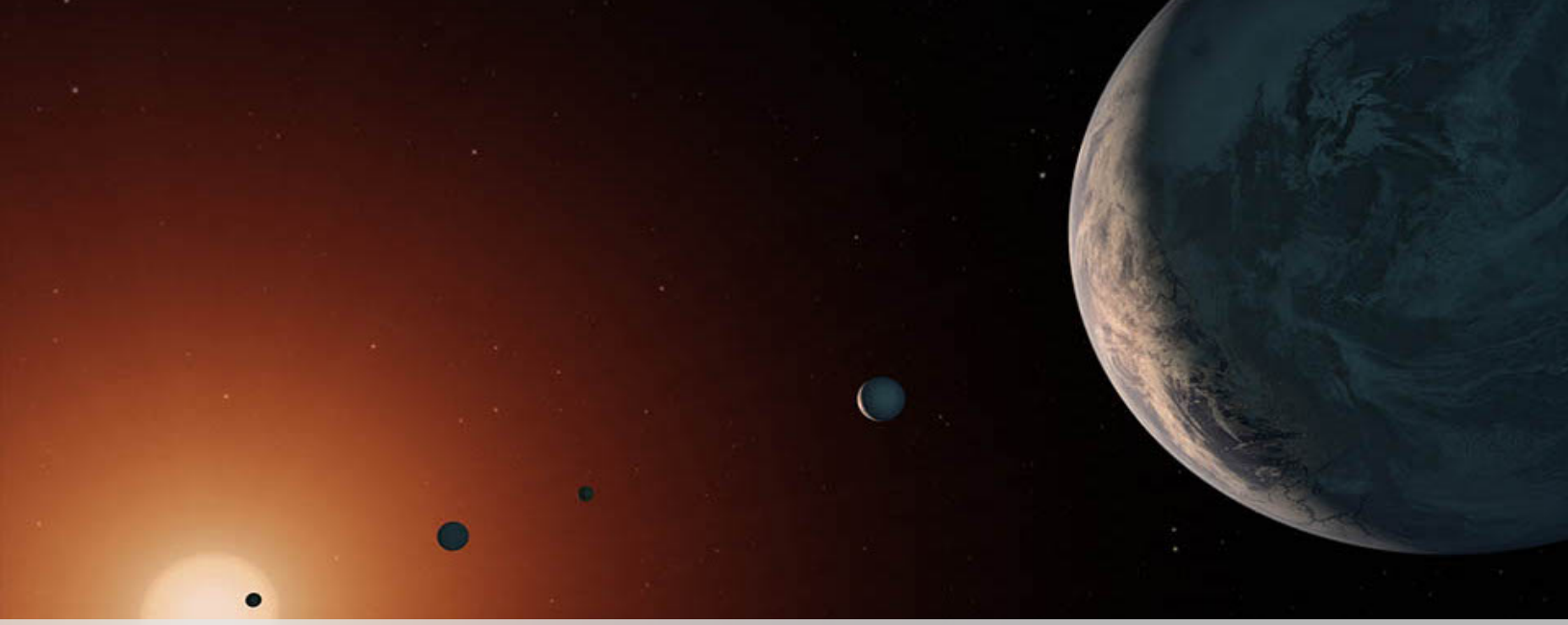

1 Introduction

The purpose of this document is to guide near-term (1–5 year) technology development for future space observatories related to NASA's Exoplanet Exploration Program (ExEP). This document provides an update to ExEP's 2019 Technology Plan Appendix [1] to reflect the recommendations of the National Academies of Science, Engineering, and Medicine 2020 Decadal Survey report *Pathways to Discovery in Astronomy and Astrophysics for the 2020s* [2].

A long-term goal of the Program is to discover and characterize worlds that could harbor life. This goal includes developing technology for a mission capable of directly imaging terrestrial planets in the habitable zones of stars in the solar neighborhood, and measuring their spectra to search for signs of life. Such a mission will require extreme starlight suppression and other new technology developments. Much of the previous space technology development in this field was developed under recommendations from the 2010 Decadal Survey [3], which included investments in starlight suppression technology as its highest priority medium scale recommendation for space.

The 2020 Decadal Survey reaffirmed the high scientific priority of the search for life in the Universe, and made two large-scale recommendations. First, the Survey recommended that NASA's Astrophysics Division (APD) should establish a Great Observatories Mission and Technology Maturation Program, to manage precursor science and technology development ahead of formulating future large missions.

Second, the 2020 Decadal Survey recommended that after a succession maturation program, NASA should realize a mission to survey 100 or more nearby Sun-like stars and detect potentially habitable planets around about

An artist's illustration depicting the TRAPPIST-1 system. Credit: NASA/JPL-Caltech/R. Hurt (IPAC).

a quarter of them. In addition, the mission will provide a transformative facility for general astrophysics. The first of the Future Great Observatories will be an Infrared/Optical/Ultraviolet Future Great Observatory (Habitable Worlds Observatory) with a roughly 6 m primary mirror and starlight suppression capabilities. The Decadal Survey acknowledges the long road to successfully achieving such an ambitious mission and set a target launch for the first half of the 2040's.

NASA's response to these recommendations began in 2022, and included an update to the Astrophysics Technology Gap List. Technology gaps are performance capabilities that exceed the current state-of-the-art but are needed to enable or enhance the recommended missions, including the Future Great Observatories and competitively selected Probe-class missions focused on far-IR and X-ray science. This technology gap process was carried out by technologists from all three of the thematic Program Offices within APD: the ExEP, Cosmic Origins (COR), and Physics of the Cosmos (PhysCOS) programs, with input from the broader community. The gaps were prioritized for closure, resulting in APD's Technology Gap List[1], published in the Astrophysics Biennial Technology Report (ABTR) [4].

The technology gaps that are related to the science goals of ExEP (Table 1.1) are described in more detail in this document than can be found in the ABTR and the Technology Gap List. The document also describes technologies that are leading candidates to close the gaps. These technologies are rapidly developing and this document is updated on a 1–2 year cadence. The greatest emphasis is placed on technologies that enable the direct imaging and spectroscopic characterization of Earth-like planets in the habitable zone of Sun-like stars, though the Program also tracks technologies for the study of broader classes of exoplanets and those that enable characterization of key properties, such as mass.

Note that, while the ExEP tracks all the listed technology gaps related to enabling and enhancing exoplanet missions, a number of gaps are cross-cutting and important to all three Astrophysics Division science themes (PhysCOS, COR, and ExEP). Several of the ExEP technology needs may be funded by the other Programs.

This document communicates overall technology needs to aid scientists, engineers, and technology managers in academia, industry, research labs, and NASA centers in deciding which technology areas they are best suited to develop. However, not all the technologies listed here are currently solicited under the Research Opportunities in Space and Earth Sciences (ROSES) Strategic Astrophysics Technology (SAT) Program (ROSES 2022, Appendix D.8)[2]. The specific technologies that are solicited under the SAT Program are described in the call for proposals. In general, an effort is made to identify and solicit proposals to mature the tallest technology tent poles within the limits of available funding, using the prioritization process described here. Please note that in the case of a discrepancy between the ROSES language and this document, ROSES has precedence.

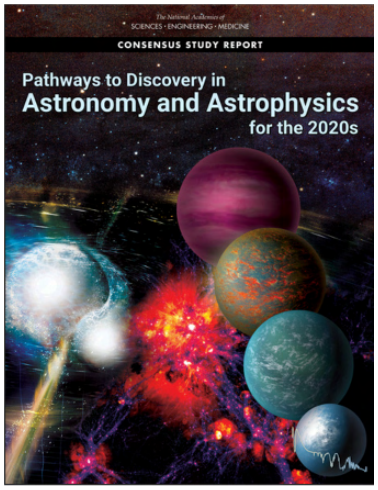

Figure 1.1: The 2020 Decadal Survey report [2].

1: The APD Technology Gap List can be found at https://apd440.gsfc.nasa.gov/tech_gap_priorities.html

Figure 1.2: The ABTR [4].

2: The SAT 2022 solicitation can be found on the NASA NSPIRES website. Facilities managed by the Exoplanet Exploration Program and made available to investigators funded under SAT are described in Appendix B

1.1 Program Goals

The ExEP aims to identify and close technology gaps to enable and enhance studying Earth-like planets around other stars, including developing technology in preparation for the Habitable Worlds Observatory recommended by Astro2020.

Earth-like exoplanets are between 10 million and 10 billion times fainter than the stars they orbit, depending on whether they are observed at mid-infrared or visible wavelengths. The presence of water, methane, and oxygen in a planet's atmosphere, revealed by reflected starlight, is therefore hidden in the noise of the star's overwhelming glare. Thus, the most important technological challenge is the demonstration that a space observatory can reject starlight, before detection, to separate the light of the planet from its parent star.

Achieving starlight suppression requires advances in the areas of high-angular-resolution sensing and high-contrast imaging, and in some architectures, improvements to the stability of space telescopes. The future space observatories might take many forms; mission concepts studied so far include designs based on coronagraphs, starshades and various hybrid designs[3]. These approaches use wavefront sensing and control, advanced optics and state-of-the-art structures, materials and mechanisms, and require specialized spacecraft subsystems. Starshades require the coordinated operation of multiple spacecraft and rely on precision in-space deployment. In all of these cases, fully testing these observatories as a complete system on the ground, prior to launch, will be challenging, and careful attention to integrated models and methods of verification and validation will be critical to mission success.

3: Recent mission concept studies directly relevant to ExEP's technology goals are the Large Ultraviolet / Optical / Infrared Surveyor (LUVOIR) [5] and the Habitable Exoplanet Observatory (HabEx) [6].

The ExEP Technology Gaps are listed in Table 1.1. The technology gaps have a broad scope and may require multiple technologies to close them.

To track the maturity of a technology with the respect to mission requirements, NASA uses the Technology Readiness Level (TRL) scale [7]. A number between 1 and 9 is assigned based on the technology's demonstrated performance and functionality as compared to a mission's performance requirements and environments. The NASA Technology Readiness Assessment Best Practices Guide [8] provides a standard framework for assessing TRL.

At this stage when no specific mission architecture has yet been defined, general classes of missions are considered. Thus, the gap list specifies performance goals and objectives, rather than formal requirements. Without a specific mission, a technology can be assessed no higher than TRL 5. It is important to note that the fidelity of requirements for technologies will improve as architecture trades are conducted in the future and performance goals (and details of the operational environment) may change.

In addition, technology requirements are tied to science goals, and are in some cases dependent on knowledge of the astrophysical universe that is still uncertain. ExEP's Science Plan and Science Plan Appendix list gaps in scientific knowledge that must be closed to fully realize ExEP's mission

goals. Some of the science gaps must be addressed in order to define a future mission. These include investigating the distribution of zodical dust around Sun-like stars (for example [9]) and more precisely determining the fraction of Sun-like stars with Earth-like planets in their habitable zones ($\eta_\oplus$).

The technology strategy for future strategic astrophysics missions typically follows NASA's procedure to advance technologies up the TRL ladder as they are matured for flight. This tends to focus effort on technologies that have already demonstrated or are close to demonstrating performance goals at the present time. Over a multi-decade effort to prepare and build future great observatories, we recognize that there may be revolutionary opportunities presented by emergent technologies, such as in photonics, machine learnning, and quantum sensing.

Chapters 2, 3, 4, 5, and 6 provide additional details on the Technology Gaps, summarize recent key developments in technologies and communicate next steps and what is planned in the near future. Alternative technologies are also presented, as appropriate. For some of the technology gaps, additional detail for potential solutions or paths forward are listed as "sub-gaps" in Table 1.1, with details found in Appendix A.

Table 1.1: The ten 2022 ExEP Technology Gaps, a subset of the APD Technology Gap List.

Technology Gap and Description	Current-State-of-the-Art	Performance Goals and Objectives
Mirror Technologies for High Angular Resolution (UV/Vis/NIR) The capability to resolve the habitable zones of nearby star systems in the UV/Vis/NIR bands with a large space telescope.	*Monolith*: 3.5-m sintered SiC with < 3 μm Surface Figure Error (SFE) (Herschel); 2.4-m Ultra Low Expansion (ULE) with 10 nm SFE (Hubble Space Telescope (HST)); Waterjet cutting is TRL 9 to 14" depth, but TRL 3 to >18" depth. Fused core is TRL 3; slumped fused core is TRL 3 (Advanced Mirror Technology Demonstration (AMTD)); 4-m class Zerodur mirrors from single boules are TRL 4. *Segmented*: 6.5 m Be with 25 nm SFE (JWST); Non-NASA: 6 Degrees of Freedom (DOF), 1-m class SiC and ULE, $<$ 20 nm SFE, and $<$ 5 nm wavefront stability over 4 hr with thermal control	Large (4—16 m) monolith and multi-segmented mirrors for space that meet SFE $<$ 10 nm Root Mean Square (RMS) (wavelength coverage 400–2500 nm); Wavefront stability better than 10 pm RMS per wavefront control time step; Coeffient of Thermal Expansion (CTE) uniformity characterized at the ppb level for a large monolith; Segmented apertures leverage 6 DOF or higher control authority meter-class segments for wavefront control. Sub-gaps that could partially or fully close this gap (Table A.1): ► Mirror Substrate and Structure ► Mirror Positioning Actuators ► Gravity Sag Offloader ► Coefficient of Thermal Expansion Characterization ► Mirror Finishing ► UV Coatings: Wavefront Effects
Coronagraph Contrast and Efficiency The capability to suppress starlight and receive planet light with a coronagraph to the level needed to detect and spectrally characterize Earth-like exoplanets in the habitable zones of Sun-like stars.	*unobscured pupil:* 4×10^{-10} raw contrast at 10% bandwidth at 550 nm, angles of 3–9 λ/D (Lyot coronagraph demo in High Contrast Imaging Testbed (HCIT)) *obscured pupil:* 1.6×10^{-9} raw contrast at 10% bandwidth across angles of 3–9 λ/D (Roman Coronagraph lab demos) *segmented/unobscured pupil:* 2.5×10^{-8} raw contrast in monochromatic light across 6–10 λ/D (Lyot coronagraph demo in High-contrast imager for Complex Aperture Telescope (HiCAT)))	Maximized science yield in imaging and spectroscopy for a direct imaging telescope/mission. $\leq 10^{-10}$ raw contrast, >10% throughput, inner working angle $\leq$ 3 λ/D, outer working angle $\geq$ 45 λ/D [TBD], 20% bandwidth; obscured/segmented pupil; For the two distinct cases of monolith and segmented primary mirrors. Sub-gaps that could partially or fully close this gap (Table A.2): ► Coronagraph Architecture ► Deformable Mirrors

Continued on next page

Table 1.1: The ten 2022 ExEP Technology Gaps, a subset of the APD Technology Gap List.

Technology Gap and Description	Current-State-of-the-Art	Performance Goals and Objectives
Coronagraph Stability The capability to maintain the deep starlight suppression provided by a coronagraph for a time period long enough to detect light from an exo-Earth.	Roman Coronagraph demonstrated ~10^{-8} contrast in a simulated dynamic environment using Low-Order Wavefront Sense and Control (LOWFS) (which obtained 12 pm focus sensitivity) Space Interferometry Mission (SIM) and non-NASA work has demonstrated nm accuracy and stability with laser metrology Capacitive gap sensors demonstrated at 10 pm 80 dB vibration isolation demonstrated *Gaia* cold gas microthrusters and LISA pathfinder colloidal microthrusters can reduce vibrations	Contrast stability on time scales needed for spectral measurements (possibly as long as days). Achieving this stability requires an integrated approach to the coronagraph and telescope, possibly including wavefront sense/control, metrology and correction of mirror segment phasing, vibration isolation/reduction This stability is likely to require wavefront error stability at the level of 10–100 pm per control step (of order 10 minutes). Sub-gaps that could partially or fully close this gap (Table A.3): ► Ultra-stable Telescope ► Integrated Modeling of Telescope/Coronagraph system ► Disturbance Reduction and Observatory Stability ► Wavefront Sensing (low-order and out-of band) ► Vibration Isolation and Pointing System Technology ► Laser Gauges for Metrology ► Segment Relative Pose Sensing and Control ► Thermal Sensing and Control ► Wavefront Sensing and Control Algorithms ► Observatory Pointing Control
Vis/NIR Detection Sensitivity The capability to detect single photons in the Vis and Near Infrared (NIR) to enable imaging and spectroscopy of Earth-like exoplanets.	*Vis:* 1k×1k silicon Electron-Multiplying Charge Coupled Device (EMCCD) detectors provide dark current of 7×10^{-4} e-/px/sec; Clock-Induced Charge (CIC) of 0.01 e-/px/frame; zero effective read noise (in photon counting mode) after irradiation when cooled to 165.15 K (Roman); 4k×4k EMCCD fabricated but still under development *NIR:* HgCdTe photodiode arrays have read noise ≤2 e- rms with multiple nondestructive reads; 4k×4k format; dark current < 0.001 e-/s/pix; very radiation tolerant (James Webb Space Telescope (JWST)), high Quantum Efficiency (QE) down to 750nm; HgCdTe Avalanche Photodiode (APD)s demonstrated dark current ~10–20 e-/s/pix, RN ≪1 e- rms and 1k×1k format *Cryogenic superconducting photon-counting, energy-resolving detectors (Microwave Kinetic Induction Device (MKID),Transition Edge Sensor (TES))*: 0 read noise/-dark current; space radiation tolerance not systematically studied; <1k×1k format	Near IR (900 nm to 2.5 μm) and visible-band (400-900 nm) extremely low noise detectors for exo-Earth spectral characterization with spectrographs or intrinsic energy resolution. NIR Read noise ≪ 1 e- RMS, dark current noise < 0.001 e-/pix/s, Vis band read noise < 0.1 e- RMS; CIC < 3×10^{-3} e-/px/frame; dark current < 10^{-4} e-/px/s, functioning in a space radiation environment over mission lifetime (5–10 years); may need large ≥ 2k×2k format Sub-gaps that could partially or fully close this gap (Table A.4): ► NIR low-noise detector ► UV/Vis low-noise detector ► Rad-Hard, High-QE, Energy Resolving, Noiseless Single Photon Detector Arrays for the NIR, VIS, and UV
Stellar Reflex Motion Sensitivity: Extreme Precision Radial Velocity Capability to measure exoplanet masses down to Earth-mass.	Ground-based Radial Velocity (RV): state-of-the-art demonstrated stability is currently 28 cm/s over 7 hours (Very Large Telescope (VLT)/ESPRESSO). Laser frequency combs demonstrated on ground-based observatories with correct mode spacing, non-NASA work is advancing miniaturization. Fiber laser-based optical frequency combs demonstrated on sounding rocket though with closer line spacing than useful for RV.	Capability to measure exoplanet masses down to Earth-mass. The radial velocity semi-amplitude of a Solar-mass star due to an orbiting Earth-mass planet at 1 AU is 9 cm/s. Technology to make radial velocity mass measurements may include using a space-based instrument to avoid atmospheric telluric lines and simultaneous measurements of stellar lines across a broad band (both Vis and NIR). Stability of the instrument and its absolute calibration must be maintained on long time scales in order to enable the measurement. Theoretical understanding of astrophysical noise sources (stellar jitter) and how to mitigate them. Sub-gaps that could partially or fully close this gap (Table A.5): ► Detectors for high-resolution, cross-dispersed spectrographs ► High-Precision, High-Throughput, High-Spectral Resolution Dispersive Optics ► Advanced Photonics for extreme-precision radial velocity spectroscopy ► Ground-based Visible-light Adaptive Optics ► Precision calibration for extreme-precision radial velocity spectroscopy

Continued on next page

Table 1.1: The ten 2022 ExEP Technology Gaps, a subset of the APD Technology Gap List.

Technology Gap and Description	Current-State-of-the-Art	Performance Goals and Objectives
Stellar Reflex Motion Sensitivity: Astrometry Capability to measure exoplanet masses down to Earth-mass.	GAIA preliminarily achieved 34 micro arcsecond error but ultimately could achieve 10 microarcseconds on bright targets after all systematics are calibrated. Demonstration of diffractive pupil showed 5.75×10^{-5} λ/D or 1.4 microarcsecond on a 4m telescope (limited by detector calibration) Preliminary study of 1-m space telescope and instrument with in-situ detector calibration can achieve 0.8 micro-arcsecond in 1 hr	Astrometric detection of an exo-Earth at 10 pc requires 0.1 microarcsecond uncertainty. Technology with the stability need to make astrometric measurements to this level, possibly requiring detector metrology and/or diffractive pupils Theoretical understanding of astrophysical noise sources (star spots) and prospects for mitigating them.
Starshade Deployment and Shape Stability The capability to deploy on-orbit a starshade that is stowed in a launch vehicle fairing to a precise shape, and to maintain that shape precision during all operational environments.	Manufacturing tolerance ($\leq$ 100 μm) verified with low fidelity 6 m prototype. Petal deployment tests conducted to demonstrate rib actuation. Petal deployment tolerance ($\leq$ 1 mm) verified with low fidelity 12 m prototype; limited environmental testing.	A system that will deploy the petals from a launch-stowed configuration to the needed shape (to better than $\leq$ 1 mm (in-plane envelope) and maintain petal edges to $\leq$ 100 micron (in-plane tolerance profile for a 7 m petal on a 34 m-diameter starshade; tolerances scale roughly linearly with starshade diameter), and be optically opaque. Performance goals are under re-evaluation for the IR/O/UV Future Great Observatory. Overall starshade diameter likely to be > 50m.
Starshade Starlight Suppression and Model Validation The capability of a starshade to suppress diffracted on-axis starlight and scattered off-axis Sunlight to levels needed to characterize Earth-like exoplanets. The capability to experimentally validate model of the starshade's optical performance at subscale.	10^{-10} contrast at inner working angle demonstrated over 10% bandpass using 24 mm starshade in Princeton testbed with F = 13. Validated optical model with demonstrated 10^{-6} suppression at white light, 58 cm mask, and F = 210. Optical model validated to within a factor 2 at 10^{-8} contrast at F=13. Etched amorphous metal edges with anti-reflection coating meet scatter specs with margin; integrated in-plane shape tolerance is to be demonstrated.	Experimentally validate at flight-like Fresnel numbers (F) the equations that predict starshade starlight contrast: total starlight contrast $\leq10^{-10}$ in a scaled flight-like geometry, F between 5 and 40, across a broad UV/optical/IR bandpass. Contrast model accuracy validated to better than 25%. Limit edge-scattered sunlight and diffracted starlight with optical petal edges that simultaneously meet scatter requirements and in-plane shape tolerances. Limit solar scatter lobe brightness to better than visual magnitude (V) ~26. Performance goals are under re-evaluation for the IR/O/UV Future Great Observatory.
UV Detection Sensitivity The sensitivity to perform imaging spectroscopy of exoplanets in the near ultraviolet.	*Lab:* Multi-Channel Plate (MCP): 0 read noise, 90 – 300 nm, spurious count rate 0.05 – 0.5 counts/cm^2/s; QE 20–45%; resolution element size 20 μm. EMCCD: 0 read noise, dark current < 0.005 e-/res/hr; QE 30-50%; resol. el. size 20 μm *Flight:* HST HRC: In relevant UV band (250 nm): QE 33%, read noise 4.7 e-, dark current 5.8×10^{-3}, 1024×1024 format	Low-noise ultraviolet (200–400 nm) detectors to characterize exoplanets with an imaging spectrograph. Read Noise: 0 e-; Dark Current: 0 e- /resolution/s; Spurious Count Rate: < 0.05 counts/cm^2/s; QE: 75% ; Resolution size $\leq$ 10 μm; Tolerant to space radiation environment over mission lifetime.
Detection Stability in the Mid-IR The capability to detect mid-infrared light with ultrastable detectors to carry out transit spectroscopy of terrestrial exoplanets in the Habitable Zone of M-dwarf stars.	JWST/MIRI is expected to achieve 10-100 ppm transit stability. Spitzer IRAC Si:As detector data have demonstrated about 60 ppm precision in transit observations of several hours	Ultrastable detectors (< 10 ppm over 5 hours) for the mid-infrared band (7 - 20 microns) enabling transit spectroscopy of rocky exoplanets in the Habitable Zone of M-dwarfs.

1.2 Previously Funded Efforts

A searchable database of APD-funded technology development projects[4] contains projects funded through both competed and directed means since 2010 [10, 11], and includes investigations in all areas of astrophysics including exoplanets.

4: http://astrostrategictech.us/

Teams funded by SAT to carry out exoplanet technology development are required to write a Milestone Whitepaper that defines quantifiable goals of the project, and a detailed plan to achieve them. ExEP technologists and an external board, the Exoplanet Technology Assessment Committee (ExoTAC), provide review of the Whitepapers. At completion, the PI writes a Final Report that assesses the results against the milestones, and discusses

any lessons learned. The Final Report is reviewed and approved by ExEP and the ExoTAC [5].

The Milestone Whitepapers and Final Reports of all the exoplanet-related SAT awards are available in the APD online database and on the ExEP website[6]. Table 1.2 lists all of the exoplanet-related SAT projects awarded prior to 2022. Note that the name Technology Development for Exoplanet Missions (TDEM), previously used to describe the SAT awards related to exoplanet missions, retired as of SAT-2018.

5: https://exoplanets.nasa.gov/exep/technology/technology-overview/

6: https://exoplanets.nasa.gov/exep/technology/TDEM-awards/

Table 1.2: Exoplanet SAT awards for proposal calls from 2009 to present. Note that the Year shown in the table indicates the proposal call year - typically the work commences 2 years after the proposal call year.

Year	PI	Institution	Proposal Title
Coronagraph Starlight Suppression Demonstrations			
2009	Mark Clampin	NASA GSFC	Visible Nulling Coronagraph Technology Maturation: High Contrast Imaging and Characterization of Exoplanets
2009	Olivier Guyon	Univ. of Arizona	Phase-Induced Amplitude Apodization Coronagraphy Development and Laboratory Validation
2009	John Trauger	JPL	Advanced Hybrid Lyot Coronagraph Technology for Exoplanet Missions
2010	Olivier Guyon	Univ. of Arizona	Advances in Pupil Remapping (PIAA) Coronagraphy: improving Bandwidth, Throughput and Inner Working Angle
2010	Richard Lyon	NASA GSFC	Compact Achromatic Visible Nulling Coronagraph Technology Maturation
2010	Jagmit Sandhu	JPL	Visible Nulling Coronagraph (VNC) Technology Demonstration Program
2010	Eugene Serabyn	JPL	Demonstrations of Deep Starlight Rejection with a Vortex Coronagraph
2013	Brian Hicks	NASA GSFC	Segmented Aperture Nulling Coronagraphy
2014	Eugene Serabyn	JPL	Broadband Light Rejection with the Optical Vortex Coronagraph
2015	Jim Breckinridge	Univ. of Arizona	Threshold Raw Retrieved Contrast in Coronagraphs is Limited by Internal Polarization
2016	John Trauger	JPL	Super Lyot ExoEarth Coronagraph
2016	Ruslan Belikov	NASA/Ames	Laboratory Demonstration of High Contrast Using PIAACMC on a Segmented Aperture
2016	Ruslan Belikov	NASA/Ames	Development of a Method for Exoplanet Imaging in Multi-Star Systems
2017	Eugene Serabyn	JPL	Vortex Coronagraph High Contrast Demonstrations
2017	Rémi Soummer	Space Telescope Science Institute	First System-level Demonstration of High-Contrast for Future Segmented Space Telescopes
2018	Ruslan Belikov	NASA/Ames	Laboratory Demonstration of Multi-Star Wavefront Control in Vacuum
2018	Dimitri Mawet	Caltech	Optimal Spectrograph and Wavefront Control Architectures for High-contrast Exoplanet Characterization
2021	J. Kent Wallace	JPL	Dual-purpose coronagraph masks for enabling high-contrast imaging with an IR/O/UV flagship mission
Starshade Starlight Suppression Demonstrations			
2009	N. Jeremy Kasdin	Princeton Univ.	Starshades for Exoplanet Imaging and Characterization: Key Technology Development
2010	N. Jeremy Kasdin	Princeton Univ.	Verifying Deployment Tolerances of an External Occulter for Starlight Suppression
2012	Suzanne Casement	Northrop Grumman Aerospace Systems	Starshade Stray Light Mitigation through Edge Scatter Modeling and Sharp-Edge Materials Development
2012	Tiffany Glassman	Northrop Grumman Aerospace Systems	Demonstration of Starshade Starlight-Suppression Performance in the Field
2012	N. Jeremy Kasdin	Princeton Univ.	Optical and Mechanical Verification of an External Occulter for Straight Suppression (transferred to starshade technologyactivity)
2013	Webster Cash	Univ. of Colorado	Development of Formation Flying Sensors
2013	N. Jeremy Kasdin	Princeton Univ.	Formation Flying for External Occulters (transferred to starshade technology activity)
2014	Mark Thomson	JPL	Optical Shield for the Starshades Inner Disk Subsystem (transferred to starshade technology activity)
Wavefront Sensing and Control			
2009	John Krist	JPL	Assessing the Performance Limits of Internal Coronagraphs Through End-to-End Modeling
2009	M. Charley Noecker	Ball Aerospace	Advanced Speckle Sensing for Internal Coronagraphs and Methods of Isolating Exoplanets from Speckles
2010	Paul Bierden	Boston Micromachines	MEMS Deformable Mirror Technology Development for Space-Based Exoplanet Detection
2010	Michael Helmbrecht	Iris AO	Environmental Testing of MEMS Deformable Mirrors for Exoplanet Detection
2010	N. Jeremy Kasdin	Princeton Univ.	Integrated Coronagraph Design and Wavefront Control using Two Deformable Mirrors
2017	Olivier Guyon	Univ. of Arizona	Linear Wavefront Control for High Contrast Imaging
2021	Kerri Cahoy	MIT	Adaptive High-order Wavefront Control Algorithms for High-contrast Imaging on the Decadal Survey Testbed
Extreme Precision Radial Velocity			

Continued on next page

Table 1.2: Exoplanet SAT awards for proposal calls from 2009 to present. Note that the Year shown in the table indicates the proposal call year - typically the work commences 2 years after the proposal call year.

Year	PI	Institution	Proposal Title
2018	Gautam Vasisht	JPL	A Novel Optical Etalon for Precision Radial Velocity Measurements
Other Technologies			
2009	Donald Figer	Rochester Inst. of Technology	A Photon-Counting Detector for Exoplanet Missions
2010	Stuart Shaklan	JPL	Coronagraph Starlight Suppression Model Validation: Coronagraph Milestone Report 3
2013	Eduardo Bendek	NASA Ames	Enhanced Direct Imaging Exoplanet Detection with Astrometric Mass Determination
2017	Bernard Rauscher	NASA GSFC	Radiation Tolerant, Photon Counting, Visible and Near-IR Detectors for Space Coronagraphs and Starshades
2018	Johannes Staguhn	Johns Hopkins University	Development of an Ultra-Stable Mid-Infrared Detector Array for Space-Based Exoplanet Transit Spectroscopy

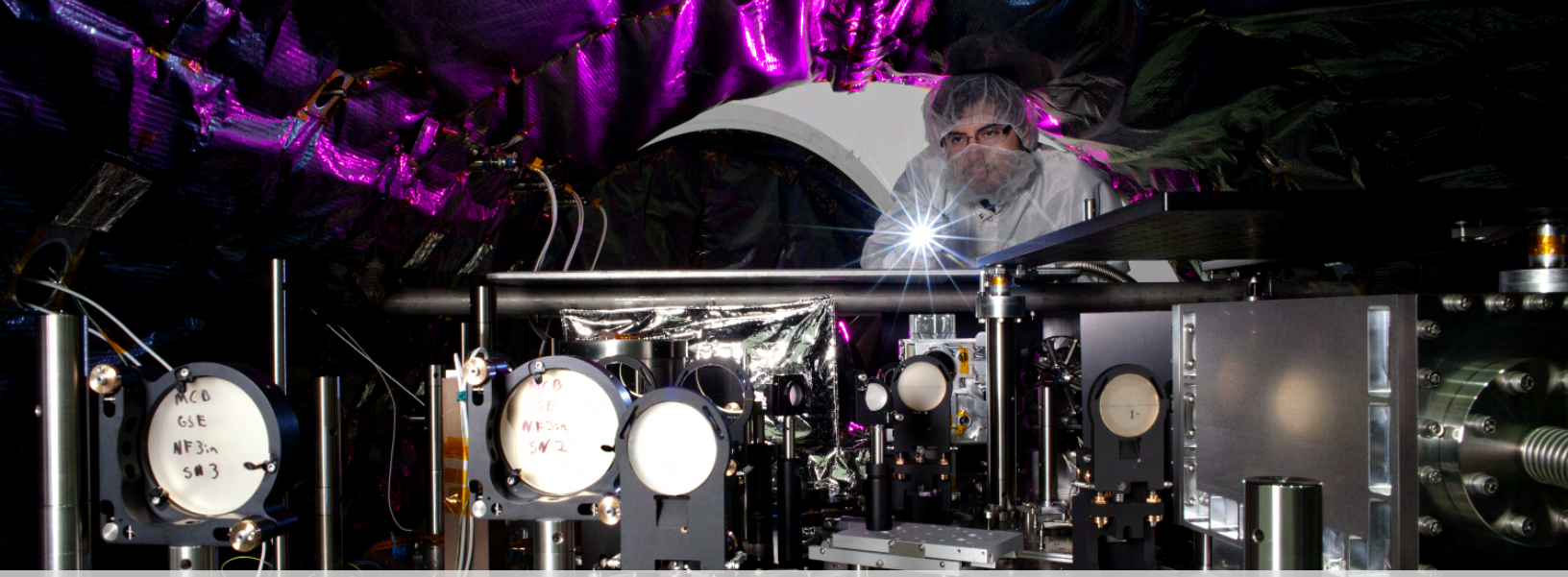

2 Coronagraph/Telescope Technology Gaps

Exo-Earth direct imaging and spectral characterization requires starlight suppression that exceeds the current best performance in ground-based observatories by several orders of magnitude. A technology that may achieve this suppression is an internal occulter, or coronagraph instrument.

Coronagraphs come in numerous architectures, each with its own strengths with respect to telescope aperture (monolithic, segmented), obscuration (unobscured, obscured by secondary mirror and its support struts), and wavefront error sensitivity (e.g. line-of-sight jitter, telescope vibration, polarization, coating non-uniformity). The design and performance of the coronagraph is closely coupled to the design and performance of the telescope that feeds it and the thermal and mechanical stability of the observatory platform; the three technology gaps in this area are:

- **Coronagraph Contrast and Efficiency** (Sec. 2.1) is aimed at starlight suppression and performing the high order wavefront control to correct quasi-static wavefront errors to achieve the necessary contrast performance, while maintaining a high throughput of planetary light.
- **Mirror Technologies for High Angular Resolution** (Sec. 2.3) addresses the capability to construct a telescope that is compatible with coronagraphy and delivers the angular resolution needed to survey enough habitable zones of nearby stars to detect the desired number of Earth-like exoplanets.
- **Coronagraph Contrast Stability** (Sec. 2.2) addresses the need to maintain deep contrast long enough for spectral measurements of very dim Earth-like planets: closing this gap may include additional wavefront control (high order or low order) or telescope-related technologies.

A vacuum optical bench for coronagraph testing located at ExEP's High Contrast Imaging Testbed facility.

There is considerable overlap between the three gaps, depending on the mission architecture choices.

In the future, the boundaries between these three technology gaps and their associated subgaps (listed in detail in Appendix A) may shift based on future architecture studies, and adapting the approach to best facilitate the practical development of the enabling technologies.

2.1 Coronagraph Contrast and Efficiency

Coronagraph optics suppress on-axis starlight while allowing off-axis planet light to transmit through the instrument, achieving a high contrast detection of the planet in close angular proximity to its host star. An ongoing program is needed to improve the performance of coronagraph masks, apodizers, beam-shaping optics, wavefront control, and post-processing techniques beyond performance levels of the Roman Coronagraph, in contrast, throughput, bandwidth, and inner working angles. To achieve maturity for a future space mission, the performance must be demonstrated in dynamic[1] vacuum environments with both segmented and unobscured pupils (i.e. relevant to a telescope with a monolithic primary mirror).

1: "Static" demonstration here and throughout implies no intentionally introduced line of sight errors or other wavefront disturbances, while "dynamic" refers to laboratory experiments where disturbances that are representative of the flight environment are deliberately introduced into the testbed.

Subgaps which may also need to be closed in order to close the Coronagraph Contrast and Efficiency gaps are listed in Table A.2. These are:

- Coronagraph Architecture - referring to the coronagraph's masks, apodizers, and other optical elements;
- Deformable Mirrors, the most mature means of performing wavefront manipulation;
- Computational Throughput on Space-rated Processors, enabling on-board high-order wavefront control;
- High-bandwidth optical communication between space and ground, enabling ground in the loop wavefront control;
- Coronagraph Efficiency: improvements in overall observing efficiency to achieve better science yield;
- Autonomous on-board Wavefront Sense and Control (WFSC) architectures: more efficienct algorithms for onboard high-order wavefront sensing and control.

Technology Gap: Coronagraph Contrast and Efficiency

- **Need:** Maximized science yield for a direct imaging telescope/mission. $\leq 10^{-10}$ raw contrast, >10% throughput, Inner Working Angle (IWA) $\leq 3\ \lambda/D$, obscured/segmented pupil
- **State-of-the-Art:** unobscured pupil: $4{\times}10^{-10}$ raw contrast at 10% bandwidth at 550 nm, angles of 3–9 λ/D (LC demo in HCIT); obscured pupil: $1.6{\times}10^{-9}$ raw contrast at 10% bandwidth across angles of 3-9 λ/D (Roman Coronagraph)
- **Subgaps are listed in Table A.2**

Current State-of-the-Art

Coronagraphs on the Hubble and James Webb Space telescopes have set the state-of-the-art for high-contrast imaging from space, albeit with no high order wavefront control needed to enable deeper contrast. Hubble's coronagraph on the Space Telescope Imaging Spectrograph (STIS) instrument has demonstrated 3×10^{-5} at 0.25″ (roughly 5 $\lambda/$D) [12]. The JWST NIRCam commissioning results have shown a 5σ detection limit of 1×10^{-5} flux ratios at angular separations of 0.5″ (5 $\lambda/$D) using the NIRCam bar mask at 3.35μm [13].

The deepest in-vacuum contrast achieved over a 10% band were 6×10^{-10} over a half-annular dark region from 3–15 λ/D with a Hybrid Lyot coronagraph at 800 nm [14], and 4×10^{-10} over a full annulus of 3–8 λ/D with a Lyot coronagraph at 550 nm [15]. Both of the demonstrations occurred in a static vacuum environment with a clear pupil (representative of a monolithic telescope) in ExEP's HCIT.

Roman Coronagraph demonstrations have achieved the state-of-the-art in coronagraph performance with a highly obscured pupil, in low light conditions, and in a simulated dynamic environment (see Table 2.1), and will establish a new space-based state-of-the-art after its launch in the mid-2020s.

Post-processing algorithms have demonstrated improvements of roughly a factor 10 starting from a raw contrast of 10^{-8} (see for example the recent Roman Coronagraph data challenge [16]).

Coronagraph demonstrations with a segmented pupil have been carried out in-air at the HiCat facility at the Space Telescope Science Institute using a hexagonally segmented deformable mirror to simulate an off-axis segmented telescope pupil with the capability to inject wavefront instabilities. To-date, the team has achieved contrast performance in monochromatic 640 nm light of 2×10^{-8} from 4.6–12$\lambda/$D with a Lyot Coronagraph in a statc environment, and 2×10^{-8} from 2–12$\lambda/$D with a Phase-Apodized-Pupil Lyot Coronagraph (PAPLC) with active low-order wavefront control [17].

A vortex coronagraph demonstration of broad-band contrast in HCIT used a static hexagonally-gridded pupil mask to demonstrate the technique of using a deformable mirror to supress diffracted light from the segmentation pattern (see Fig. 2.1).

Recent Progress

Roman Space Telescope Coronagraph Instrument

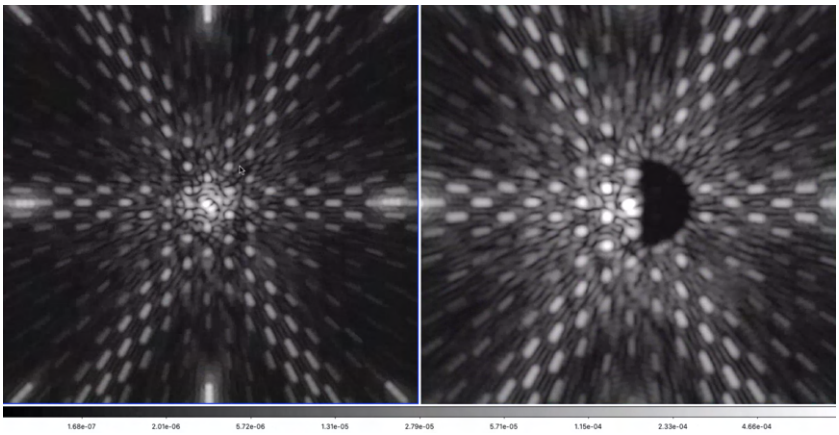

Figure 2.1: A vortex coronagraph dark hole in the presence of a static pupil mask mimicking a hexagonal segmented primary mirror. On the left, the diffraction pattern due to the segmented hex pattern is apparent; the right panel shows the same scene after electric field conjugation was used to null the diffracted light in a dark zone [18].

The Coronagraph Instrument on the Roman Space Telescope is a technology demonstration instrument that is capable of characterizing exoplanets in the visible band at contrast levels of 10^{-8} or better. As the first space coronagraph with active wavefront control, the Roman Coronagraph will establish a new state-of-the-art performance and demonstrate many technologies that could feed forward to the envisioned future exo-Earth direct-imaging mission. These include coronagraph architectures, a low-order wavefront sensing and control system, deformable mirrors, photon-counting visible-band EMCCD detectors, and post-processing techniques [19].

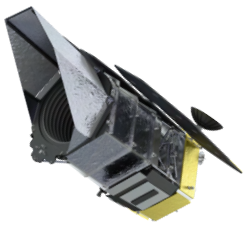

Figure 2.2: The Roman Space Telescope

In June 2022, the Roman Coronagraph passed its System Integration Review and the instrument is now undergoing a flight build for launch aboard Roman in the mid-2020's. Over the course of pre-formulation technology development activities and early phases of the flight mission, the Coronagraph team demonstrated a number of performance milestones with increasingly challenging configurations. Table 2.1 shows the to-date laboratory performance of the instrument.

The coronagraph masks that will be included for the purposes of achieving the technology demonstration goals of the instrument include a hybrid Lyot optimized for small inner working angle imaging; a spectroscopy-optimized shaped pupil with a broader bandwidth (17%) and a partial field-of-view; and, a shaped pupil optimized for a wider field of view. These masks were designed to work with the highly obscured pupil of the donated Roman telescope. Contributed masks from the Exoplanet Exploration Program Office, which can be used to perform additional on-orbit demonstrations and measurements, include a multi-star wavefront control mask and a transmissive Zernike wavefront sensor[2]. Figure 2.3 shows a flight mask positioning mechanism with shaped pupil and multi-star masks. The full complement of Roman flight masks and bandpasses are described in [21].

2: The Zenike sensor is being demonstrated for future exoplanet direct imaging missions as a method to measure changes in light phase to sub-pm precision [20], such as drifts in deformable mirror actuator position.

Strategic Astrophysics Technology awards

Many of the recent technology advances in space coronagraphy have been funded by awards from NASA's Strategic Astrophysics Technology program (See Table 1.2).

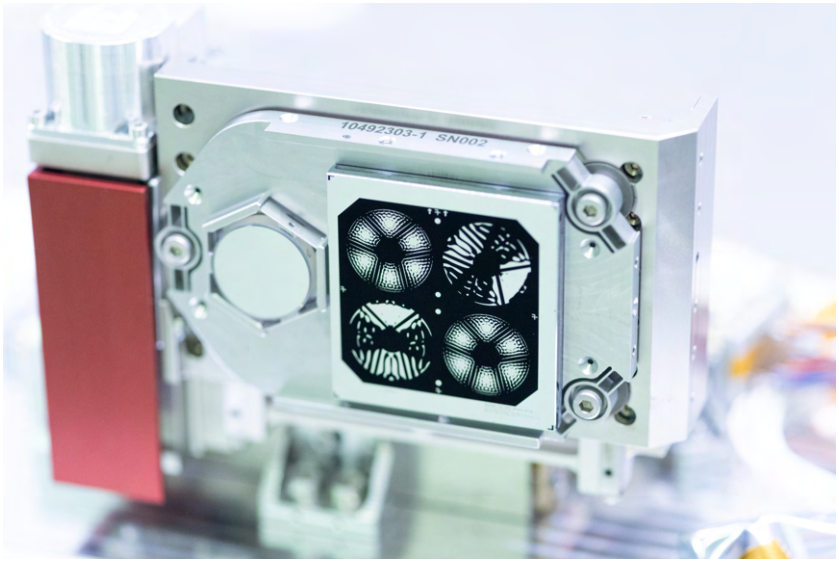

Figure 2.3: The Roman Coronagraph pupil plane mask flight mechanism. A simple fold mirror is used for the Hybrid Lyot mode. The other four masks are shaped pupil masks for limited-field-of-view slit spectroscopy in two orientations, as well as wide field of view imaging with and without the dot grid pattern multi-star masks contributed by ExEP. Image Credit: Ryan Lannom (JPL).

The SAT-2015 Breckinridge (University of Arizona) polarization modeling effort delivered a Milestone Final Report [27], completing three milestones characterizing the effects of polarization aberrations on coronagraph performance. The work influenced both the HabEx and LUVOIR designs, as the teams included design changes to their telescopes and coronagraphs to help mitigate the effect of polarization. Breckinridge and his team also provided an independent simulation of the polarization aberrations induced by the Roman Space Telescope fore-optics and found agreement with the Roman Coronagraph team.

The SAT-2018 Belikov award focused on Phase-Induced Amplitude Apodized / Complex Mask Coronagraph (PIAACMC). The team completed testing in vacuum with a static segmented pupil, and is currently writing a Milestone Final Report assessing limiting factors in contrast performance. The design under consideration is more robust to tip/tilt errors (and thus also to stellar diameter) than previous PIAACMC designs.

HCIT hosted several rounds of testing of vortex coronagraphs for the SAT-2014 and SAT-2017 Serabyn awards in 2021 and 2022. Vortex masks can offer reduced sensitivity to most low order aberrations, and were chosen as the baseline coronagraph for both the HabEx and LUVOIR-B studies. The testing achieved new contrast records for the vector vortex at 10% bandwidth between 3–9 λ/D of 1.5×10^{-9} and 6×10^{-9} at 20% bandwidth. A demonstration of high contrast with a static hexagonal segmented pupil mask (Fig. 2.1) validated the previously predicted ability to correct diffraction from segment gaps using wavefront control. The limiting performance factor appears to be small-scale retardance errors in the vortex masks; improvements in the mask fabrication are underway and new masks will be tested in the near future [18, 28].

A Trauger SAT-2016 has begun work on a next-generation Hybrid Lyot Coronagraph known as the Super Lyot Exo-Earth Coronagraph (SLEEC) aiming to demonstrate $<10^{-10}$ contrast in broadband [29]. Mask designs have been developed and fabrication is underway. Initial vacuum testbed

Table 2.1: Coronagraph contrast demonstrated in laboratory testbed settings by the Roman Coronagraph team. Adapted from Seo (private communication).

Year	Accomplishment	Contrast	λ (nm)	Band	Angle (λ/D)	Reference
2015	Narrowband 360° Hybrid Lyot contrast with 2 DMs and Roman pupil	6.92×10^{-9}	550		3–9	[22]
2015	Broadband Hybrid Lyot demo	8.54×10^{-9}	550	10%	3–9	[23]
2015	Broadband Shaped Pupil demo	8.80×10^{-9}	550	10%	3–9	[23]
2017	Broadband Hybrid Lyot	1.60×10^{-9}	550	10%	3–9	[24]
2017	Broadband Shaped Pupil	4.3×10^{-9}	550	10%	2.8–8.8	[24]
2017	Broadband Shaped Pupil and Hybrid Lyot dynamic environment[a]	$<1\times10^{-8}$	550	10%	3–9	[24]
2017	Integral Field Spectrograph contrast demo	1.00×10^{-8}	660	18%	3–9	[25]
2018	Broadband Disc mask contrast	3.46×10^{-9}	660	10%	6.3–19.5	[26]
2019	Band 1 Hybrid Lyot	3.58×10^{-9}	575	15%	3–9	
2020	Integral Field Spectrograph contrast demo	4.83×10^{-9}	760	18%	3–9	

[a] Sensing and control of flight-like tip, tilt, and focus aberrations only.

runs with a simple Lyot coronagraph have been shown to replicate the testbed commissioning contrast [15].

See Figure 2.4 for contrast vs. working angle for recent coronagraph demonstrations in the HCIT vacuum testbeds.

A SAT-2017 (PI Soummer, Space Telescope Science Institute) kicked off an effort to demonstrate an Apodized Pupil Lyot Coronagraph (APLC) at a contrast of $<10^{-7}$ level over a 6% band on an in-air testbed (HiCat; [30–37]) in the presence of dynamic wavefront errors expected from a simulated segmented telescope. The demonstrations have successfully achieved the contrast goals in monochromatic (639 nm) light [17] and broadband demonstrations are expected in 2023. APLC technology is the leading coronagraph architecture for segmented/obscured space telescopes and was the baseline coronagraph technology by the LUVOIR-A (on-axis) mission concept.

In addition to coronagraph architecture investigations, several SAT-funded groups have investigated novel wavefront control techniques that have the potential to enhance their stability and/or open up novel applications for coronagraphy.

A wavefront control technique known as Multi-Star Wavefront Control is being developed under an Internal Scientist Funding Model (ISFM) award to Belikov (NASA/ARC). The aim is to simultaneously suppress light from a star and light from a closely separated companion star. It is accomplished by introducing a grating into the coronagraph and performing wavefront control to suppress starlight around a dispersed higher order of the companion star. Since the majority of nearby Solar-type stars are found in

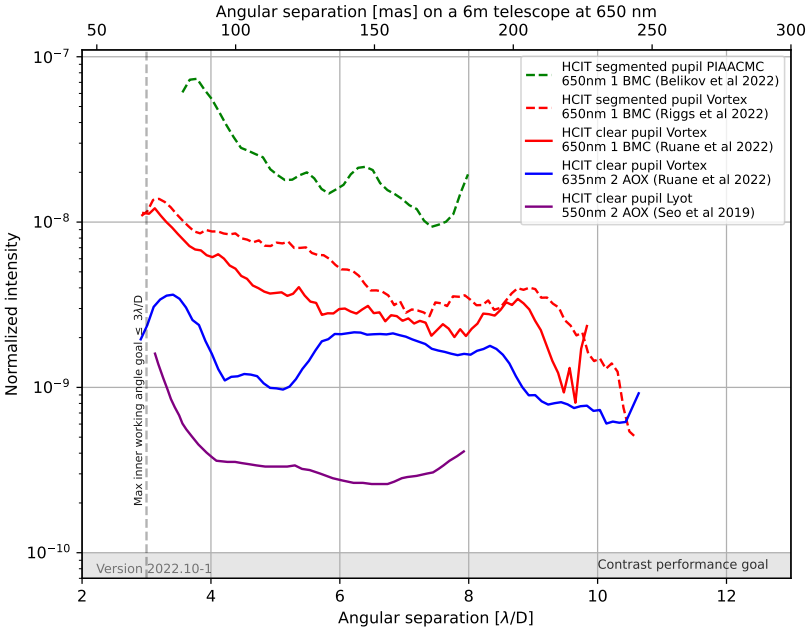

Figure 2.4: Recent broadband ($\Delta\lambda/\lambda$ = 10%) coronagraph performance demonstrations in ExEP's HCIT facility. The upper x-axis scale shows the equivalent angle in milli-arcseconds corresponding to a 6 m telescope at 650 nm. The labels "1 BMC" and "2 AOX" describes the set of deformable mirrors used to perform high-order wavefront control in the demonstration: a single Micro-Elecrical Mechanical Sensor (MEMS) Deformable Mirror (DM) from Boston Micromachines, or two electrostrictive DMs built by Northrup Grumman's AOA Xinetics, respectively.

multi-star systems, it has the potential to expand greatly the target list of exo-Earth direct imaging missions.

The technique was successfully demonstrated in in-air laboratory tests [38–40]. Initial laboratory demonstrations of the technique in ExEP's vacuum testbed [41, 42] are underway (See Fig. 2.5). A key challenges is demonstrating the technique in broadband. The Roman Coronagraph accepted an ExEP-contributed multi-star wavefront control mask that may enable the search for planets orbiting both stars in the nearby α-Centauri system [43].

Mawet's SAT-2017 is advancing improved architectures to couple a spectrograph to a coronagraph. In addition to hardware demonstrations in-air, the investigation is developing a novel wavefront control technique to enable deeper contrast and wider bandwidth ($\Delta\lambda/\lambda \geq$30%) over a smaller focal plane region. The concept allows higher signal-to-noise ratio spectral characterization when the location of the planet is known. The software has been implemented for the vacuum testbed and results from initial tests with a vortex coronagraph are forthcoming.

Next Steps

A gap remains between present capabilities and the needed 10^{-10} contrast ratio, with 3 λ/D inner working angle and 10% bandwidth with a coronagraph. Laboratory demonstrations and continuing modeling work are needed to achieve this goal and to mature coronagraph technology for infusion into a flight mission.

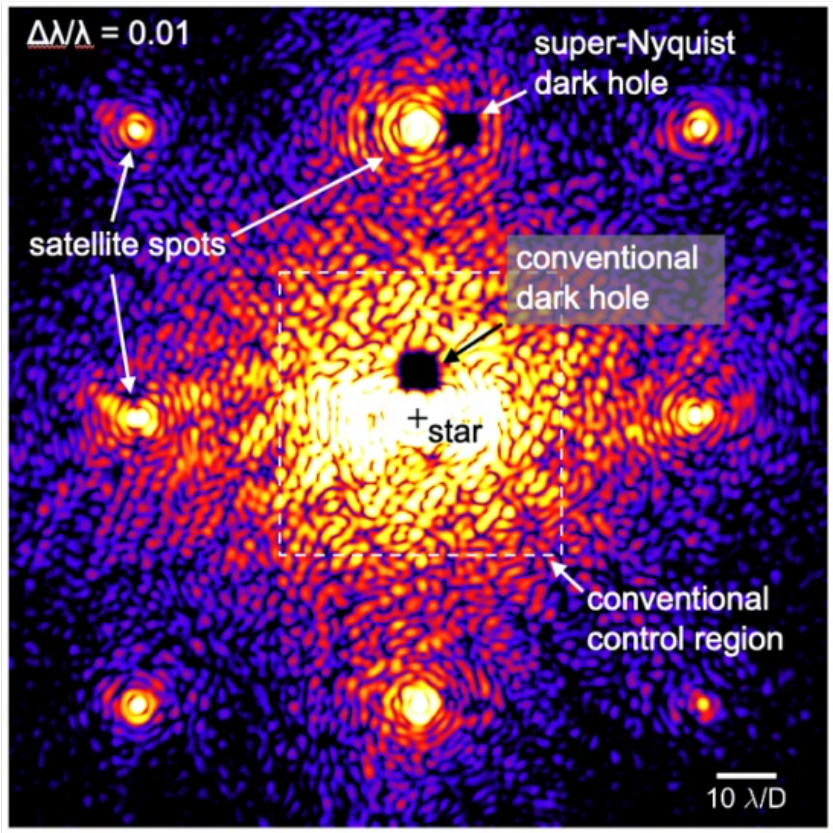

Figure 2.5: Super-Nyquist wavefront control demonstration with a double dark hole, a critical step towards enabling observations of binary star systems. (Image credit: Garreth Ruane).

In addition, the preparatory work within Great Observatories Maturation Program (GOMAP), architecture and science trades may lead to adjustments of the performance goals for coronagraphy in wavelength coverage, inner working angle, throughput, and contrast. Other performance goals will need to be quantified as science goals are developed – for example the Outer Working Angle (OWA) of the coronagraph[3].

The SAT-funded efforts in vortex coronagraphs, next-generation hybrid Lyot coronagraphs, and apodized pupil Lyot coronagraphs will continue towards these goals. Other promising coronagraph architectures under investigation include scalar vortex [44, 45] and Phase-Induced Amplitude Apodized (PIAA)/Vortex [46].

In addition to meeting the contrast, bandwidth, and working angle requirements, coronagraph demonstrations may focus on improvements in outer working angle and wider spectral bandwidth that could benefit the survey efficiency and science yield of a future mission. Coronagraph design and modeling efforts will focus on robustness to realistic telescope wavefront errors (see Sect. 2.2 below) and to polarization aberrations (for example [47]).

Two new SAT awards in 2022 will advance coronagraph technology. One will demonstrate a technique known as dark-hole maintenance that updates the wavefront control settings at a higher rate (SAT-2022 Cahoy, MIT). This approach has been demonstrated in-air [48] and the SAT will attempt to demonstrate the technique at high contrast in vacuum. In addition, a

3: The LUVOIR study specified a coronagraph OWA of 40 λ/D in the UV and 64 λ/D in the Visible and Near Infrared (Table 1-8 of [5]), while HabEx used 32 λ/D (Table C.2-2 of [6]). The OWA requirement maps to the actuator count of the deformable mirror used for wavefront control.

technique will be investigated to develop dual-purpose masks that can simultaneously perform high contrast imaging and high order wavefront sensing with a Zernike dimple (SAT-2022 Wallace, JPL).

A detailed study of near-ultraviolet coronagraphy may be needed; The science cases described in the HabEx and LUVOIR reports called for high contrast imaging capability down to a wavelength of 200 nm. This represents a factor of 2 shorter wavelength than has been demonstrated to-date in a laboratory coronagraph, and additional challenges are expected in the areas of polarization aberrations, reflectivity/scattering, contamination issues, and wavefront control.

Post-processing algorithms should be evaluated for ~10^{-10} raw contrast to determine whether algorithms demonstrated at shallower contrast can still achieve gains in extracting terrestrial planets in the presence of realistic speckle noise.

The ExEP is commencing two activities in 2023 to help guide the next steps: a Coronagraph Architectures Survey, and a Coronagraph Roadmapping Activity. The Coronagraph Architecture Survey is a fact-finding activity that will gather a team of experts to capture the status of coronagraph architectures that could benefit the Habitable Worlds Observatory. It will aim to address the questions of which coronagraph architectures offer the highest likelihood of success and which merit investment and demonstration opportunities.

The LUVOIR [5] and HabEx [6] reports included detailed technology development plans for coronagraphs. The Coronagraph Roadmapping Activity will assemble a team to create an updated maturation plan for coronagraphs for the Habitable Worlds Observatory. The team will consider coronagraph architectures along with wavefront control, interfaces with the telescope, and consider facilities and ground support equipment that may be needed such as telescope simulators. The activity will also make recommendations for detectors.

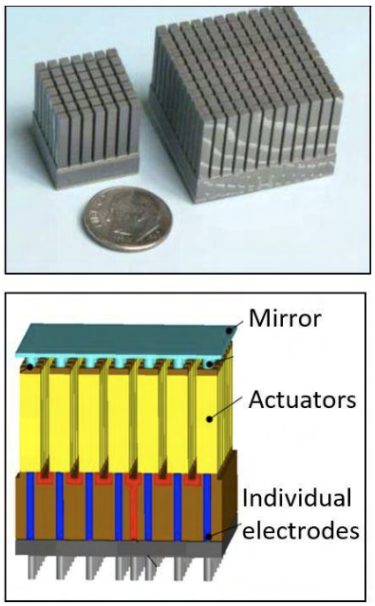

Figure 2.6: Deformable mirror technology from AOA Xinetics (AOX). The top panel shows the electrostrictive actuators. The bottom panel is a diagram showing a side-view of the assembly including the deformable mirror surface ("face sheet"), actuators, electrodes, and connector pins.

2.1.1 Deformable Mirrors

DMs, available in a variety of architectures and designs, offer the most technologically mature means of applying corrections as part of a wavefront sensing and control system, and are likely to serve in this role in a future space coronagraph instrument. They do so with actuators that displace a reflective surface on scales that are a small fraction of a wavelength and can thus apply phase changes to the light in a coronagraph.

Key performance parameters for this technology include actuator count (the number of actuators), actuator pitch, resolution, actuator stroke, actuator response time, actuator stability, and low cross talk. Specific requirements on these parameters depend on coronagraph and mission architecture. The needed actuator stroke and resolution is a function of the coronagraph architecture. The actuator pitch will set the overall scale of the coronagraph design and for space-based applications, smaller is generally advantageous

for volume and mass considerations. Higher actuator counts enable control of more spatial modes across the pupil.

Current State-of-the-Art

The deformable mirrors for Roman Coronagraph are space-qualified, with flight mirrors delivered. These devices supplied by Northrop Grumman's AOX, are based on electrostrictive actuators using lead-magnesium-niobate (PMN) materials (Figure 2.6). Most of the vacuum high contrast performance demonstrations carried out in the HCIT have relied on this type of mirror.

MEMS devices are an alternative architecture that is commonplace in ground-based adaptive optics systems. This technology is manufactured using industrial semiconductor processing techniques, and electrostatic forces are used to deform a continuous face-sheet mirror. Low-actuator-count MEMS devices (Boston Micromachines Corporation (BMC) 140) have flown and successfully operated in a low-Earth orbit on the DEMI cubesat [49], though not as part of a high contrast imaging instrument. A BMC 1K mirror has flown on the PICTURE-C telescope and demonstrated high-order wavefront control on a stratospheric balloon-borne platform [50].

MEMS devices (BMC 1K - shown in Figure 2.7 - and BMC 2K) have also demonstrated functionality in a coronagraph after exposure to launch-load random vibe and demonstrated in-lab repeatable performance [51, 52].

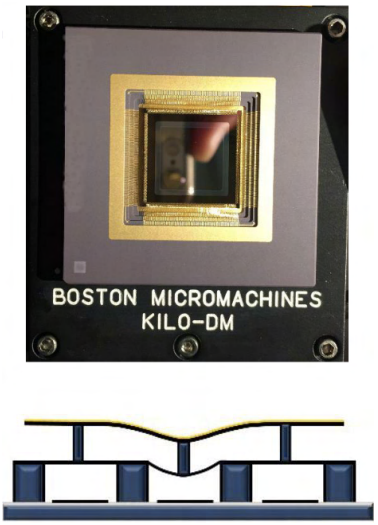

Figure 2.7: MEMS deformable mirror from Boston Micromachines Corp. (BMC). The upper panel shows a 1K (one thousand actuator) deformable mirror. The bottom panel shows how voltages applied to individual actuators deform the mirror surface through electrostatic forces.

Recent Progress

ExEP carried out a worldwide deformable mirror survey to document viable deformable mirror technologies for future missions, and to make recommendations for maturing these technologies based on a number of factors such as mission performance requirements, estimated development cost, and technology readiness [4]. The top two candidates were electrostrictive technology by AOX (the vendor providing DMs for Roman) and MEMS technology by BMC. A third vendor, ALPAO builds DMs based on electromagnetic coil actuation, has demonstrated 64×64 actuator architecture with aims to space qualification [53], and is scaling to a 128×128 actuator mirror for ground-based extremely large telescope applications.

A balloon flight in September 2022 of PICTURE-C demonstrated a "woofer-/tweeter" approach with a 97-actuator ALAPO deformable mirror to correct low-order aberrations and a BMC MEMS mirror to perform the high order wavefront control [50] with a minaturized deformable mirror controller [54].

Launch-load random vibration testing of MEMS has demonstrated promising results. A project funded by SAT-2010 Bierden performed random vibration testing on an earlier generation of MEMS deformable mirrors, showing they survived launch loads [51], with further demonstrations of random vibration survivability of a BMC 2K mirror by ExEP [52].

4: See an ExEP Technology Colloquium Series talk from August 19, 2021 for more details.

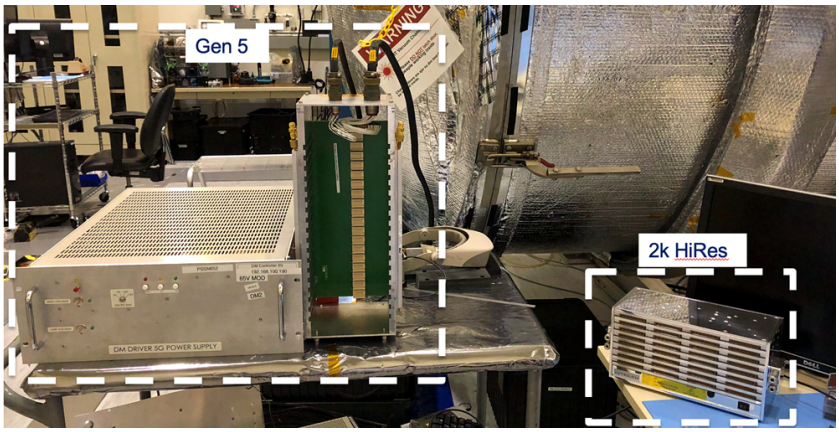

Figure 2.8: A photograph of new higher bi-resolution deformable mirror drive electronics (right: "2k HiRes") showing the compactness as compared to a previous version of drive electronics (left "Gen 5") [54] (Image credit: Eduardo Bendek).

Modeling and demonstrations of BMC MEMSs deformable mirrors in a coronagraph setting has shown that surface figure errors due to print-through effects creates a performance limit (Fig. 2.4) [28], improved processing techniques to mitigate this effect are under study by BMC.

Modeling of the effects of quantization errors in the drive electronics on the final coronagraph contrast has demonstrated the need for improvement in Digital-to-Analog Converter (DAC) resolution so that the DAC's least significant bit corresponds to a finer physical actuator displacement [55] while maintaining the overall throw of the actuators. New compact designs for drive electronics have been developed with a 18-bit resolution (as opposed to 16-bit used in the Roman Coronagraph) and better scalability to high actuator count (Fig. 2.8) [54].

Next Steps

The ExEP is initiating a Deformable Mirror Roadmapping activity to commence in 2023. This activity will assemble a team of experts to create a strategy to mature deformable mirrors for the Future Great Observatory, including electronics, cables, and interfaces. This activity will determining detailed requirements, including working with the science community to select a format size and includes the electronics, cables, and interfaces, and also gather the lessons learned from the Roman Coronagraph.

The activity is likely to look at scaling of deformable mirrors, their drive electronics, and interconnects to higher actuator counts (up to 128×128). Deformable mirror stability must be investigated, and MEMS devices surface figure (in particular, quilting patterns) must be improved.

An ongoing effort to develop and test parabolic deformable mirrors under an ISFM (lead, Tyler Groff, GSFC) partnering with ALPAO, could lead to a reduction in the size and complexity of space coronagraphs [56].

Deformable mirrors are the most mature technology to perform wavefront corrections, but less mature alternatives such as Spatial Light Modulators (SLM) [57] and architectures based on photonic lanterns [58] may be investigated in the future.

2.2 Coronagraph Contrast Stability

A coronagraph must maintain its contrast performance long enough to directly image or spectrally characterize a planet, during exposures that may last days or weeks. Depending on the system's architecture, the stability requirements on wavefront error can be 10–100 pm over a control loop step (of order minutes). Typical disturbances are thermal drifts, mechanical vibrations, and transient disturbances (such as thermal relaxation or micrometeroid strikes). The necessarily stability can be achieved with some combination of active control of wavefronts within the coronagraph, active control of the telescope segments/surfaces, passive stability of the telescope and coronagraph optics, robustness to disturbance, and disturbance reduction. There is overlap with the technology gaps Mirror Technologies for High Angular Resolution and Coronagraph, as the coronagraph and telescope must be considered as a system.

Identified sub-gaps that may partially or fully close the Coronagraph Contrast Stability gap are:

- Ultra-stable Telescope - active control of primary and secondary telescope mirrors to achieve stability requirements;
- Integrated Modeling of Telescope/Coronagraph system - the capability to rapidly and precisely model the system;
- Disturbance Reduction and Observatory Stability - reducing onboard vibrations, for example by replacing reaction wheels with microthrusters;
- Wavefront Sensing (low-order and out-of band) - measuring wavefront errors over a variety of spatial and temporal bands to inform control systems;
- Vibration Isolation and Pointing System Technology - the ability to isolate the telescope/coronagraph from onboard disturbances;
- Laser Gauges for Metrology - providing on-board metrology if needed;
- Segment Relative Pose Sensing and Control - the relative positioning of mirror segments;
- Thermal Sensing and Control - to maintain thermal stability;
- Wavefront Sensing and Control Algorithms - algorithms to use wavefront error information to control coronagraph;
- and, Observatory Pointing Control - the capability to precisely point the space observatory during an observation.

Technology Gap: Coronagraph Stability

- **Need:** Contrast stability on time scales needed for spectral measurements (possibly as long as days). Achieving this stability requires an integrated approach to the coronagraph and telescope, possibly including wavefront sense/control, metrology and correction of mirror segment phasing, vibration isolation/reduction This stability is likely to require wavefront error stability at the level of 10-100 pm per control step (of order 10 minutes).
- **State-of-the-Art:** Roman Coronagraph demonstrated ~10^{-8} contrast in a simulated dynamic environment using LOWFS (which obtained 12 pm focus sensitivity).
  SIM and non-NASA work has demonstrated nm accuracy and stability with laser metrology. Capacitive gap sensors demonstrated at 10 pm. 80 dB vibration isolation demonstrated. *Gaia* cold gas microthrusters and *LISA* pathfinder colloidal microthrusters can reduce vibrations.
- **Subgaps are listed in Table A.3.**
  - **Ultra-stable Telescope**
  - **Integrated Modeling of Telescope/Coronagraph system**
  - **Disturbance Reduction and Observatory Stability**
  - **Wavefront Sensing (low-order and out-of band)**
  - **Vibration Isolation and Pointing System Technology**
  - **Laser Gauges for Metrology**
  - **Segment Relative Pose Sensing and Control**
  - **Thermal Sensing and Control**
  - **Wavefront Sensing and Control Algorithms**
  - **Observatory Pointing Control**

Current State-of-the-Art

The state-of-the art in high contrast coronagraph stability remains the laboratory demonstrations of the Roman coronagraph contrast stability in a dynamic environment, using a LOWFS [24].

Preliminary results from JWST indicate 10–20 nm of wavefront error stability on scales of two days, limited by segment motion [59].

Many demonstrations of components and subsystems that may be needed to achieve the coronagraph stability have also set state-of-the-art performance.

LISA Pathfinder's colloidal microthrusters have demonstrated thrust noise better than $\mu\text{N}/\sqrt{\text{Hz}}$ in the 0.01 to 5 Hz bands. These thrusters can be adapted to replace reaction wheels, as baselined for HabEx [60].

In the lab,capacitive metrology has been demonstrated to better than 3.3 pm over a >10 Hz bandwidth [61], a concept that may be scalable to a segment edge sensor with picometer sensitivity.

Picometer-accuracy laser metrology was demonstrated by the SIM with large beam launchers. More compact beam launchers, lightweight enough to mount to the edges of segments, have been developed over the last

few years for non-NASA customers but were designed to operate at the nanometer-precision level. Additional development in laser metrology is needed if a laser metrology truss is to be used for sensing segment positioning.

The disturbance-free payload system has demonstrated vibration isolation at 68 dB level and a design was developed for the LUVOIR mission concept to isolate the telescope and coronagraph instrument from vibrations from the attitude control system [62].

Work at NASA/Marshall Space Flight Center (MSFC) funded by an ISFM demonstrated better than 2 mK thermal stability control of a 1.5 m ULE mirror in a relevant thermal-vacuum environment [63].

Recent Progress

The LUVOIR final report presented a telescope architecture that was designed together with the coronagraph instrument as a coupled system and thus addressed coronagraph contrast stability as a systems problem. The report developed a observatory architecture with multiple layers of active stability control: vibration isolation, active segment control in the primary mirror and wavefront control in the coronagraph [5]. The HabEx final report presented an architecture that took the approach of reducing disturbance sources and using the passive stability of a massive monolithic primary mirror, as well as wavefront control in the coronagraph, to achieve stability requirements [6]. Each of these approaches offer detailed reference points and important concepts for future architecture studies to consider.

Activities have continued on wavefront sensors and control algorithms that could be used to fully or partially achieve the necessary stability. Demonstrations of a coronagraph using closed-loop wavefront control to correct separately injected segmented mirror dynamics have been made in monochromatic light at the 3×10^{-8} level on the HiCAT in-air testbed [17], and have demonstrated Kalman-filter-like algorithms [48] to stabilize the dark zone.

To improve wavefront sensing capabilities, Zernike wavefront sensors have been developed and demonstrated to sense sub-picometer wavefront errors over a wide variety of spatial scales [20, 64]. Future work will address temporal bandwidth of these sensors and how they can fit in to a coronagraph/telescope system.

Guyon's SAT-2017 is advancing a technique known as Linear Dark Field Control to use information in residual starlight outside the coronagraph's dark zone, either spatially or spectrally, to update the high order wavefront control settings at a faster rate than otherwise possible using signal inside the dark zone. This technique has been successfully demonstrated on an in-air coronagraph testbed at NASA/Ames [65] achieving the first milestone of the investigation. Subsequent lab demonstrations at the Subaru Coronagraphic Extreme Adaptive Optics (SCExAO) testbed showed a factor of 30 improvement in coronagraph contrast starting from a $\sim10^{-6}$ contrast [66, 67]. Second and third milestones in the investigation aim in the coming

year to demonstrate the technique at deeper contrast in a vacuum testbed and to attempt dark field control with out-of-band spectral information [68].

In addition, the industry-led architecture studies of telescope/coronagraph systems have continued. The first phase of these studies focused on system-level studies of segmented telescope architectures, making important progress identifying key technology challenges. In the second phase, component level technologies that may contribute to the overall success of the architecture are being matured.

The Ultra-Stable Large Telescope Research and Analysis – Technology Maturation (ULTRA-TM) work led by Ball have also initiated lab demonstrations of picometer-scale edge sensing and actuation [61] as well as advancing other technologies, such as thermal sensing and control, mirror mounting, passive structural damping [69]. Integrated modeling [70] and thermal architecture [71] has also played a role.

Pueyo et al. [72] have investigated a number of wavefront control architectures, using the LUVOIR-A and LUVOIR-B telescopes and coronagraph instruments as references. In all cases, additional wavefront sensing beyond science focal plane images provides advantages in control loop speed and correction, either a low-order sensor similar to the one on Roman Coronagraph or a high-order Zernike wavefront sensor. Improvements are limited by the number of photons that the wavefront sensor receives, however the use of predictive control algorithms can enable shorter exposure times on fainter stars.

The TechMast team is working to develop a prototype for a CubeSat demonstration of the Disturbance-Free Payload concept [73] in order to improve maturity of this technology for a future flagship-class mission. They have also developed a photonic laser gauge demonstrated 20 pm RMS sensitivity in a laser heterodyne measurement [74] and continued studies of the stability of telescope architectures similar to LUVOIR-B [75].

The Ultra-Stable Structures (USS) lab at GSFC, funded by a COR SAT award (PI: Babak Saif, NASA/GSFC), has demonstrated the capability to measure surface RMS drift rates to 3 pm/s. The facility is designed to measure both specular and diffuse surfaces and could be instrumental in studying material stability and validating performance of components for an ultra-stable observatory [76].

Segmented Coronagraph Design and Analysis study

ExEP's Segmented Coronagraph Design and Analysis (SCDA) study continued to design and model coronagraph architectures for contrast and mission exo-Earth yield sensitivities to realistic wavefront error dynamics, simulated by finite-element engineering models of telescope structures. The SCDA teams worked with the TechMast and ULTRA-TM teams to incorporate higher fidelity models of the telescope dynamics, using the two LUVOIR architectures as models.

[77] presented a study of an integrated model of LUVOIR-A.

The Fast Linearized Coronagraph Optimizer (FALCO) modeling software [78–81] developed in part through the SCDA effort, is now publicly available[5].

5: Python and Matlab versions of FALCO are available on GitHub.

The SCDA team looked at opportunities for wavefront control by analyzing TechMAST simulations of vibration modes of the LUVOIR-A and LUVOIR-B telescopes. An adaptive optics system can reduce telescope dynamic wavefront errors of 100 pm RMS to 30 pm RMS with a magnitude 0 star, improving the contrast performance by a factor of 15. Artificial guide stars can potentially be used to correct disturbances further. In addition, the off-axis design with fewer segments (LUVOIR-B) produces a factor 5 or so less contrast-degrading wavefront disturbance than the larger, on-axis model (using similar mechanical damping factors), thereby resulting in a factor of 25 or so better contrast [82].

Most importantly, the SCDA work has begun a framework for combining detailed coronagraph contrast performance modeling with structural dynamics models of telescope systems. This framework will be critical for future architecture trades as an approach to ultra-stability is developed.

Next Steps

As the GOMAP commences architecture trades, the approaches to stability of the telescope/coronagraph system described in the LUVOIR and HabEx Final Reports will provide important starting points for engineering and for choosing technology solutions. Coronagraph lab performance demonstrations (see Sect. 2.1) are likely to require the development of a representative dynamical testbed, with the ability to introduce flightlike wavefront errors and also with optics that are scalable to flight telescope optics, by including the full range of angles of incidence.

In the near term, the industry-led segmented telescope technology efforts will continue to push forward with component-level technology development and system-level modeling. The SCDA modeling effort will continue and aims to include polarization aberrations and near-angle scattering.

The JWST and Roman Space Telescope missions will provide lessons and ideas for closing the coronagraph stability gap for the future great observatory. In 2022, JWST successfully deployed, aligned, and phased a 6.5 m segmented telescope in space. As JWST continues operations, lessons will be learned about stability challenges in the Earth-Sun Second Lagrange Point (L2) environment that will be crucial for developing technology for theHabitable Worlds Observatory.

When the Roman Space Telescope launches in the mid-2020's, the Coronagraph's technology demonstration mission will test operations and stability of a high-contrast coronagraph, using wavefront control, in a space environment [19].

2.3 Mirror Technologies for High Angular Resolution

The ability to probe terrestrial regions around stars (e.g. the habitable zone) requires a minimum aperture size. The more distant the star, the larger the telescope aperture is needed to probe these regions.

The habitable zone of an exo-Earth at 10 pc has an angular resolution of 100 mas at planet quadrature. To detect such a planet at 400 nm, a telescope should have an angular resolution of 25 mas if we conservatively assume a coronagraph with 3 λ/D inner working angle. However, our end objective is spectral biosignatures. Imposing the same parameters for detecting the planet at the 760 nm oxygen line would then require a 6.3 m telescope; water at 940 nm would require a telescope aperture approaching 8 m. Thus, improvements in the coronagraph inner working angle, or using a starshade for long wavelength spectral measurements, can help drive the aperture size down.

Large primary mirrors also reduce science integration time due to greater collecting areas and throughput, and enable probing of a larger number of more distant stars' habitable zones. The telescope's primary mirror size and architecture (monolithic or segmented, obscured or unobscured) is among the most important decisions a space telescope design team will have to make, especially when considering optimizing the performance of a coronagraph.

Simulations of mission science yield - the mean number of exo-Earths a mission will characterize - have been developed in order to inform trades[6]. The Decadal Survey recommended a roughly 6 m primary mirror diameter in order to probe the habitable zones of about 100 nearby stars for terrestrial planets.

6: The two standard methods for evaluating exo-Earth yields are ExoSIMs [83] and Altruistic Yield Optimization [84].

However, the biggest unknown quantity needed to select the telescope size is the fraction of Sun-like stars with Earth-size planets in their habitable zones, also known as $\eta_\oplus$. As $\eta_\oplus$ increases, fewer planetary systems will need to be observed in order to build sufficient statistics about the habitability of exoplanets. If $\eta_\oplus$ is near 0.1, then a 10m-class telescope is required to detect and characterize approximately 30 candidate habitable zones for exo-Earths. If $\eta_\oplus$ is greater than 0.8 then only a 4m-class telescope would be required to observe the same number of candidate habitable zones.

Determining $\eta_\oplus$ is an ongoing scientific investigation; as of this writing, a reasonable value to adopt is $\eta_\oplus \sim 0.3$ acknowledging uncertainties of a factor 3. See [85] for a recent review of exoplanet demographics. The latest results from Kepler find $\eta_\oplus = 0.37^{+0.48}_{-0.21}$ [86], though another analysis sets an upper limit at $\eta_\oplus < 0.27$ and recommends that future mission designs remain robust to values between 0.06 and 0.76 [87]. A recent analysis focused on correcting Kepler results for former sub-Neptune planets finds an occurrence rate of habitable zone terrestrial planets of $0.15^{+0.06}_{-0.04}$ [88].

If a coronagraph is used for starlight suppression, the telescope must be capable of ultra-stability (Sect. 2.2) and be designed to avoid or reduce

disturbances as much as possible. These disturbances typically include mechanical vibration induced by observatory pointing (such as reaction wheels), thermal deformations, and the micro-meteoroid environment in the observatory's orbit (possibly L2).

Characterization of exoplanets requires broadband performance of the primary and secondary telescope optics, extending into the UV. Exo-Earth atmospheric characterization demands spectra down to 200 nm, while general astrophysics science cases may desire 100 nm or shorter. Currently, the most advanced solution providing good performance ranging from the UV to IR is aluminum with a protective overcoat[89, 90]. Coated aluminum provides a lower reflectance in the visible and near-IR bands compared to silver (e.g. [91]), however silver does not reflect wavelengths shorter than ~400 nm. The coatings must be applied in a uniform way so as not to induce significant aberrations that wavefront control cannot correct.

Telescope designs must mitigate or account for wavefront error degradation with time due to micrometeroid impacts in the operating environment. JWST has observed micrometeroid fluxes at L2 that are largely consistent with models. However a single event impacting one segment caused an increase of post-realignment 5–10 nm RMS wavefront error in the telescope. The rate of such large events is currently unknown [59]. Future design teams may consider observatory features to mitigate these events, as enclosing the primary optics. A specific working group to address these concerns within Future Great Observatory architectures may be needed.

The large primary mirror can be either segmented or a monolith. The detailed requirements on the telescope are system-dependent and trades can be made with other subsystems. In this particular technology area, we consider the manufacturability of the mirror substrate, coating, and backing structures. Technologies for maintaining segment phasing, low order wavefront sense and control, and vibration isolation and disturbance reduction are considered as separate, though closely related, technologies for closing the Contrast Stability technology gap.

In order to be compatible with coronagraphy, the telescope must have certain characteristics that allow ultra-stability of the entire optical system. The mirror substrate, reflective surface, protective coating, backplane, mounting structures and mechanisms must themselves be highly stable. The coefficient of thermal expansion of the material at the telescope operating temperature must be < 5 ppb/K and highly uniform. Uncertainty in gravity sag corrections to the surface figure must be <10 nm, and must be better than 2–4 nm for spatial frequencies outside the correction capabilities of an adaptive optics system. Because the telescope will operate with active control systems, it may be advantageous to divide surface figure requirements into spatial frequency bands.

Identified sub-gaps that may partially or fully close the Mirror Technologies for High Angular Resolution gap are:

- Mirror Substrate and Structure - the capability to create mirror substrates and backing structures that meet stiffness, launch survivability and are capable of meeting stability requirements;

- Mirror Positioning Actuators - achieve rigid body positioning of mirror segments (and potentially mirror surface figure), accurate and stable to the picometer level;
- Gravity Sag Offloader - the capability to accurately predict a mirror's surface figure on-orbit from measurements on the ground;
- Coefficient of Thermal Expansion Characterization - the ability to measure the coefficient of thermal expansion of mirror substrates to the parts-per-billion level;
- Mirror Finishing - the capability to polish mirror substrates to achieve surface figure requirements (on the order of 10 nm RMS);
- UV Coatings: Wavefront Effects - achieve a mirror surface coating that provides high reflectivity from the UV into the infrared and minimizing wavelength-dependent phase shifts that might limit the bandwidth of coronagraph wavefront control..

Technology Gap: Mirror Technologies for High Angular Resolution (UV/Vis/NIR)

- **Need:** Large (4–16 m) monolith and multi-segmented mirrors for space that meet SFE $\leq$ 10 nm RMS (wavelength coverage 400–2500 nm); Wavefront stability better than 10 pm RMS per wavefront control time step; CTE uniformity characterized at the ppb level for a large monolith; Segmented apertures leverage 6 DOF or higher control authority meter-class segments for wavefront control.
- **State-of-the-Art:**
  Monolith: 3.5-m sintered SiC with <3 μm SFE (Herschel); 2.4-m ULE with ~10 nm SFE (HST); Depth: Waterjet cutting is TRL 9 to 14″, but TRL 3 to >18″. Fused core is TRL 3; slumped fused core is TRL 3 (AMTD).
  Segmented: 6.5 m Be with 25 nm SFE (JWST); Non-NASA: 6 DOF, 1-m class SiC and ULE, < 20 nm SFE, and < 5 nm wavefront stability over 4 hr with thermal control.
- **Subgaps are listed in Table A.1**
  - Mirror Substrate and Structure
  - Mirror Positioning Actuators
  - Gravity Sag Offloader
  - Coefficient of Thermal Expansion Characterization
  - Mirror Finishing
  - UV Coatings: Wavefront Effects

2.3.1 Large Monolithic Mirrors

Monolith primary mirrors in an off-axis telescope provide an ideal unobscured pupil for a coronagraph, but are more limited in size than a deployable segmented mirror. The maximum size monolithic mirror has been limited to approximately 4 m by currently available 5-m-class launch vehicle fairings. For example, the largest monolithic space telescope ever flown was Herschel's 3.5 m primary mirror. With the advent of NASA's Space Launch System (SLS) and SpaceX's Starship, with planned 8-m class fairings, it is possible to consider monolithic 4- to 8-m-class mirrors.

Current State-of-the-Art

The largest monolith mirror optimized for performance in the visible-band is the Hubble Space Telescope, made of ULE glass with 10 nm surface figure error. The Roman Space Telescope will be the same size. A 3.5 m monolith primary mirror (made of SiC) flew as part of the Herschel observatory, though it was optimized for mid and far-infrared wavelengths, and had a surface figure error of 3 μm. Glass mirrors in the 8 m or larger class achieving 7-8 nm surface figure error have been manufactured for use in ground-based observatories (Subaru, VLT) though space missions usually require mirrors with lower density per area, and a higher resonant frequency (stiffness).

Recent Progress

The HabEx study presented a roadmap for maturing large monolith space mirror technology, specifically studying a 4 m diameter primary mirror made of Zerodur; see Appendix E of [6].

Next Steps

The GOMAP may consider large monolithic primary mirrors in future architecture options. The HabEx study of developing technology for a 4 m monolith should be revisited for the case of the recommended 6 m primary mirror to understand scaling issues.

The ISFM-2022 award to Stahl will address several issues related to large monolithic primary mirrors, including gravity sag measurements.

2.3.2 Large Segmented Mirrors

The development of large segmented mirrors and their supporting structures will enable astronomy to build telescopes of ever-increasing sizes that can advance both exoplanet and general astrophysics science, beginning with JWST. Technical challenges specific to segmented mirrors involve segment-to-segment rigid body motion (i.e., tip/tilt and piston). The impact of diffraction from segment gaps has been explored in coronagraph modeling and lab demonstrations (see e.g. [18]), though edge roll-off of mirror segments remains as an area needed further investigation.

Because independent mirror segments must be controlled to maintain them operating collectively as a single phased telescope, additional stability considerations relates this technology closely to the Coronagraph Contrast Stability gap discussed above in Sect. 2.2.

Current State-of-the-Art

JWST is state-of-the-art for segmented telescopes in space. Its primary aperture is 6.5 m in diameter composed of 18 gold-coated beryllium segments, each 1.32 m tip-to-tip. Working in the near- to mid-infrared, the telescope operates at a temperature below 50 K.

Mirror subtrate materials more suitable for operating in the UV/Vis/NIR bands rather than the near- and mid-infrared may include ULE glass, Zerodur, or silicon carbide (SiC).

Recent Progress

The successful deployment and telescope phasing of JWST in 2022 demonstrated the feasibility of on-orbit deployment and phasing of 18 mirror segments to achieve a telescope operating at the diffraction limit at a 1.1 μm wavelength [92], achieving better than 100 nm RMS wavefront error at the NIRCam focus [93].

The LUVOIR design study team explored the scientific benefits and technology needs of future large segmented primary mirrors, providing detailed studies of two telescope architectures operating at shorter wavelengths. The team considered both an on-axis (LUVOIR-A) and an off-axis (LUVOIR-B) architecture. Architecture A used 120 ULE glass hexagonally-shaped segments (1.223 m flat-to-flat) and architecture B used 55 segments (0.955 m flat to flat). The segments included no radius-of-curvature actuation. The segments are based on technology demonstrated by the Advanced Mirror Segment Demonstrator project [94]. Each segment was connected to a composite backplane structure with a thermal control system calable of 1 mK control (similar to that considered for Advanced Technology Large-Aperture Space Telescope (ATLAST) [95]). The interim report does consider the benefits of highly actuated, silicon carbide segments and considers this approach to be a viable backup alternative, though with less heritage than ULE glass.

The in-Space Assembled Telescope (iSAT) study considered possible cost and risk advantages of a robotically assembled segmented space telescope [96], which can also be considered in architecture trades by a Future Great Observatory, as can opportunities for on-orbit servicing (refueling and instrument replacement).

Next Steps

By operating at a warmer temperature than JWST, because of its focus on UV to near-infrared observations, a Future Great Observatory will use materials other than beryllium for its optical components and structure. These include ULE glass, Zerodur, and silicon carbide with a nanolaminate coating, which have demonstrated better than 5 nm RMS SFE on 1 meter-class segments.

Ultimately, maturing this technology at the level required for exo-Earth direct imaging will require building and testing multiple segments together. This will require demonstrating relative phasing, integrated thermal control, and surface figure actuation as needed. The LUVOIR final report [5] includes a technology roadmap for the telescope system that can act as a starting point.

Alternative Telescope Designs

Alternative space telescope architectures have been proposed and may provide useful considerations for future mission architecture teams. These include a telescope based around lightweight refractive optics [98]. A large rectangular-shaped primary mirror that can form an synthetic aperture in software post-processing by combining observations at multiple roll angles [97] (Fig. 2.9) is a concept that may be well-suited to the mid-IR [99]. Alternatives to hexagonal segments have been proposed to reduce or eliminate the periodic layout's sharp grating lobes in the telescope's point-spread function [100], which may assist a coronagraph's wavefront control. Nulling interferometry is another approach to achieving high angular resolution, though NASA is not currently pursuing it (see Sect. 6.3).

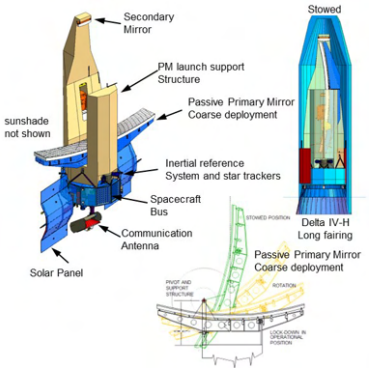

Figure 2.9: A schematic of the Rotating Synthetic Aperture telescope concept; reproduced from Fig. 13 of [97].

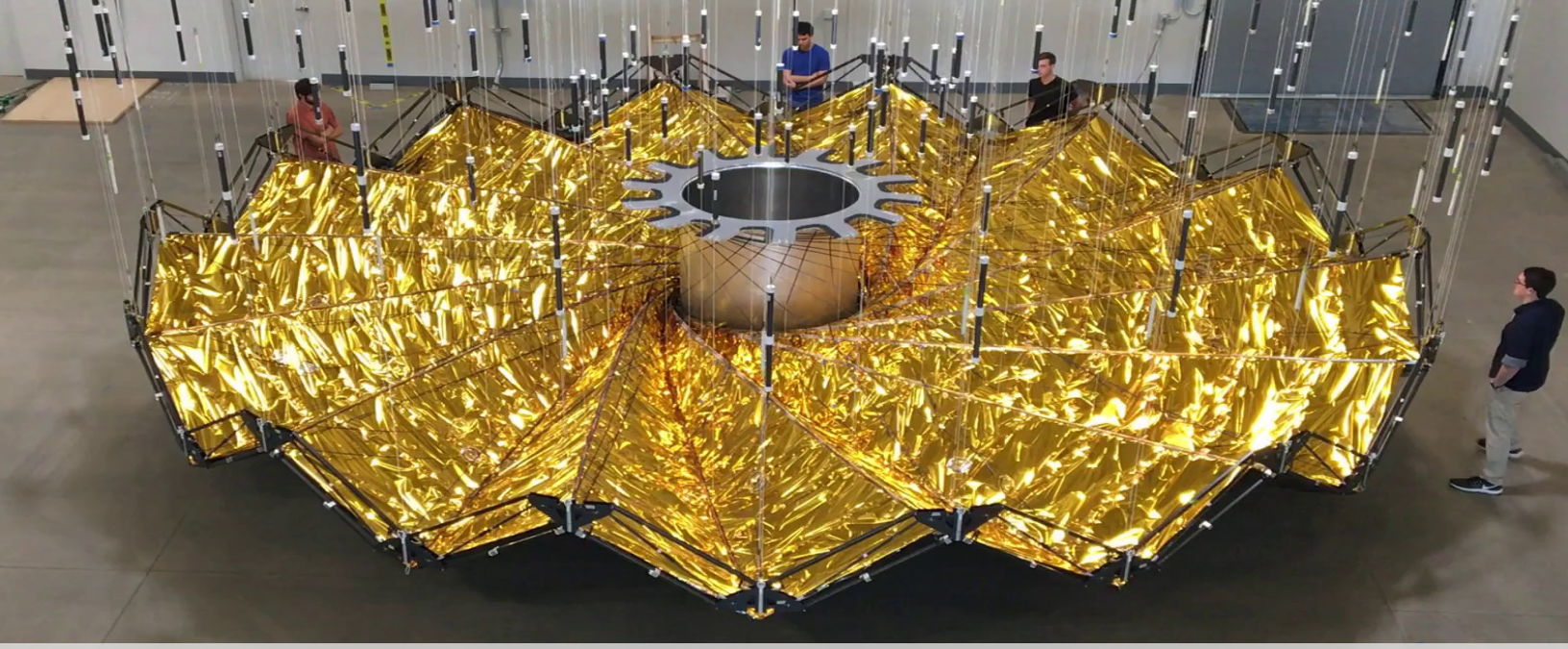

3 Starshade Technology Gaps

An external occulter, or a starshade, is a technology that performs starlight suppression with a structure deployed on a spacecraft at a distance from the telescope so that minimal on-axis starlight reaches the entrance pupil, while off-axis planet light passes the occulter. The starshade structure is designed to avoid an Arago spot with petal-shaped structures that redirect diffracted light away from the telescope. Depending on the size of the telescope and wavelength range, this typically requires the starshade to be tens of meters in diameter and positioned tens of thousands of kilometers from the telescope (Fig. 3.1). To position the shadow on the telescope, the two spacecraft must maintain formation and the starshade petals must hold the correct shape to produce the desired reduction in starlight relative to the light reflected by the planet. It must also be opaque and limit the amount of sunlight scattered from the petal edges into the telescope.

Among other benefits, missions using starshades to perform starlight suppression have relaxed telescope wavefront error stability requirements as compared to those using coronagraphy [102], albeit with the added complexity of launching and deploying a second spacecraft and operating

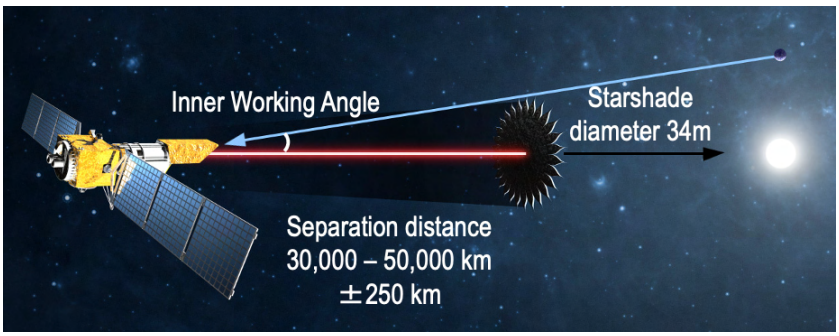

Figure 3.1: Notional configuration of a starshade and a space telescope to image Earth-like exoplanets [101]. An animation of the on-orbit separation and deployment of a co-launched starshade and space telescope can be found at https://exoplanets.nasa.gov/resources/1015/

it in tandem with a space telescope. Another benefit is that the starshade's inner working angle is only an indirect function of wavelength - potentially enabling much broader band survey's of nearby habitable zones.

Several mission concepts have considered starshades. Of particular note are: Exo-S, Roman Rendezvous, and HabEx. Three technology gaps must be closed to enable a starshade operating with a space telescope. One of these - Formation Sensing and Control (see Sect. 3.2) - was formally closed in January 2019, having achieved TRL 5 for the requirements of a Roman rendezvous mission. While no longer formally on the APD Technology Gap List, this capability is described here because further evaluation may be needed to determine whether the gap remains closed for the Habitable Worlds Observatory with a ~6 m primary mirror.

The two remaining technology gaps: 1. Starshade Starlight Suppression and Model Valdiation; and 2. Deployment Accuracy and Shape Stability are described in Sections 3.1 and 3.3 respectively.

The Starshade Technology Development Activity [103], also known as S5, was stood up by NASA in 2016 to develop starshade technology[1]. Their Starshade Technology Development Plan [104], adopted in 2018, defined a plan to advance five technologies to close the three technology gaps by 2023, with a series of series of milestones to track progress.

1: https://exoplanets.nasa.gov/exep/technology/starshade/

In 2022, NASA made the decision to transition starshade technology investments from the directed approach to a competed approach. In doing so, future funding for S5 is ceased, and SAT-2022 allows proposals for starshade technology. Several facilities developed by S5 are now available to proposers to SAT[2].

2: Appendix B lists details of facilities available to SAT and how to access them.

At this stage, the accomplishments of S5 have matured starshade technology enough that starshade technology is a viable option for consideration in architecture trades in preparation for the Habitable Worlds Observatory. In particular, unique to starlight suppression techniques, subscale laboratory demonstrations have already achieved the overall performance goal of better than 10^{-10} in broadband over a range of working angles needed for a future great observatory.

The number of targets that can be observed using a starshade is ultimately limited by the on-board fuel needed to reposition the starshade; thus, starshades could also benefit from on-orbit servicing capabilities that could extend the fuel lifetime of the starshade.

While most starshade mission concepts operate in tandem with a space telescope, concepts for a starshade in low-Earth orbit, enabling starlight suppression for a ground-based observatory, are being explored [105, 106]. The technology gaps needed for such a mission may be different from those considered here which are aligned towards the needs of a flagship space telescope mission with capabilities for exoplanet direct imaging and characterization.

MS #	Milestone	Report Completion Date	Exo-TAC Confirm by Decadal	% Risk Retired by Decadal
1A	Small-scale starshade mask in the Princeton Testbed demonstrates $1x10^{-10}$ instrument contrast at the inner working angle in narrow band visible light and Fresnel number ≤ 15.	1/28/19	X	100
1B	Small-scale starshade mask in the Princeton Testbed demonstrates $1x10^{-10}$ instrument contrast at the inner working angle at multiple wavelengths spanning $\geq 10\%$ bandpass at the Fresnel number ≤ 15 at the longest wavelength.	3/30/19	X	100
2	Small-scale starshade masks in the Princeton Testbed validate contrast vs. shape model to within 25% accuracy for induced contrast between 10^{-9} and 10^{-8}.	1/15/20	X	100
3	Optical edge segments demonstrate scatter performance consistent with solar glint lobes fainter than visual magnitude 25 after relevant thermal and deploy cycles.	11/1/19	X	100
4	Starshade Lateral Alignment Testbed validates sensor model by demonstrating lateral offset position accuracy to flight equivalent of $\pm$ 30 cm. Control system simulation using validated sensor model demonstrates on-orbit lateral position control to within $\pm$ 1 m.	11/14/18	X	100
5A	Petal subsystem with *shape critical features* demonstrates shape stability after deploy cycles (deployed) consistent with a total pre-launch shape accuracy within $\pm$ 70 µm.	12/20/19	X	80
5B	Petal subsystem with *all features* demonstrates total pre-launch shape accuracy (manufacture, deploy cycles, thermal cycles deployed, and storage) to within $\pm$ 70 µm.	6/2/23		
6A	Petal subsystem with *shape critical features* demonstrates on-orbit thermal stability within $\pm$ 80 µm by analysis using a validated model of critical dimension vs. temperature.	12/20/19	X	80
6B	Petal subsystem all *features* demonstrates on-orbit thermal stability within $\pm$ 80 µm by analysis using a validated model of critical dimension vs. temperature.	6/2/23		
7A	Truss Bay *longeron and node subassemblies* demonstrate dimensional stability with thermal cycles (deployed) consistent with a total pre-launch petal position accuracy within $\pm$ 300 µm. (Note: SBIR funding dependency)	12/20/19	X	80
7B	Truss Bay *assembly* demonstrates dimensional stability with thermal cycles (deployed) and storage consistent with a total pre-launch petal position accuracy within $\pm$ 300 µm.	6/2/23		
7C	Inner Disk Subsystem with optical shield assembly that includes *deployment critical features* demonstrates repeatable accuracy consistent with a total pre-launch petal position accuracy within $\pm$ 300 µm. (Note: SBIR funding dependency)	12/20/19	X	80
7D	Inner Disk Subsystem with optical shield assembly that includes *all features* demonstrates repeatable accuracy consistent with a total pre-launch petal position accuracy within $\pm$ 300 µm.	6/2/23		
8A	Truss Bay *longeron and node subassemblies* demonstrate on-orbit thermal stability within $\pm$ 200 µm by analysis using a validated model of critical dimension vs. temperature.	12/20/19	X	80
8B	Truss Bay *assembly* demonstrates on-orbit thermal stability within $\pm$ 200 µm by analysis using a validated model of critical dimension vs. temperature.	6/2/23		

Figure 3.2: Summary of S5 Milestones, reproduced from the Starshade to TRL5 (S5) Technology Development Plan. As of mid-2022, ten of the fifteen milestones have been achieved; only all higher-fidelity mechanical deployment milestones (5B, 6B, 7B, 7D, and 8B) remain open.

3.1 Starlight Suppression

The primary goal of the starshade optical edges is to provide the correct apodization function to suppress starlight to levels sufficient for exoplanet direct imaging. However, in order to do so, light emanating from sources other than the target star must also be taken into consideration as this has the potential to significantly degrade the image contrast. Of greatest importance is light from our Sun reflecting off the optical edges and entering the telescope. This solar glint appears primarily as two lobes, originating from a few petals oriented with edges broadside to the Sun. The overall intensity of scattered light must be limited to low enough levels (typically below the noise floor set by the exozodiacal background) that measurement integration times are not significantly impacted. A detailed imaging noise budget can be found in [107].

To demonstrate pre-launch that a full-scale starshade achieves $\leq 10^{-10}$ contrast is unfeasible; the Fresnel number of the starshade/telescope configuration (8–20) demands separation distances larger than the diameter of the Earth. Sub-scale flight demonstrations, along with model validation,

at a flight-like Fresnel number are thus carried out along with other sub-scale tests to validate an error budget.

To close the Starshade Starlight Suppression and Model Validation technology gap, subscale demonstrations of a starshade (Sect. 3.1.1) must show agreement with model predictions, and demonstrations of petal edges (Sect. 3.1.2) must be carried out.

Technology Gap: Starshade Starlight Suppression and Model Validation

The capability of a starshade to suppress diffracted on-axis starlight and scattered off-axis Sunlight to levels needed to characterize Earth-like exoplanets. The capability to experimentally validate model of the starshade's optical performance at subscale.

- **Need:** Experimentally validate at flight-like Fresnel numbers (F) the equations that predict starshade starlight contrast: total starlight contrast $\leq 10^{-10}$ in a scaled flight-like geometry, F between 5 and 40, across a broad UV/optical/IR bandpass. Contrast model accuracy validated to better than 25%.
  Limit edge-scattered sunlight and diffracted starlight with optical petal edges that simultaneously meet scatter requirements and in-plane shape tolerances. Limit solar scatter lobe brightness to better than visual magnitude (V) ~26.
  Performance goals are under re-evaluation for the Habitable Worlds Observatory.
- **State-of-the-Art:** 10^{-10} contrast at inner working angle demonstrated over 10% bandpass using 24 mm starshade in Princeton testbed with F = 13. Validated optical model with demonstrated 10^{-6} suppression at white light, 58 cm mask, and F = 210. Optical model validated to within a factor 2 at 10^{-8} contrast at F=13.
  Etched amorphous metal edges with anti-reflection coating meet scatter specs with margin; integrated in-plane shape tolerance is to be demonstrated.

3.1.1 Starlight Suppression and Model Validation

Several experiments over the last decade demonstrate the viability of creating a dark shadow with a starshade to contrasts better than 10^{-10} just outside the petal edge. Legacy laboratory demonstrations took place at the University of Colorado [109, 110], Northrup Grumman [111, 112], the McMath Pierce solar observatory [113], and in a dry lakebed [114]. The S5 project focused on demonstrations at the Frick testbed at Princeton [115], which provided a flight-like Fresnel number in a stable environment. In the Frick testbed, the testbed tube was 80 m long, with a 1 cm diameter starshade.

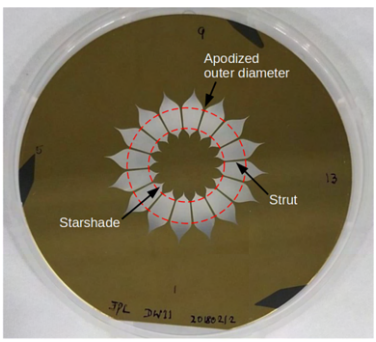

Figure 3.3: Subscale starshade used for the S5 contrast demonstrations; reproduced from Figure 4 of [108]

The S5 Activity set out two milestones (1A and 1B) aiming to demonstrate, with a sub-scale starshade in a flight-like configuration, better than 10^{-10} contrast at the inner working angle, first in narrow-band then in broadband ($\Delta\lambda/\lambda = 10\%$) visible-band light, for a Fresnel number ≤ 15 (at the longest wavelength). A third Milestone (2) uses the same testbed to measure the

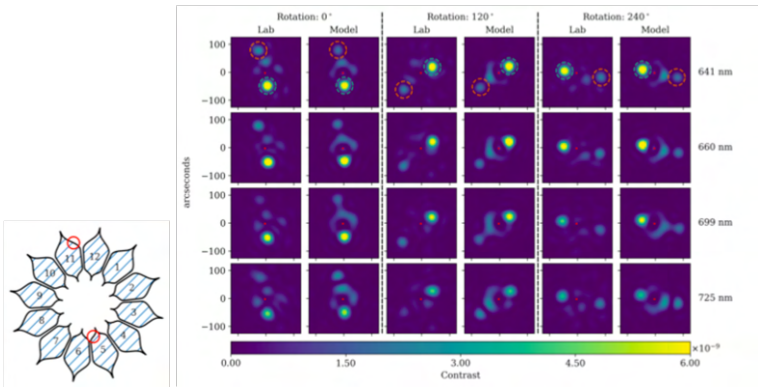

Figure 3.4: Comparison of diffraction models of starshades and laboratory measurements (right) of deliberate shape perturbations introduced in a subscale starshade.(left) [118].

performance of a set of sub-scale starshades with deliberately introduced defects with the goal of showing that the diffraction models agree with measurement to within 25% or 100%, for shape perturbations and petal position perturbations, respectively.

Current State-of-the-Art

Milestones 1A and 1B demonstrated high contrast ($\leq 10^{-10}$) at flight-like Fresnel numbers on a subscale starshade in both monochromatic and broadband light in the Frick testbed at Princeton [116, 117]. The demonstrations across a 10% band centered on 660 nm had a noise floor of 2×10^{-11} [108], exceeding all other laboratory high contrast demonstrations in depth (including coronagraph demonstrations), and showing agreement with optical diffraction models to better than 35%.

Recent Progress

The Milestones 1A and 1B demonstrations on average achieved the contrast needed for exo-Earth direct imaging and characterization, but two brighter lobes appeared that are not predicted by scalar diffraction theory. These have been traced to polarization effects related to the narrow valleys in between the petals; the petal gaps are only several wavelengths wide and behave similarly to waveguides. A vector diffraction model of this effect shows that when scaled to a flight-like geometry, where the narrow valleys are no longer similar in scale to the wavelength of light, the lobes will be reduced by a factor 10^6 (see Appendix B of [108]).

Tests for Milestone 2, validating models against testbed measurements of deliberately misshapen subscale starshades (Fig. 3.4), have been accomplished [119]. The results demonstrated agreement to within 25% of shape perturbations and 100% for petal position perturbations. A Milestone Final Report passed a review by the ExoTAC in October 2022 [118].

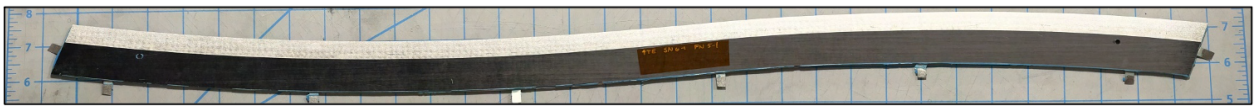

Figure 3.5: Starshade edge 75 cm test article.

Next Steps

In principle since the diffraction models are scalable to any physical dimensions with the same Fresnel number, changes in the diameter of the telescope or starshade for Habitable Worlds Observatory will not have a strong impact on the applicibility of the validated models.

While the starlight suppression and polarization lobes are well-described by a vector diffraction model, a future starshade technology effort may wish to reduce risk by demonstrating in a scaled up testbed in order to show that the effects scale as predicted and will indeed not be relevant in a flight mission[3].

3: Note that in order to maintain flight-like Fresnel number, testbed sizes scale linearly with the starshade size: a 1 m diameter starshade would requre a 8 km-long testbed.

3.1.2 Controlling Scattered Sunlight

The starshade requires an optical edge that can (1) be integrated to the petal's structural edge, (2) meet and maintain precision in-plane shape requirements after deployment and over a broad thermal environment, and (3) limit the intensity of solar glint to acceptable levels. Based on analyses for an Exo-S petal architecture it was determined that the optical edges should have a sharp beveled edge and/or low reflectivity to meet the requirement on solar glint. A guideline resulting from the Exo-S study [120] is that the product of edge radius and reflectivity should be less than or equal to 12 μm-%, while at the same time maintaining a stable in-plane shape, limiting thermal deformation of the petal and accommodating any stowed bending strain (some mechanical deployment architectures may not have bending strain issues).

The scatter of sunlight from the petal edges into the space telescope will create two bright lobes (referred to as solar glint lobes) which must be dim enough that they can be measured and removed from observations without contributing significant noise.

Previous investigations explored a wide variety of materials and coatings to act as a petal edge, but the approach taken by the S5 project to address the issue was to manufacture petal edges from uncoated amorphous metals, which provide very sharp (radius of curvature $< 0.5\mu$m) and stable edges that can be manufactured in meter-class segments [121, 122].

Current State-of-the-Art

Edge scatter performance was demonstrated in the S5 Milestone #3 report [123]. A custom scatterometer (Fig. 3.7) was used to measure reflectivity of an amorphous metal petal edge (Fig. 3.5) manufactured in the shape needed

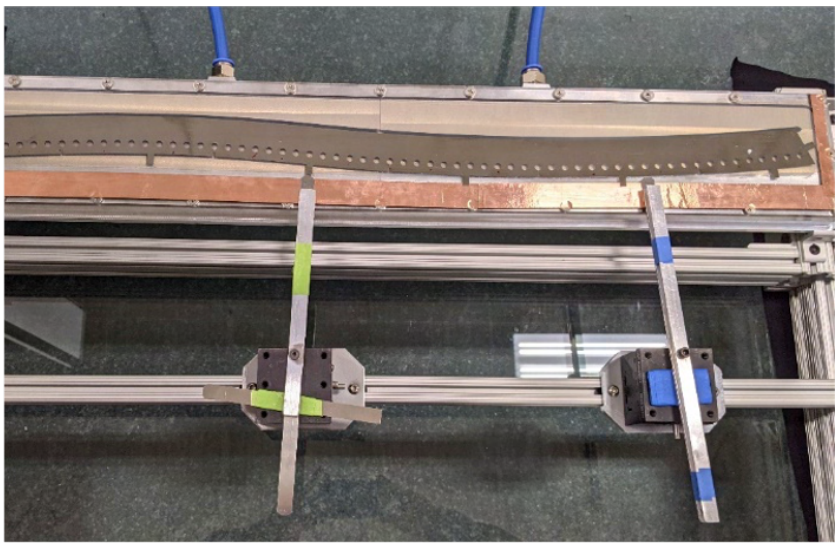

Figure 3.6: Starshade edge shape adjustment fixture.

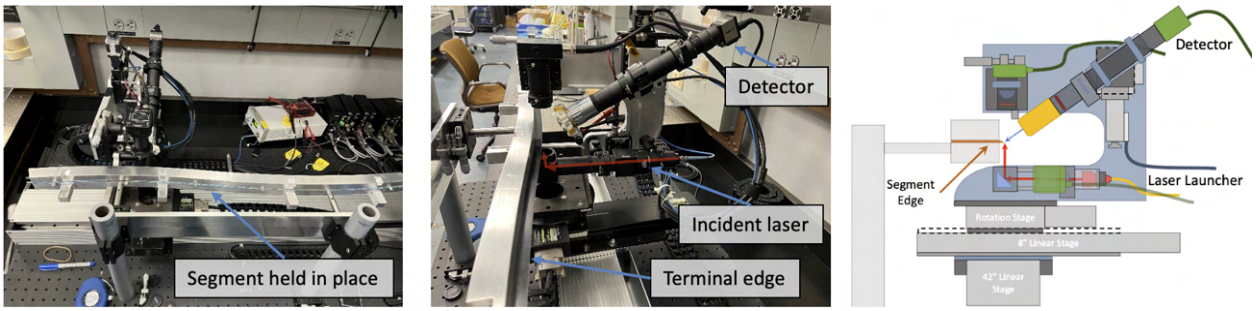

Figure 3.7: Starshade edge scatterometer, designed to measure the scatter of a petal edge segment as a function of wavelength and position along the segment at a fixed angle. Left panel shows the edge segment held in place in the apparatus. The center panel shows the orthogonal view. The right panel is a diagram showing the orientation of the laser, the detector and the translation stages.

for a petal (Fig. 3.6) and showed that it traced to solar glint requirements [124].

Recent Progress

While the uncoated amorphous metal petal edges meet requirements, a thin coating process by ZeCoat can provide another factor 20 in glint reduction, providing further margin [125].

Next Steps

The performance needed to close the technology gap is written in terms of an equivalent surface brightness of solar glint lobes and their brightness with respect to exozodiacal background; future missions with larger apertures may need to revisit the requirement based on the aperture size of the telescope.

3.2 Formation Sensing and Control

Maintaining precise alignment of the telescope, starshade, and target star is imperative to achieving the science goals of an exo-Earth-finding mission as the starlight suppression function rapidly degrades as a starshade and space telescope moves radially out of alignment. A starshade spacecraft must control its lateral position to within about ±1 m of the telescope boresight to keep the telescope in the darkest shadow. The challenge for the mission is in sensing the misalignment (to around ±30 cm). The control aspect is not particularly challenging, especially in the benign gradients of Earth-Sun L2 or in an Earth-trailing orbit; better than 10 cm-level-control is regularly achieved in low Earth orbit for rendezvous and docking.

The approach taken by S5 to is to use a pupil-plane camera operating at a wavelength where the starshade apodization function no longer fully suppresses, but a spot of Arago is detectable at a reasonable signal-to-noise ratio[4]. Based on this concept, a sensing and control system was devised for the Roman rendezvous mission and demonstrated with subscale laboratory measurements [126, 127]. Other subscale tests have also demonstrated a similar pupil-plane sensing scheme simultaneous with high contrast focal plane measurements [128].

4: See https://exoplanets.nasa.gov/resources/2186 for an animation of a simulation of the pupil-plane lateral sensing concept.

This technology gap formally closed with S5 Milestone # 4 [129] and is no longer included on the Astrophysics Technology Gap List.

Next Steps

In principle, the approach taken by S5 to the formation sensing and control problem is applicable to any mission in an L2 halo orbit, including the ~6 m Habitable Worlds Observatory mission recommended by Astro2020. Further work or architecture studies should investigate whether to keep the gap closed or if new mission requirements suggest further work in this area. A recent study of several operations concepts and sensing/control architectures can be found in [130].

3.3 Deployment Accuracy and Shape Stability

To function as an occulter and casting a dark shadow on the formation-flying telescope, the starshade must accurately deploy to, and maintain the correct shape. There are two technologies that must be matured in order to close this gap. First, the petals must meet the in-plane shape and maintain that shape stably over the full range of operational environments. Second, Petal Positioning and Opaque Structure is the technology needed to deploy petals from their stowed launch configuration to within the required tolerances and maintain that position with an opaque barrier to starlight.

The starshade mechanical architecture chosen by S5 is described in detail in [131]. The concept relies on designs for deployable structures that have

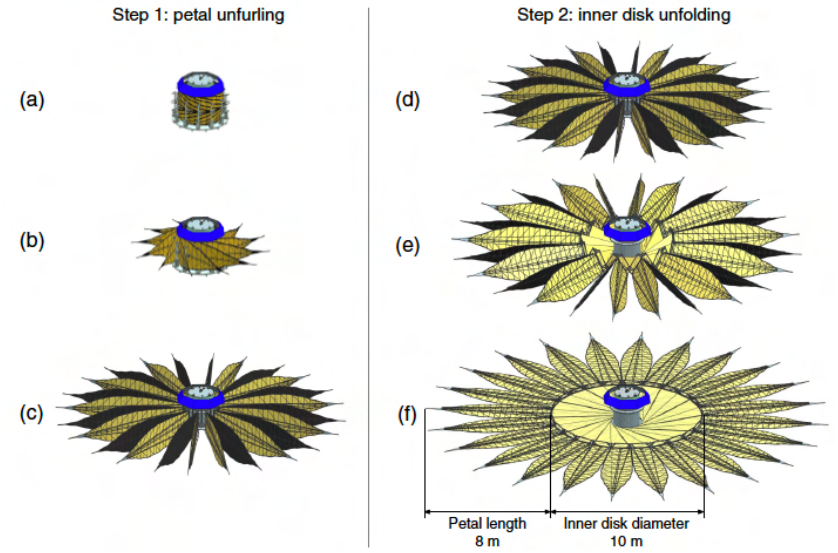

Figure 3.8: The concept for deploying a starshade from a stowed configuration adopted by the Starshade Technology Activity - Figure 1 of [131]. See `https://exoplanets.nasa.gov/resources/2185/starshade-deployment-animation/` for an animation of this deployment concept.

flown in multiple space missions, in particular the peremiter truss of the Astromesh antenna [132]. A perimeter truss is used for the deployment of the starshade's opaque inner disk; it consists of a ring of truss bays connected by hinges that rotate from stowed vertical positions to locked horizontal deployed positions. Each truss bay has a flexible petal attached to it; at launch, all of the petals are wrapped around the stowed truss bays (See Fig. 3.8 for an illustration of the deployment process).

To close the two technology gaps, the S5 Technology Development Plan defined ten milestones related to the Deployment Accuracy and Shape Stability technology gap (Milestones 5A to 8B in Fig. 3.2). The series of milestones are based on demonstrating performance and stability of key petal and inner disk sub-assemblies at increasing levels of integration. The design aimed for a 26 m starshade with 8 m-long petals and a 10 m-diameter inner disk. The HabEx mission concept included a starshade twice as large (52 m diameter), and it was determined that the S5 work was also directly relevant to this design [103].

Five of the ten mechanical milestones have been completed as of this writing with no showstoppers identified. Though the technology gap remains open, the risk to a future starshade has been greatly reduced.

If the Habitable Worlds Observatory requires a signficantly larger starshade, the mechanical architecture should be revisited to determine whether it is still applicable or whether the technology gap needs revision. Preliminary considerations for a 6-m space telescope point towards a starshade with a total diameter of 55-70 m, with petals and inner disk sizes in-family with the current prototyping work.

Technology Gap: Starshade Deployment Accuracy and Shape Stability

The capability to deploy on-orbit a starshade that is stowed in a launch vehicle fairing to a precise shape, and to maintain that shape precision during all operational environments.

- **Need:** A system that will deploy the petals from a launch-stowed configuration to the needed shape (to better than ≤ 1 mm (in-plane envelope) and maintain petal edges to ≤ 100 micron (in-plane tolerance profile for a 7 m petal on a 34 m-diameter starshade; tolerances scale roughly linearly with starshade diameter), and be optically opaque.
  Performance goals are under re-evaluation for the Habitable Worlds Observatory. Overall starshade diameter likely to be > 50m.
- **State-of-the-Art:** Manufacturing tolerance (≤ 100 μm) verified with low fidelity 6 m prototype. Petal deployment tests conducted to demonstrate rib actuation.
  Petal deployment tolerance (≤ 1 mm) verified with low fidelity 12 m prototype; limited environmental testing.

3.3.1 Petal Shape and Stability

This technology is the mechanical realization of the starlight apodization function needed to carry out the starlight suppression; it consists of petals that achieve the required shape and can stably maintain that shape over the range of thermal and strain environments that the starshade will experience.

Current State-of-the-Art

A low-fidelity 6 m prototype petal has been shown to meet manufacturing tolerances < 100 μm. Furl/unfurl and limited thermal testing has demonstrated stability.

Recent Progress

Shape measurements of a full-scale petal prototype validated that critical shape features are accurate to within requirements (Milestone #5a [133]) and maintained stability of the petal shape after experiencing stow and unfurl cycles; additional details can be found in [131] (See Fig. 3.9).

In parallel, on-orbit thermal stability requirements were demonstrated with thermal cycling tests and supporting thermal and mechanical modeling (Milestone #6a [134]).

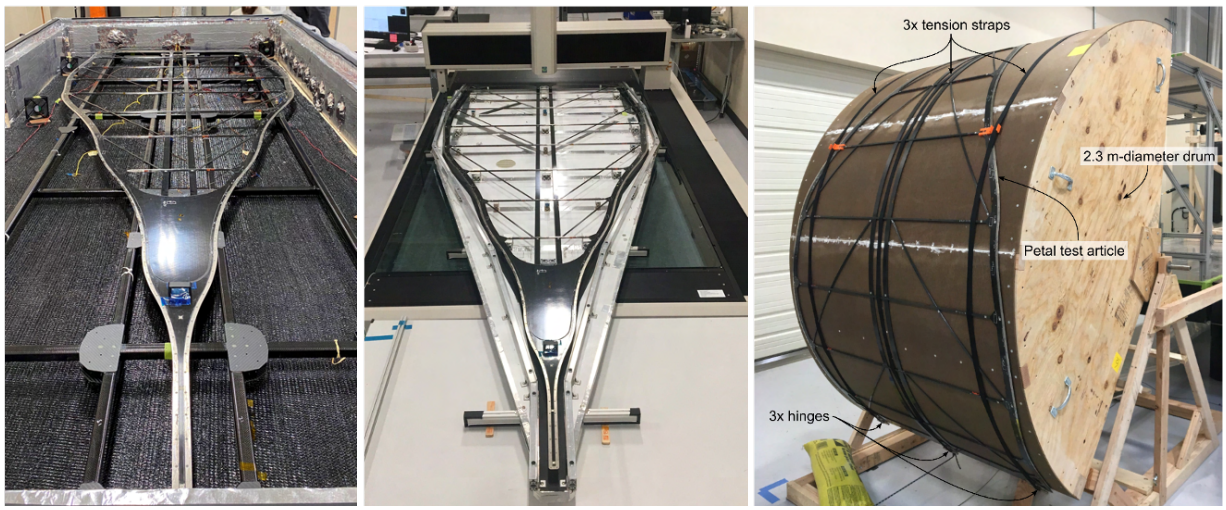

Figure 3.9: Full-scale starshade petal test article in thermal testbed (left), metrology testbed (center), and stow/deploy test jig (right).

Next Steps

Two milestones relevant to petal shape and stability remain to be achieved. Milestone 5B and 6B will repeat the measurements of petal stability to stow/deploy and thermal cycles with a higher fidelity petal subsystem at 3/4 scale that includes all features, including the optical edges. As starshade funding from APD transitions from directed to competed, a new strategy for completing the remaining milestones is under development.

As mission architectures are considered for the Habitable Worlds Observatory, the mechanical design of a potential starshade will need to be revisited to determine whether performance goals are still relevant. In the current design, shape and stability tolerances scale roughly linearly with starshade dimension, and thus become more relaxed at larger sizes. At some point the limits of launch vehicle fairings may be reached and different mechanical designs may need to be considered.

3.3.2 Petal Positioning Accuracy and Opaque Structure

This technology provides the capability of the inner disk assembly to deploy the petals to their correct locations at the outer edge of the starshade within relatively tight tolerances. It also maintains an opaque central disk to block the on-axis starlight.

Current State-of-the-Art

A low-fidelity inner disk has been shown to meet mm-scale shape tolerances after deployment with limited environmental testing.

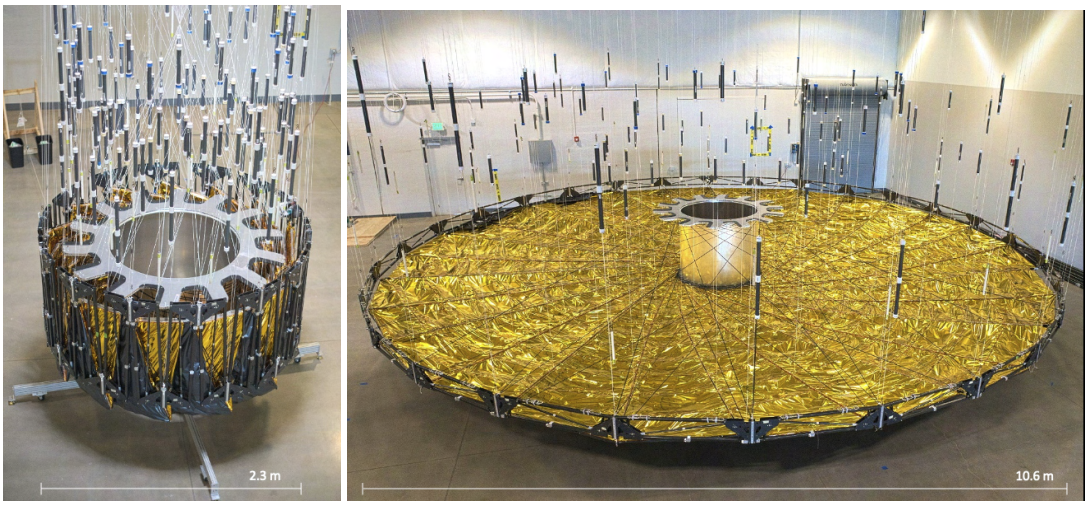

Figure 3.10: Starshade Inner Disk full-scale(10 m diameter) prototype in stowed (left) and deployed (right) configurations. See https://exoplanets.nasa.gov/resources/2218/10m-starshade-inner-disk-deployment/ for a video of the autonomous deployment of this prototype.

Recent Progress

Three mechanical milestones have been achieved. First, critical features of the inner disk deployment were tested. The dimensional stability of a truss bay longeron and node subassembly prototype after thermal cycles was demonstrated to be stable to within 300 μm after repeated thermal cycling [135]. A thermal model, validated against measurements, demonstrated the truss bay will be thermally stable to within 200 μm on-orbit [136]. Together, these give confidence that the petals will be correctly positioned as the ring of truss bays deploys.

Finally, a full scale 10-meter inner disc subsystem prototype that includes deployment critical features will be shown to deploy within 300 μm [137] (See Fig. 3.10).

Next Steps

The three completed milestones have successfully demonstrated the riskiest portions of the deployment architecture but three milestones relevant to deployment remain to be achieved (7B, 7D, and 8B). As starshade funding from APD transitions from directed to competed, a new strategy for achieving the goals of the remaining milestones is under consideration.

As mission architectures are considered for theHabitable Worlds Observatory, the mechanical design of a potential starshade will need to be revisited to determine whether the existing performance goals are still relevant. In the current design, shape and positioning tolerances scale roughly linearly with starshade dimension, and thus become more relaxed at larger sizes. However, at some point the limits of launch vehicle fairings may be reached and different mechanical designs may need to be considered.

The starshade's opaque inner disk is currently made robust to micrometeroid pinholes by fabricating it from multiple layers of black Kapton separated by a spacer material, such as open cell foam. If the JWST mission makes discovies about the micrometeroid environment at L2, this design may need additional scrutiny.

A NASA Small Business Innovation Research (SBIR) awarded to ZeCoat will investigate a black coating applied to a membrane that may improve the optical performance of the inner disk.

4 Detection Sensitivity Technology Gaps

Another capability required for exo-Earth direct imaging is detection sensitivity across the wavelength band of interest. With single aperture telescopes, the science goals of measuring spectral features of biomarkers like O_3, CO_2, CH_4, and H_2O, while also maintaining telescope angular resolution ($\sim \lambda/D$) capable of resolving habitable zones is likely to drive future missions to observe in the ultraviolet, visible, and near infrared. Earth-like exoplanets orbiting Solar-type stars are dim sources (magnitude 30 or dimmer) that even with large telescopes, integration times are likely to be on the order of hours. Consequently, the detectors for both imaging and spectroscopy behind a starshade or a coronagraph must be highly sensitive, have ultra-low noise, and must be radiation hardened to operate in space with a service lifetime of >5 years (Goal lifetime >10 years). In addition, the need for low spectral-crosstalk spectroscopy and large outer working angles to study stellar disks and exoplanets at greater angular separation may lead to the requirement for larger detector format: 2k×2k pixels or larger.

Two technology gaps track this sensitivity need: Vis/NIR Detection Sensitivity (Sec. 4.1), and UV Detection Sensitivity (Sec. 4.2). There is overlap between the two Gaps - the boundaries of the wavelength regimes are flexible and some technologies may address both.

4.1 Vis/NIR Detection Sensitivity

Several classes of photoconducting detectors are candidates for achieving detection sensitivity goals in the wavelength range of 0.4–2 μm. Technologies based on silicon, such as Charge Coupled Device (CCD), EMCCD, and Complementary Metal Oxide Semiconductor (CMOS) offer sensitivity

This artist's concept show a massive asteroid belt in orbit around a star the same age and size as our Sun. Credit: NASA/JPL-Caltech/T. Pyle (Spitzer Science Center)

shortward of 1 μm. Several p-channel doped silicon devices are under development for astronomical applications including Skipper CCDs, and Hole-Multiplying Charge Coupled Device (HMCCD). The quantum efficiency tends to fall off steeply close to 1 μm, reducing sensitivity to the 930 nm oxygen absorption feature, though thicker (250 μm) devices have been shown to have 80% QE at 930 nm [138, 139]. P-channel Skipper CCDs were originally developed for particle physics experiments, and have demonstrated photon counting; however, to-date the devices have extremely slow read times if all pixels are required to have sub-electron read noise at all times [140]. Coupling to parallel read channels (standard for CMOS detectors) is a path to creating a practical visible-band detector for astronomical use [138]. In addition, readout software schemes could create regions-of-interest within detectors that are read out in a ultra-low-noise mode while accepting higher noise in the rest of the detector.

MCP amplifiers can enable photon-counting detectors in the visible band. Commercially available GaAs photocathodes are sensitive to wavelengths 350–850 nm and achieve very low dark current of order 0.2 counts/px/hr with modest cooling to -30°C. Similar designs are currently operating in space (UVOT on SWIFT, S20 cathode) [141].

In the near infrared, HgCdTe-CMOS hybrid detectors have been used in multiple astrophysics missions in near-Earth and L2 orbits (for example HST, WISE, JWST NIRCAM/NIRSPEC) and are part of several planned missions in the coming decade (Euclid, Roman, SPHEREx, NEOSurveyor, ARIEL/CASE). This material has a tuneable long-wavelength cutoff - typically available with cutoffs at either 2.3 μm or 5 μm (though devices with cutoffs as long as 10 μm have been matured for flight - Sect. 5.2.1). On the short wave side, these devices are typically operated to 750 nm but could be engineered for sensitivity to wavelengths as short as 400 nm. These detectors are radiation tolerant, have very low dark current ($<10^{-3}$ e$-$/s), though correlated double sample read noise is still well above 1 $e-$ and are thus far from intrinsic photon-counting.

Adding a stage of avalanche gain to each HgCdTe pixel, for example in Saphira [142] and Linear-Mode Avalache Photodiode (LMAPD) detectors, promises photon-counting in the infrared. Current challenges involve reducing multiplexer glow (which introduces spurious dark counts much like a dark current) and a tunnelling dark current which turns on at high detector bias voltages.

In addition, several types of cryogenic detectors are candidates to close this technology gap. Cryogenic superconducting detectors such as MKIDs and TESs have no read noise or dark current, eliminating the spurious count rate problem associated with non-cryogenic devices. These devices are scalable to large arrays via multiplexed readouts [143]. Transition edge sensor microcalorimeter arrays are another candidate cryogenic detectors with modest built-in energy resolution (and thus reducing need for dispersive optics) like the MKIDs. Nanowire single photon detection arrays can operate at somewhat higher cryogenic temperatures and can also support multiplexing [144]. Cryogenic detectors will require solutions for dynamic isolation, particularly from their cooler vibrations, and resolution (pixel

count). The immediate challenge will be providing near-zero-vibration cooling to maintain compatibility with coronagraph instruments (though a starshade-only space mission will have less stringent vibration requirements). While cooling is not a detector technology, future telescope architectures must minimize vibrations sources to enable the coronagraph performance to reach the dual driving instrument goals of 10^{-10} contrast ratios at $<3\ \lambda/D$. Radiation tolerance has not yet been assessed.

Technology Gap: Vis/NIR Detection Sensitivity

- **Need:** Near IR (900 nm to 2.5 μm) and visible-band (400-900 nm) extremely low noise detectors for exo-Earth spectral characterization with Integral Field Spectrographs. NIR read noise $\ll 1$ e^- RMS, dark current noise < 0.001 e^-/pix/s, Vis band read noise < 0.1 e- RMS; CIC < 3×10^{-3} e^-/px/frame; dark current $<10^{-4}$ e^-/px/sec , functioning in a space radiation environment over mission lifetime; large $\geq$ 2k×2k format
- **State-of-the-Art:** Vis: 1k×1k silicon EMCCD detectors provide dark current of 7×10^{-4} e^-/px/sec; CIC of 0.01 e^-/px/frame; zero effective read noise (in photon counting mode) after irradiation when cooled to 165.15 K (Roman); 4k×4k EMCCD fabricated but still under development NIR: HgCdTe photodiode arrays have read noise $\lesssim$2 e^- rms with multiple nondestructive reads; 2k×2k format; dark current < 0.001 e^-/s/pix; very radiation tolerant (JWST); HgCdTe APDs dark current ~10–20 e^-/s/pix, Read noise $\ll 1$ e^- RMS, and < 1k×1k format Cryogenic superconducting photon-counting detectors (MKID,TES): 0 read noise/dark current; radiation tolerance is unknown; <1k×1k format
- **Subgaps are listed in Table A.4.**

Current State-of-the-Art

The Roman coronagraph instrument will use the e2v CCD201-20 detector (1024×1024; 13×13 μm pixel pitch) for the coronagraph science camera and the LOWFS camera. The Roman team [145]. This detector was baselined as a visible-band detector by the HabEx and LUVOIR concepts, but but falls short in several ways for the Habitable Worlds Observatory Future Great Observatory. The lifetime of the detectors in the radiation environment may not be acceptable. In addition, the photon-counting mode of EMCCDs has a limited dynamic range, a fact that may need evaluation as requirements are developed.

SAT-funded demonstrations of LMAPD devices (PI: Mike Bottom, University of Hawaii) have shown that a 1k×1k device achieves 2 e- per read with a 3×10^{-3} e-/s spurious count rate, thought to be due to the onset of a tunneling current as the gain is increased[146].

Recent Progress

An ISFM-funded investigation (PI Bernie Rauscher, GSFC) has evaluated several types of p-channel-doped detectors for exoplanet characteriaztion in

the 400–1000 nm band that are likely to offer improved radiation hardness with respect to EMCCDs. An important finding is that HMCCD devices show a high risk of degradation due to the impact ionization used in the gain stage [138].

CMOS sensors in principle have intrinsically lower radiation degradation due to their single-pixel readouts. For example, Quanta Image Sensors (QIS) have been demonstrated to have photon-counting capabilities in the visible band while maintaining dynamic range [147]. These devices are being investigated for astronomical applications in space by an SAT award (PI: Don Figer, Rochester Institute of Technology; award managed by COR program office). So far the team has shown that engineering devices can achieve photon-counting performance, with high dynamic range (on order 250), simultaneously with <0.001 e-/s dark noise at a relatively warm operating temperature (258 K) [148]. The detectors have been exposed to radiation dosing and are awaiting post-exposure testing. A further advantage of QIS devices is the small pixel pitch size (on order 1μm) which can enable smaller mass and volume of optical instruments.

A charge damage analysis of six years of data from GAIA, which has 106 CCDs at a L2 orbit, showed a slight increase in charge transfer inefficiency due to radiation damage [149] but still dominated by pre-flight defects.

Saphira devices, which have a relatively small format, have been superceded by new 1k×1k LMAPD devices, also manufactured by Leonardo. The devices are close to achieving photon counting noise performance, and have been shown to have intrinsic dark current consistent with zero; however spurious dark counts due to multiplexer glow is still slightly above performance goals [146]. Multiplexer glow effects tend to be localized on the detector, again suggesting a observing and readout scheme that creates a region-of-interest.

Next Steps

The ISFM-funded work will investigate further optimizing Skipper devices for astronomical applications in coordination with Department of Energy (DOE) investments, likely by coupling with Application Specific Integrated Circuit (ASIC) for Control And Digitization of Imagers for Astronomy (ASIC) readouts developed for Roman Wide Field Instrument (WFI) [150] and carrying out further testing. An Astrophysics Research and Analysis (APRA)-2021 (PI Drlica-Wagner, U Chicago) will also advance the technology, focusing on several areas of interest to the future Habitable Worlds Observatory flagship - including radiation tolerance.

The work on QIS plans to continue testing, post-radiation exposure testing, and considering a re-design of the QIS tailored to likely requirements of an exoplanet direct imaging mission.

The SAT-funded team advancing LMAPD plans to continue with lab characterization measurements of another iteration of detectors, with new results expected in 2023. The detector will also be radiation-tested, and used on an observatory to gain experience with on-sky measurements.

An MKID camera will be tested on a future flight of the PICTURE-C balloon payload [151].

Longer-term, operating the EMCCD detectors on Roman's Coronagraph Instrument will provide lessons in using these detectors in flight operations. This will enable addressing several issues involving the photon counting mode, including tuning the exposure time to balance detected photons against the level of spurious counts (from boosted dark current and CIC noise).

4.2 UV Detection Sensitivity

Measuring broad atmospheric features in the near ultraviolet (UV) band is necessary for spectral characterization of terrestrial planets exoplanets. At wavelengths shortward of 300 nm, the reflectivity of planets with O_3 in their atmosphere (as in an Earth-like planet) is very low. The challenges of achieving coronagraph contrast and efficiency in the UV are noted in Section 2.1, but beyond the starlight suppression, but in addition, mature ultraviolet detectors are needed to perform spectroscopy on Earth-like planets. The reflected-light brightness of the target planets in the UV is typically even lower than in the Vis/NIR (due to decreasing stellar flux), and thus achieving the necessary sensitivity is likely to require photon-counting, radiation-hard detectors.

The technology gap described here describes the capabilities needed for exo-Earth spectroscopy in the 200–400 nm. Wavelengths shorter than 200 nm are not likely to benefit exoplanet science; other technology gaps describe ultraviolet detection capabilities needed for other astrophysical applications.

Technology Gap: Vis/NIR Detection Sensitivity

- **Need:** Low-noise ultraviolet (200–400 nm) detectors to characterize exoplanets with an imaging spectrograph.

  Read Noise: 0 e-; Dark Current: 0 e- /resolution/s; Spurious Count Rate: < 0.05 counts/cm^2/s; QE: 75% ; Resolution size $\leq$ 10 μm; Tolerant to space radiation environment over mission lifetime.
- **State-of-the-Art:** *Lab:* MCP: 0 read noise, 90 – 300 nm, spurious count rate 0.05 – 0.5 counts/cm^2/s; QE 20–45%; resolution element size 20 μm. EMCCD: 0 read noise, dark current < 0.005 e-/res/hr; QE 30-50%; resol. el. size 20 μm

  Flight: HST HRC: In relevant UV band (250 nm): QE 33%, read noise 4.7 e-, dark current 5.8×10^{-3}, 1024×1024 format

Current State-of-the-Art

Delta-doped EMCCD and MCP both meet all sensitivity requirements, though lifetime in the L2 radiation environment is not known. Current state-of-the-art format of 1k × 1k is acceptable.

Recent Progress

The LUVOIR mission concept's coronagraph instrument (ECLIPS) included a UV channel (200–400 nm) for both the LUVOIR-A (on-axis telescope) and LUVOIR-B (off-axis telescope) architectures. Delta-doped EMCCD detectors were baselined for the LUVOIR coronagraph instrument ECLIPS [5] and for HabEx's starshade camera [6]. Possibilities enabled by 2D delta-doping [152].

Next Steps

Future mission architecture trades should consider overall benefits and challenges of measuring UV spectra of exo-Earths, including more detailed detector requirements.

A SAT-2021 award to Shouleh Nikzad (JPL) titled "High Efficiency, UV/Optical Photon Counting Detectors" will work to develop EMCCD detectors that are delta-doped for UV sensitivity.

Radiation hardness of delta-doped EMCCDs for the near UV should be investigated. In addition, architecture trades may consider alternatives to delta-doped EMCCD detectors. CMOS detectors, such as those under consideration for the UVEX Explorer concept, are likely to present significant radiation hardness advantages as compared to EMCCD devices, though they have yet to demonstrate photon-counting capabilities [153]. Cryogenic MKID and TES detectors, which are photon-counting and energy resolving, can also potentially operate in this band.

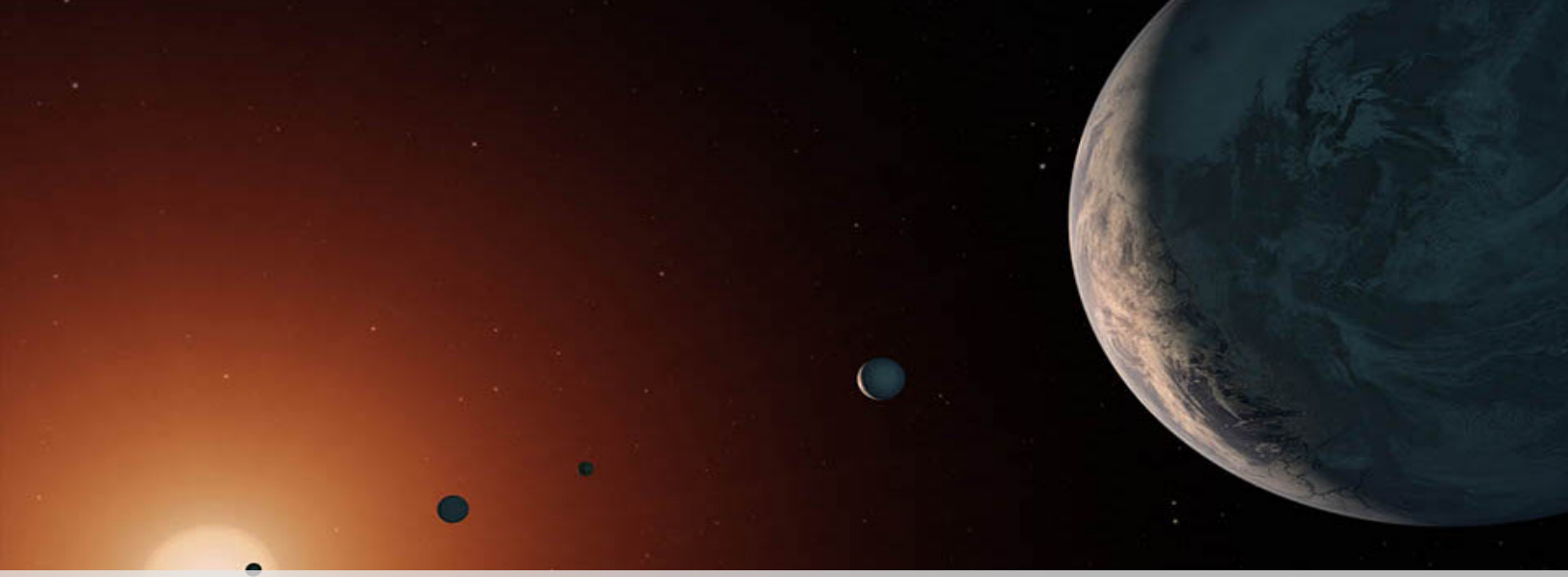

5 Other Technology Gaps

5.1 Stellar Reflex Motion Sensitivity

Interpreting spectral measurements of a planetary atmosphere requires measurement of the planet's mass, typically inferred from the reflex motion of the star due to an orbiting planet. This can be done through multi-epoch precise measurements of the angular position of the star relative to distant background stars (astrometry; Sect 5.1.2) or measurement of the Doppler shift in stellar absorption as the star moves along the line of sight (extreme precision radial velocity; Sec 5.1.1). In both techniques, improvements in technology are needed to enable mass measurements to the level of Earth-mass.

Mission architectures may consider either or both of these techniques to support the science objectives, see Table 5.1 for a comparison of the two techniques.

5.1.1 Extreme Precision Radial Velocity

Extreme Precision Radial Velocity (EPRV) techniques measure the Doppler shift in stellar absorption lines as orbiting planets cause a gravitational recoil in the star. RV is a historically important technique for discovering exoplanets, and recently was used to discover a planet orbiting our closest neighboring star, Proxima Centauri [154].

The capability to measure RV could support the Habitable Worlds Observatory in two ways: first, ground-based RV instruments could support a space mission by detecting and characterizing the masses and orbits of direct imaging targets [155]; or second, a dedicated RV instrument could

An artist's illustration depicting the TRAPPIST-1 system. Credit: NASA/JPL-Caltech/R. Hurt (IPAC).

EPRV (<9 cm/s)	**Astrometry (< 0.3 μarcsec)**
Ground-based achievement of sensitivity may be possible; advantages to observing in space	Must go to space for necessary precision
Stellar jitter mitigation must be improved by 10× at least	Astrophysical limits may be less stringent (or simply may not have been studied thoroughly)
sin(i) effects rule out many targets	No orbital inclination angle effects
Limited by photometry of target star	May be limited by photometry of reference stars
Technology tall poles: detectors, gratings, calibration (See Table A.5)	Technology tall poles (for an imaging-type mission): optical distortion calibration, detector plate scale calibration. Interferometry is another possibility.

Table 5.1: Comparison of Extreme Precision Radial Velocity and Astrometry for exoplanet mass measurement. The 9 cm/s target for RV refers to the signal for a Earth-mass planet orbiting a Solar-mass planet. The astrometry 0.3 μarcsec refers to the angular motion of a Sun-like star at 10 parsecs due to an orbiting Earth analog. The measurement noise and systematic error floor must be significantly lower than these targets to enable robust detections.

be included on a space telescope to accomplish these ends. Both paths are likely to require new technologies.

The vast majority of research and expertise in the field focuses on ground based radial velocity measurements, which typically require specialized ultra-stable and precisely calibrated wide-band stellar spectrograph instruments [156]. The recent EarthFinder Probe concept studied advantages and challenges of carrying out precision radial velocity measurements from space. Advantages include access to a broad wavelength band unaffected by residual atmospheric effects; challenges include reducing the size, mass and power of critical components, including calibration technology [157].

The NASA-NSF Exoplanet Observational Research (NN-EXPLORE) program[1] has invested in RV in three ways: developing the NEID radial velocity instrument, providing access to southern-hemisphere RV observing opportunities, and establishing an EPRV Working Group to develop a plan for a strategic EPRV initiative. The EPRV working group delivered a report in July 2021 [158], which included recommendations for advancing technology via an EPRV instrumentation testbed. As part of the 2022 gap list process, members of the working group submitted five candidate technology gaps which were accepted as sub-gaps to partially or fully close the EPRV gap (Table A.5). These were: Detectors for high-resolution, Cross-dispersed Spectrographs; High-Precision, High-Throughput, High-Spectral Resolution Dispersive Optics; Advanced Photonics for extreme-precision radial velocity spectroscopy; Ground-based Visible-light Adaptive Optics; and Precision Calibration for Extreme-Precision Radial Velocity Spectroscopy.

1: https://exoplanets.nasa.gov/exep/NNExplore/

Detectors are estimated to contribute 8.1 cm/s to the RV error budget of NEID [159] due to systematic errors in the CCD. Larger format devices (up to 8k×8k or larger) providing wider spectral coverage, result in systems that are more straightforward to calibrate. In addition, CMOS detectors may come to replace CCD as the standard astronomical detectors in the visible band.

New types of dispersive optics for a R~100,000 spectrograph with lower wavefront error, larger size, and higher efficiency may improve the RV

precision. Lithographic fabricated gratings may be a candidate technology that provide these characteristics.

Extracting science from EPRV measurements requires combining measurements taken over many years; frequency references that are stable over those time periods are needed. Traditionally laser frequency combs (Astrocombs) have been used successfully and reduce frequency calibration error well below any other term in the error budget. But devices in use at current RV facilities have proven to be massive, high-power, expensive and require periodic maintenance. Etalon-based calibration sources could be an alternative that is also potentially scalable to a flight mission.

A ground-based visible light adaptive optics system would enable the use of a single-mode fiber-fed spectrograph, vastly reducing the size and enabling greater stability of future RV instruments.

Adapting various techniques from photonics, such as "spectrographs on a chip" could also greatly simplify future RV instruments.

Technology Gap: Stellar Reflex Motion Sensitivity: Extreme Precision Radial Velocity

- **Description:** Capability to measure exoplanet masses down to Earth-mass.
- **SOA:** Ground-based RV: state-of-the-art demonstrated stability is currently 28 cm/s over 7 hours (VLT/ESPRESSO). Laser frequency combs demonstrated on ground-based observatories with correct mode spacing, non-NASA work is advancing miniaturization. Fiber laser-based optical frequency combs demonstrated on sounding rocket though with closer line spacing than useful for RV.
- **Needed capability:** Capability to measure exoplanet masses down to Earth-mass. The radial velocity semi-amplitude of a Solar-mass star due to an orbiting Earth-mass planet at 1 Astronomical Unit (AU) is 9 cm/s. Technology to make radial velocity mass measurements may include using a space-based instrument to avoid atmospheric telluric lines and simultaneous measurements of stellar lines across a broad band (both Vis and NIR). Stability of the instrument and its absolute calibration must be maintained on long time scales in order to enable the measurement.
  Theoretical understanding of astrophysical noise sources (stellar jitter) and how to mitigate them.

  Sub-gaps that could partially or fully close this gap (Table A.5):

  - Detectors for High-Resolution, Cross-dispersed Spectrographs
  - High-Precision, High-Throughput, High-Spectral Resolution Dispersive Optics
  - Advanced Photonics for Extreme-precision Radial Velocity Spectroscopy
  - Ground-based Visible-light Adaptive Optics
  - Precision Calibration for Extreme-precision Radial Velocity Spectroscopy

Current State-of-the-Art

The current generation of ground-based RV spectrographs, ESPRESSO [160], EXPRES [161], MAROON-X [162], and NEID [163], have achieved intrinsic instrumental sensitivity between 20 and 30 cm/s.

Recent Progress

The EPRV working group reported several recommendations relevant to developing technology [158], some of which entered the Technology Gap list process in the detailed descriptions of EPRV subgaps (Table A.5).

Other recommendations of the EPRV working group focus on improving understanding of the variability of the host stars by "immediately implementing a long-term, large-scale, interdisciplinary research and analysis program in this area." In response to this recommendation, NASA issued a focused call for proposals under ROSES in 2020 called Extreme Precision Radial Velocity Foundation Science, and selected eight proposals to investigate techniques to mitigate stellar variability.

The NASA/NSF-funded NEID instrument has been deployed to the WIYN 3.5 m telescope on Kitt Peak, Arizona. The NEID archive [2] contains not only publicly available processed NEID data for science targets, but 8 regularly-observed radial velocity standard stars, and solar RV data taken during the daytime [164]. The latter two types of data may be useful for investigating stellar variability effects on radial velocities.

2: https://neid.ipac.caltech.edu/search.php served by the NASA Exoplanet Science Institute (NExScI).

A project funded by an SAT award (SAT-2018 Vasisht) is developing a whispering gallery mode etalon to use as a calibration source for an EPRV spectrometer [165]. The miniaturized packaging makes it convenient for ground-based applications but also useful for a space-based RV instrument.

Next Steps

The Habitable Worlds Observatory 6 m class future great observatory may explore a variety of avenues to achieving planetary mass measurements in support of its science goals. This may include radial velocity capabilities, either ground-based, or in a specialized space instrument or separate mission. These choices are likely to set the detailed requirements in technology development.

In the meantime, following the recommendations of the EPRV report, further theoretical understanding of stellar variability and telluric atmospheric effects, taking into account results from the EPRV Foundation Science awards will evaluate the limitations of EPRV.

In the near term, more EPRV instruments at the ~30 cm/s sensitivity level will come online (for example the Keck Planet Finder instruments [166] was commissioned in November 2022), giving the community more

opportunities to study systematic errors and stellar activity at that level of sensitivity.

Additional improvements in instrumental stability and calibration will be needed beyond the current generation of RV spectrometers. The establishment of a EPRV technology testbed, another recommendation of the EPRV report, may be considered in the future.

5.1.2 Astrometry

The Exoplanet Science Strategy report [167] found that astrometry is a viable option for determining the mass of exoplanets, but considered it as a backup to extreme precision radial velocity. There are some key cases, however, such as in observing the nearest Solar-type stars, where astrometric techniques may prove superior to RV.

As multi-epoch precision astrometric measurements become more readily available from *Gaia* and VLT/GRAVITY, inference of the mass of an orbiting planet via astrometry is becoming a more common occurrence (see for example [168]). Thousands of Jupiter-mass planets are expected to be discovered in the coming decade via analysis of many epochs of *Gaia* measurements.

Due to the need for long term stability and precise calibration of systematic errors, a space-based platform is likely to be necessary for sub-micro-arcsecond measurements. These measurements could be carried out either with an instrument on a space observatory (likely requiring some form of in-situ calibration) or with a dedicated astrometry mission.

A study shows that in principle the Roman Space Telescope's WFI instrument may be capable of 10 μ-arcsec measurements using diffraction spikes [169]. LUVOIR's interim report explored the possibility of making 0.1μ-arcsecond measurements with its wide field imager (and a 15 m telescope).

Future dedicated astrometry mission concepts capable of exo-Earth detection may require new technology. Recent mission concepts such as Theia [170], Toliman [171], and Micro-Arcsecond Small Satellite (MASS) [172], have identified key technical challenges: in particular calibrating optical field distortion and the detector plate scale, both of which can vary with time and introduce systematics in the angular position measurement.

Technology Gap: Stellar Reflex Motion Sensitivity: Astrometry

- **Description:** Capability to measure exoplanet masses down to Earth-mass.
- **SOA:** *Gaia* preliminarily achieved 34 micro arcsecond error but ultimately could achieve 10 microarcseconds on bright targets after all systematics are calibrated. Demonstration of diffractive pupil showed 5.75×10^{-5} λ/D or 1.4 microarcsecond on a 4m telescope (limited by detector calibration). Preliminary study of 1-m space telescope and instrument with in-situ detector calibration can achieve 0.8 micro-arcsecond in 1 hr
- **Needed capability:** Astrometric detection of an exo-Earth at 10pc requires 0.1 microarcsecond uncertainty. Technology is needed to obtain the stability need to make astrometric measurements to this level, possibly requiring detector metrology and/or diffractive pupils. Theoretical understanding of astrophysical noise sources (star spots) and prospects for mitigating them is needed.

Current State-of-the-Art

Gaia Data Release 3 (June 2022), based on 34 months of observations, has a median 5-parameter astrometry position fit uncertainties of 10–20 μ-arcsec for stars brighter than *Gaia* magnitude 15 [173].

Ground based interferometric measurements using VLT/GRAVITY have achieved 10–100 μ-arcsec in K band (2.2 μm) [174] . This experiment was designed to measure the dynamics of the Galactic center but has been used to measure relative star-planet positions in combination with direct imaging [175].

In the lab, demonstrations of calibration of optical distortion using a diffractive pupil [171] and calibration of the detector plate scale using interference fringes [176] trace to the micro-arcsecond level.

Recent Progress

Recent mission studies continued to investigate the benefits and challenges of astrometry for planetary mass measurements beyond *Gaia*. The MASS smallsat study showed 6 μ-arcsec sensitivity per hour-long exposure is enough to achieve sensitivity to temperate Earth-mass planets for dozens of the nearest Solar-type stars [172].

An APRA-funded dedicated astrometry test bench at JPL is under construction (Fig. 5.1) and will soon demonstrate state-of-the-art optical distortion calibration with a diffractive pupil in a stable vacuum environment [177] (Fig. 5.2). Initial results have demonstrated 0.48 μas astrometric sensitivity when scaled to a Hubble-sized telescope.

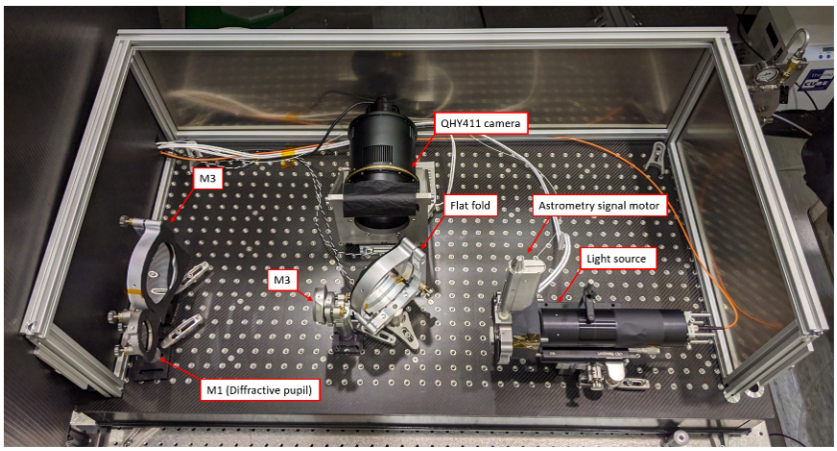

Figure 5.1: The sub-microarcsecond astrometry demo bench at JPL (PI: Eduardo Bendek, JPL; Image credit: Matt Noyes, JPL-Caltech).

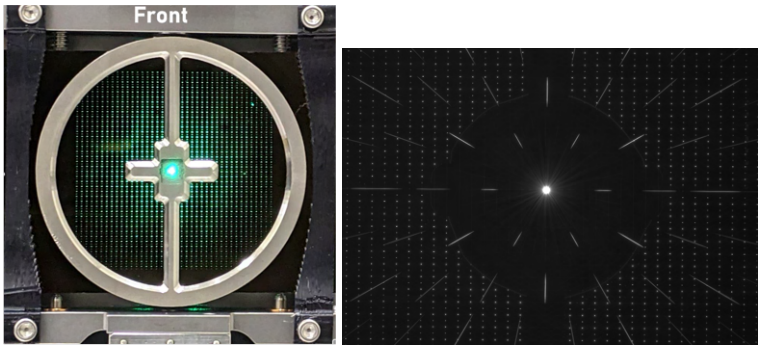

Figure 5.2: Left: A diffractive pupil to enable sub-micro-arcsecond astrometry (PI: Eduardo Bendek, JPL; Image credit: Matt Noyes, JPL-Caltech). Right: a focal plane image of a diffracted source in the astrometry demo testbed.

Next Steps

Future *Gaia* data releases are expected to include thousands of discoveries of planetary companions down to of order Jupiter-mass [178]. Data Release 4, based on 66 months of data, is scheduled to include the first release of an exoplanet catalog. In addition, a detailed assessment of *Gaia*'s systematic errors and on-orbit stability, including thermal relaxation effects and micrometeroid impacts, will be critical for designing future missions.

Given the importance of mass measurements for understanding the potential habitability of exo-Earths, the ~6 m Habitable Worlds Observatory may explore astrometric capabilities. A coronagraph starlight suppression system will require extreme telescope wavefront error stability, which may in turn provide a platform capable of excellent astrometric measurements. The diffractive pupil design may enable astrometric solutions at the sub microarcsecond level for a large mission concepts. A working group analagous to the EPRV Working Group could provide expert assessments.

While it is thought that astrometry is less susceptible to systematic errors from stellar activity than EPRV [179], an updated assessment of these effects may be important.

5.2 Transit Spectroscopy

Transit spectroscopy is an technique for characterizing the atmospheres of exoplanets. Like photometric transits, transit spectroscopy looks at the decrease in brightness of a host star as a planet crosses the line of sight to the star. By observing the transit in multiple wavelengths, spectroscopic absorption features in the atmosphere of the transiting planet can be measured. Similarly, secondary eclipse spectroscopy measures the spectrum of light emitted from a transiting planes by comparing signals during and outside of secondary eclipse, when the host star completely occults the planet. These techniques have been used historically to study the atmospheres of giant planets with HST and Spitzer data, and are now being used to study smaller planets in the mid-IR with Mid-Infrared Instrument (MIRI) on JWST [180].

The Origins large mission concept study included an instrument capable of performing transit spectroscopy to higher precision than JWST [181]. The key performance metric for these observations is the stability of the instrument response during the transit, secondary eclipse, or planetary orbit phase curve (typically on the time scale of hours to days). For missions beyond JWST, the responsivity stability of mid-IR detectors need to be improved to a level of roughly 5 ppm on time scales of hours- expected to be a factor of several beyond what JWST achieves.

The Astro2020 Decadal Survey did not prioritize the science enabled by transit spectroscopy beyond JWST, but one of the recommended far-IR flagship or probe missions could potentially choose to include mid-IR transit measurements as an enhancing capability.

5.2.1 Detection Stability in the Mid-IR

Technology Gap: Detection Stability in the Mid-IR

- **Description:** The capability to detect mid-infrared light with ultrastable detectors to carry out transit spectroscopy of terrestrial exoplanets in the Habitable Zone of M-dwarf stars.
- **SOA:** Spitzer IRAC Si:As detector data have demonstrated about 60 ppm precision in transit observations of several hours. JWST/MIRI is expected to achieve 10–100 ppm transit stability.
- **Needed capability:** Ultrastable detectors (< 10 ppm over 5 hours) for the mid-infrared band (7 - 20 microns) enabling transit spectroscopy of rocky exoplanets in the habitable zone of M-dwarfs.

Current State-of-the-Art

Spitzer IRAC Si:As detectors have demonstrated about 60 ppm precision in transit observations of several hours. JWST/MIRI has demonstrated similar performance in early commissioning; improvements may be seen as understanding of instrumental systematics, post-processing techniques, and calibration improve during the JWST mission.

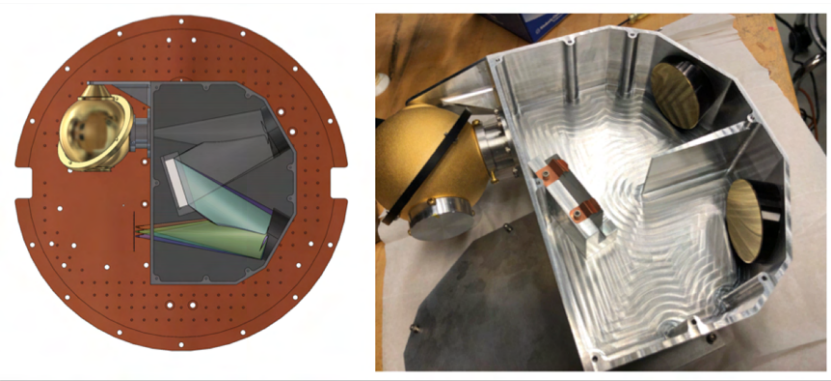

Figure 5.3: Integrating sphere for testing ultra-stable mid-infrared detectors [182] (PI Johannes Staguhn, JHU; Image credit: Johannes Staguhn)

Recent Progress

JWST successfully commissioned its near and mid-infrared instruments for transits, reporting transit depth precision in NIRSPEC and MIRI of <100 ppm at R=100 (<5 μm)and R=50 at longer wavelength, with improvements expected as analysis improves [59].

In the lab, a SAT-2018 (PI Staughn, Johns Hopkins University) was awarded to demonstrate the mid-infrared stability of TES. Sub-Kelvin TES. detectors are sensitive to single photons over a wide band. The investigation includes a novel out-of-band calibration technique. A testbed is set up and nearly ready to carry out the demonstrations (Fig. 5.3) [182].

Next Steps

The far-IR Probes and Far-IR Future Great Observatory recommended by Astro2020 will develop their science cases and architectures in the coming years and investigate the benefits of developing better transit sensitivity. In support of this work, astrophysical limits should be examined further to show that they will not be limitations for transit measurements at sensitivity levels beyond those achievable by JWST.

The SAT demonstration of the stability of TES detectors will complete in the next year and publish results.

A new class of HgCdTe photoconducting arrays with a wavelength cutoff at 10μm [183, 184] have been developed as part of the Near Earth Object (NEO) Surveyor project. These may also be a candidate technology offering the necessary stability in the mid-infrared.

6 Technology Watch List

In addition to the technology gaps prioritized for investment, ExEP maintains a list of four "Watch List" gaps; These gaps, if closed, may be beneficial to exoplanet science. If future architecture or mission choices deem closing these gaps to enable or enhance one of the future strategic missions, these may move to the prioritized gap list.

6.1 Low-Vibration Cryogenic Systems

Energy-resolving photon-counting detectors for exoplanet characterization provide a number of advantages with respect to photoconducting detectors (Sect. 4.1). This type of detector typically requires cryogenic cooling, and in most cases, sub-Kelvin cooling. Below 25 K, passive cooling in space is not practical and active cryocooling is necessary. While recent missions have achieved sub-Kelvin cooling for many years to support far-infrared and millimeter wave detectors (for example *Planck* [185] and *Herschel*), additional technology development may be needed in heat lift, lower mass, lower volume, and lifetime. In addition, vibration disturbances from cryogenic cooling must be at a level compatible with the sub-nanometer wavefront stability needed for coronagraphy. A discussion of cooling technology suitable for cryogenic detectors and associated challenges can be found in [186].

6.2 Mid-Infrared Coronagraphy

The ExEP has traditionally focused its coronagraph technology development on visible wavelengths because for a fixed telescope aperture size, the

This artist's conception illustrates a storm of comets around a star near our own, called Eta Corvi. NASA/JPL-Caltech/R. Hurt (IPAC).

available inner working angle to study the habitable zones of nearby stars degrades linearly with wavelength. However, in the mid-infrared where a planet could be detected in thermal emission rather than in reflected starlight, the starlight suppression requirement is less stringent. There are science benefits to directly imaging and spectral characterization of cool giant exoplanets.

The state-of-the-art in mid-IR coronagraphy will be set by JWST in the coming years. JWST's instruments have several coronagraph modes, including four-quadrant phase masks on JWST-MIRI. The high contrast imaging mode was predicted to achieve contrasts to 10^{-4} at 10.65 to 15.5 μm wavelengths with inner working angles of 0.33 - 0.49″ in wide bands (no spectral dispersion) [187].

If future great observatories, such as the far-IR mission, prioritize direct imaging of exoplanets in the mid-IR, technology development may be needed to obtain deeper contrast and improved inner working angle. Some development in coronagraph optics and architecture technology will overlap with developments in the visible band and near infrared, but there are specific optimizations that are needed for the mid-infrared band. In particular, the coronagraph instrument may need to operate entirely at cryogenic temperatures to reduce background noise, including the deformable mirrors [188].

6.3 Nulling Interferometry

Nulling interferometry is an alternative starlight suppression technique to interfere light from multiple apertures to null on-axis starlight. The technique may prove useful at spectral measurements of Earth-like exoplanets to seek biomarkers in the mid-infrared, where single aperture telescopes will be limited in angular resolution. Instruments on the Large Binocular Telescope (LBT) [189] and VLT [190] have employed the technique to great success - to the point of performing near-IR spectroscopy of an exoplanet from the ground [175]. Space-based nulling interferometry [191] has been studied on and off over decades.

The 2018 Exoplanet Science Strategy recommended that NASA begin to consider technologies to enable a mid-infrared interferometry mission that could follow up biosignature measurements from a UV/Vis/NIR direct-imaging mission. In 2021, ExEP conducted a study (PI: Bertrand Mennesson, Study Manager: Pin Chen) to survey technological advancements in the past ~15 years, revisit mission architecture and scientific objectives, and identify current technology gaps. The study found that the NASA Terrestrial Planet Finder Interferometer (TPF-I)'s main scientific goals and objectives are still applicable, as well as the TPF-I Emma mission architecture. The study produced a number of reports, including a detailed technology gap list. Distribution of these reports is on a per-request basis.

However, the Astro2020 decadal survey did not recommend a space mission that entails mid-IR interferometry and NASA is currently not investing in this approach.

Going forward, the *LIFE* mission concept in Europe continues to investigate the benefits and technological challenges of a nulling interferometry mission [192].

Aside from multi-aperture nulling for mid-IR spectroscopy, single-aperture nulling using sub-aperture interference or vortex-fiber nulling, can fill an important gap in discovery space, especially for near-IR characterization. For example, a 60 mas IWA at 1.8 μm translates to 1 λ/D for a 6-meter aperture. This very narrow IWA poses a severe challenge for coronagraphy, while nulling technology has inherent advantages for achieving small IWA [193].

6.4 Technosignatures

In 2021, the ExEP commenced a fact-finding technosignatures technology gap study to understand where it can make a positive impact towards the search for technological life. The study will help ExEP and the community better understand the landscape and needs of the field if investments in this field are considered again.

The study is systematically creating a database that will include:

- technosignature search approaches;
- technology needs and gaps;
- and other needs to advance technosignature searches (such as access to existing facilities and future facilities that may be needed).

The study will conclude in 2023 by delivering the database to the community via a public website.

A ExEP Technology Subgaps

Table A.1: Subgaps of **Mirror Technologies for High Angular Resolution (UV/Vis/NIR)**.

Subgap Name and Description	Current-State-of-the-Art	Performance Goals and Objectives
Mirror Substrate and Structures Mirror substrate material advancements will likely be required to meet 10 pm/10 minute Wavefront Error (WFE) stability requirements, with particular emphasis in homogeneity and isotropy. Additional characterization, material processing understanding, and potential advancements in structural composite materials may be required to ascertain long term dimensional changes which may drive critical actuator stroke range and capabilities. Advances in latch mechanisms will be necessary to reach precision, stability, and hysteresis levels likely required.	JWST: Beryllium mirror segments, 1.32-m flat-to-flat with 25 nm surface figure error. Multiple Mirror System Demonstrator (MMSD) demonstrated fabrication or partial fabrication of five, 1.4-meter point-to-point ULE mirror segment substrates, achieving 10 kg/m^2 areal density and a production schedule of 3 mirrors on three-week centers. One of the five mirror segment substrates was flight qualified. Thermal modeling performed with as-measured CTE distributions indicate that these fabricated mirrors can achieve the necessary thermal stability when properly controlled. Materials with near-zero CTE are desired for optimal thermal stability. Thus, candidate mirror segments using closed-back ULE or open-back Zerodur are under consideration. (a) Study indicates <10mK temperature stability in ULE mirror required to bound uncorrected wavefront errors due to higher spatial frequency mirror surface figure errors to <6 pm rms[194], which may be achievable[62]. Less thermally stable segmented PM designs may be susceptible to launch acoustics. JWST beryllium Primary Mirror (PM) segments are State-of-the-Art (SOTA) metallic mirror substrates. Need: Additional characterization/process advancements for thermal stability/homogeneity and characterization of consistent long-term crack growth parameters to demonstrate safe life. (b) JWST OTIS structures made from various graphites with 954-6 cyanate ester thermoset resin are SOTA precision composite structures. Other resins exist with low outgassing, moisture uptake, high fiber compatibility. Observation efficiency, dimensional stability, & micro dynamics will be impacted by thermal microcracking & moisture desorption. Need SOTA characterization of these properties. (c) Mechanism deployment repeatability and stability are critical for WFE stability. Latches with <1nm/N hysteresis have been demonstrated[195].	Surface Figure Error: ~5 nm RMS First Free Mode: > 400 Hz Areal Density: <19 kg/m^2 ► Perform system performance studies to determine detailed homogeneity requirements for critical mirror substrates ► Demonstrate ability to characterize material inhomogeneity to required resolutions ► Characterize long-term crack growth behavior of mirror substrates within required precision to assure mission safe life ► Characterize microcracking & moisture absorption/desorption of critical telescope composite structures ► Demonstrate through similitude to potential flight structures low/no microcracking & moisture absorption/desorption meeting mission requirements ► Determine detailed requirements for latched mechanisms with emphasis on repeatability, hysteresis, and stability ► Build and demonstrate latches suitable for incorporation into a UVOIR mission based on segmented architecture ► Demonstrate mitigation of support print-through.

Continued on next page

Table A.1: Subgaps of **Mirror Technologies for High Angular Resolution (UV/Vis/NIR)**.

Subgap Name and Description	Current-State-of-the-Art	Performance Goals and Objectives
Mirror Positioning Actuators Rigid-body positioning of the primary mirror segments will require actuators that simultaneously have high dynamic range (millimeters of travel) and ultra-fine resolution (picometer step sizes). For the ultra-fine actuation, Piezo-electric (PZT) actuators are the primary candidate.	The JWST mechanical bipod actuators currently achieve the necessary level of coarse and fine stage actuation. Commercial off-the-shelf PZT actuators with 5 picometer resolution are available and have been demonstrated in controlled laboratory environments [196]. However, development is needed to incorporate PZT actuators with the coarse and fine stage mechanical bipod actuators. PZT launch survivability and reliability must also be studied and developed. The ULTRA-TM program recently demonstrated closed loop gap stability of a capacitive sensor and 3 ultra-fine actuators to <2.5 pm RMS in gap (0.01–10 Hz)	Stroke: 10 mm Resolution: < 10 pm Creep: < 1 pm / 10 min. Design an initial test article actuator that incorporates mechanical coarse stage motion and PZT ultra-fine stage motion. Co-develop the necessary drive electronics to manage the actuator motion. Fabricate a test article actuator and verify its performance in a laboratory setting to achieve TRL 4. Following the TRL 4 demonstration, design and fabricate a complete, flight-like bipod actuator, and electronics. Complete functional and performance testing of the actuator with a mirror segment mass simulator (TRL 5) and complete environmental qualification testing to bring the actuator technology component to TRL 6. Incorporate actuators into full-scale mirror segment assembly to raise system-level TRL to 6. (see [5] for more detailed plan, schedule, and cost)
Gravity Sag Offloader Capability to trace surface figure error measurements in 1-g to the 0-g environment.	Ability to characterize gravity sag and compensate for it is TRL-9 for space telescopes such as Hubble, Kepler, and Webb. But, it is TRL-4 for a potential 4 to 6 m monolithic Habitable Worlds Observatory exoplanet mirror. The reason is amplitude. For a potential 4 to 6m mirror, it is necessary to characterize and compensate for several millimeters of gravity sag with an uncertainty of <4 nm RMS. The Hubble, Kepler and Webb mirrors had gravity sags of a few 10s to 100s micrometer.	To meet the Decadal 2020 identified gap, technology is needed to characterize and compensate primary mirror gravity sags on the order of several millimeters with an uncertainty of <4 nm RMS.
Coefficient of Thermal Expansion Characterization Capability to characterize the homogeneity of the CTE in mirror substrates to the parts-per-billion (ppb) level.	'Zero' CTE materials such as Zerodur® made by SCHOTT and ULE® made by Corning have flown in space and thus are TRL-9 in sizes from 1-m to 2.4-m. And both Corning and SCHOTT have standard processes for characterizing CTE. However, the CTE maps produced by these standard processes do not have sufficient spatial resolution to predict the mirror's thermal performance at the fidelity needed for coronagraphy with a Habitable Worlds Observatory telescope. Furthermore, Structural Thermal Optical Performance (STOP) models created with state of art CTE maps have not correlated well with measured mirror cryo-deformation.	To meet the Decadal 2020 identified gap, technology is needed to characterize the primary mirror's CTE homogeneity < ± 5-ppb/K at spatial frequencies up to 100 cycles/diameter. And ideally, this technology needs to be able to assess if a mirror blank compliance with this specification before it is made into a mirror.
Mirror Finishing Habitable Worlds Observatory mirror requirements allow only nanometers of deviation from a perfect optical performance. This is approximately 5 – 10× better than JWST. Areas in need of development include: polishing techniques to control SFE to achieve a high-quality optical surface out to the edge of the part, radius matching of mirror segments to meet UV-quality phasing requirements, CTE uniformity, ultra-stable mirror mounting methods, gravity offloading uncertainty management consistent with requirements to fabricate a Habitable Worlds Observatory, zero g surface in a 1 g environment, and mirror coating uniformity. Advanced mirror manufacturing, polishing, and coating technologies are required to avoid individual mirror segment figure control in the optical telescope assembly which would lead to a significant increase in wavefront sensing and control complexity. Advancing modeling methodologies need to continue to quantify spatial and temporal surface figure errors on coronagraph contrast to inform mirror requirements and wavefront sensing/control architectures. Coating performance at segment edges.	Studies of Capture Range Replication (CRR) indicate it is possible to achieve Habitable Worlds Observatory mirror SFE over spatial frequency bands using precision mandrels in lieu of traditional mirror generating, grinding, and polishing processes. These methods reduce cost and schedule [197]. Closed-back ULE mirror substrates achieve 7.5 nm RMS SFE with no actuated figure correction; first free mode <200 Hz; ~10 kg/m^2 areal density [102]. CTE homogeneity distribution of 3 – 6.5 ppb/°C in a Zerodur mirror produces a thermal deformation SFE distribution of <6 nm RMS [194]. Integrated model correlation of both ULE and Zerodur mirrors have shown gravity sag prediction agreement to within 31 nm RMS difference between predicted and measured values [194].	Advanced mirror technologies demonstrating the following: (a) Segment-to-segment alignment and radius matching with SFE < 5 nm RMS over low spatial frequencies (6 Cycles per Aperture (cpa)). (b) Correct mid-spatial frequency (6 – 60 cpa) errors through deterministic finishing to <5 nm RMS. (c) Achieve <1.5 nm RMS SFE in high-spatial frequencies (>60 cpa) using stiffness polishing tools. (d) Demonstrate 0.5 nm RMS microroughness through optimized polishing parameters, slurry selection, and improved polishing tools consistent with a high-rate production schedules. (e) consideration of active surface figuring with actuators if required.

Continued on next page

Table A.1: Subgaps of **Mirror Technologies for High Angular Resolution (UV/Vis/NIR)**.

Subgap Name and Description	Current-State-of-the-Art	Performance Goals and Objectives
UV Coatings: Wavefront Effects Mirror coatings allowing broadband performance into the UV while maintaining high reflectivity and low polarization aberrations over a broad band.	Al coating with combination of MgF_2, LiF, and/or AlF_3 overcoat: 90–120 nm: < 50% reflectivity 120–300 nm: 85% reflectivity 300 nm–2 μm: > 90% reflectivity Polarization differences between orthogonal polarization states, uniformity, and durability of coatings on large optics is unknown. Flight: HST uses MgF_2; 85% reflectivity λ > 120 nm; 20% reflectivity λ < 120 nm	Mirror coatings that enable high reflectivity to wavelengths as short as 90 nm while maintaining good performance in Vis/NIR band. Coating uniformity must be good enough that polarization phase and amplitude difference < 1% between orthogonal polarization states across the whole wavelength band.

Table A.2: Subgaps of **Coronagraph Contrast and Efficiency**.

Subgap Name and Description	Current-State-of-the-Art	Performance Goals and Objectives
Coronagraph Architecture Coronagraph masks and architectures that perform the necessary starlight suppression to image exo-Earths orbiting Sun-like stars, for a variety of telescope architectures, for both segmented and monolithic apertures.	Roman: Demonstration of $\sim 10^{-8}$ contrast at an IWA of 3 λ/D over a 10% bandpass with a significantly obscured monolithic aperture, but at limited throughput of the planet Point-Spread Function (PSF). Decadal Survey Testbed: A classical Lyot coronagraph with an unobscured aperture, 10% bandpass, and IWA of 3 λ/D has achieved 3.8×10^{-10} contrast over a full dark-hole region. APLC: The SCDA study resulted in several designs that achieve the necessary contrast, IWA, bandpass, and throughput to enable the LUVOIR science. Additional modeling has characterized the performance of the APLC masks in the presence of low-order, segment-level, and polarization aberrations, as well as stellar diameter. Masks have been fabricated and testbed demonstrations at moderate contrast and in air are underway. Vortex Coronagraph (VC): 1.8×10^{-0} contrast demonstrated at 10% Bandwidth (BW) from 3-8 λ/D on a clear aperture, 5×10^{-9} demonstrated on a simulated off-axis segmented static pupil. Nulling Coronagraph (NC): A lateral shearing NC was demonstrated at 10^{-9}contrast at the necessary IWA, but narrowband and with no shear implemented. This demonstration was performed with a segmented DM at a pupil, thus constitutes a demonstration with a segmented aperture. Hybrid Lyot Coronagraph (HLC): Roman Coronagraph has demonstrated 10^{-8} contrast as part of the Roman Coronagraph technology development program, with a significantly obscured aperture. PIAA: 10^{-8} contrast achieved in 10% band with a a simulated off-axis segmented static pupil.	Raw Contrast: 1×10^{-10} Bandpass: >10% Inner Working Angle: < 4 λ/D High contrast spanning 300 nm to 2.5 microns High efficiency: an optimized combination of throughput, inner working angle, tolerance to aberrations, and bandwidth. Robust to stellar diameter and jitter. Telescope pupil shear compatible with contrast/inner working angle.
Deformable Mirrors State-of-the-art coronagraphs rely on deformable mirrors to perform wavefront control. There is a need for flight-qualified, large-format, stable deformable mirrors to perform wavefront control and diffraction suppression for high-contrast coronagraph instruments, for both segmented and monolithic apertures.	Roman Coronagraph: Electrostrictive PMN-based Xinetics DMs have been used in laboratory demonstrations of 3.8×10^{-10} contrast and are being baselined for the Roman Coronagraph instrument. Segmented MEMS DMs have been used in a laboratory setting to achieve 5×10^{-9} contrast with a visible nuller coronagraph. Continuous facesheet MEMS DMs have been used in a laboratory setting to achieve 2×10^{-9} contrast with a vortex coronagraph. ExEP Deformable Mirror Trade Study provides further information (E. Bendek, JPL)	Actuator Format: Minimum 64 × 64; >96 × 96 preferred low surface figure error (of order ~3 nm, pending trades)

Continued on next page

Table A.2: Subgaps of **Coronagraph Contrast and Efficiency**.

Subgap Name and Description	Current-State-of-the-Art	Performance Goals and Objectives
Computational Throughput on Space-rated Processors High-order wavefront control on future missions will require performing many Trillions of Floating-Point Operations (TFLOP). These operations would have to be computed within seconds to minutes to keep up with the instabilities of the primary telescope mirrors. Such computational throughput is not supported by existing radiation-hardened processors suitable for a Class-A mission as they lag by decades behind the commercial off-the-shelf components. Additionally, memory-access times are currently poorly constrained and might further degrade computational performance by an order of magnitude. Both the stability requirements on the primary mirrors and the contrast of the coronagraph are tightly connected to our ability to efficiently and quickly control the higher-order wavefront on space-rated processors.	The BAE RAD5545 is currently the most advanced radiation-hardened processor. It has a throughput of about 0.006 TFLOP/s (not including memory access time.) and supports 16 GB memory. A LUVOIR-type telescope will perform wavefront control at a cadence of seconds to minutes [198] and require about 0.5 TFLOP and 250 GB to compute a single deformable mirror command [199]. Radiation-hardened Field-Programmable Gate Array (FPGA)s generally have better performance than processors, at least in terms of raw throughput. FPGAs were descoped for the Roman Space Telescope due to the complexity involved with programming them. A lower-class co-flyer, similar to the Mars Cube One, can also expand the computational bottleneck by employing more powerful and replaceable but less radiation-tolerant processors. Defining and maturing a higher capability approach is a major effort. It is critical to immediately start developing computing capability and port wavefront control algorithms to space-rated hardware and increase their TRL to be able to achieve science requirements.	Achieve 1 TFLOP/s computation throughput with 1 TB optical science simulation models on a computational architecture that can reliably withstand the radiation levels at L2.
High-bandwidth Optical Communication between Space and Ground High-order wavefront control on Habitable Worlds Observatory with many degrees of freedom my require ground-in-the-loop wavefront control, requiring bandwidth improvements.	Free-space laser communications has long been known for its ability to efficiently communicate at high rates over long distances. Examples include the Lunar Laser Communication Demonstration (LLCD) program, which successfully demonstrated 622 Mbit/s downlink rates over the 400,000 km Earth-Moon link in 2013, and the recently launched Laser Communications Relay Demonstration (LCRD), which will support downlink rates up to 1.2 Gb/s from Geosynchronous Equatorial Orbit (GEO). Another near-term lasercom program is the Terabyte Infrared Delivery (TBIRD) program, which will field a Low Earth Orbit (LEO) cubesat-based satellite that can support 200 Gbit/s data rates. Using a 1 W and 1.2 cm transmission on the space terminal, a pair of up-screened wavelength division multiplexed (WDM) 100 Gbit/s commercial coherent transmitters will generate transmission waveforms from the LEO satellite that will be received at the ground station with a commercial 40 cm telescope.	256 Gbps continuous downlink speeds
Coronagraph Efficiency There is a need for greater coronagraph "efficiency". By "efficiency" we mean a combination of throughput, inner working angle, tolerance to aberrations, and bandwidth (i.e. factors that depend on coronagraph design), and exclude contrast, contrast stability (which are already listed as separate gaps), and exclude mirror reflectivities, detector QE, etc (i.e. factors that depend on component technologies). Because coronagraph parameters can be traded against each other, it makes sense to treat their combination as a single gap of "efficiency", rather than consider gaps in each parameter separately. We quantify this "efficiency" as the ratio of expected exoplanet yield between a real coronagraph and a theoretically optimal coronagraph (for a given target contrast, telescope, and Design Reference Mission (DRM)). Assuming that a coronagraph drives mission performance but not the cost, it is cost-effective to improve the coronagraph and other instrument technologies to theoretical limits, enabling savings on telescope requirements.	Current coronagraph designs considered for LUVOIR and HabEx (APLC, VC, PIAA, Lyot Coronagraph (LC), NC – see table 11-1 in [5] and table 11.1-1 in [6]) can still be substantially improved. As shown in [200] (Figure 10), theoretically optimal coronagraphs have 2–3× greater exoplanet yields for a given mission, even assuming no improvements in contrast, bandwidth, or component efficiencies. There are two possible general technology directions that can close this gap: "classical" architectures (mentioned above), and less common ones such as photonic chips and fiber bundle arrays. The former has the advantage of greater maturity, but it is not known whether they can fully close this gap, even in theory (although latest designs already improve yield by ~1.5× relative to LUVOIR/HabEx final reports). Conversely, photonic chips can close the full gap in theory, but it is not known how challenging that would be in practice.	The goal is to (a) design and (b) demonstrate a coronagraph that achieves at least 80% efficiency, for at least some points in the trade space of the Habitable Worlds Observatory mission (preferably for telescopes with obstructed apertures and relaxed stability requirements). This efficiency can be measured by yield estimators such as AYO or EXOSIMS for a given mission and DRM. Abstracted theoretically optimal coronagraphs can be used as a reference benchmark for this measurement of efficiency.

Continued on next page

Table A.2: Subgaps of **Coronagraph Contrast and Efficiency**.

Subgap Name and Description	Current-State-of-the-Art	Performance Goals and Objectives
Autonomous On-board WFSC Architectures If onboard high-order wavefront control is required, A mismatch exists between the state-of-the-art algorithms for High-Order Wavefront Sensing and Control (HOWFSC), and the computing and storage capabilities required to implement them in onboard flight software, and this will be exacerbated by the steep scaling of performance cost vs. deformable mirror size. The tallest poles are for precomputation activities (e.g. computing and storing a "Jacobian" for use by wavefront control), but high-order wavefront sensing, high-order wavefront control, and alignment/calibration activities such as phase retrieval form the next set of limits.	Current algorithmic state of the art for HOWFSC is "pairwise probing" [201] for wavefront sensing and "electric field conjugation" (e.g. [202]), which have demonstrated $<4\times10^{-10}$ contrast in the ExEP Decadal Survey Testbed (e.g. [15]). Projections of computational usage and available flight-qualified computing hardware project that this implementation would be marginally-feasible to infeasible for CPU-based onboard computation for missions in the HabEx-to-LUVOIR scale [199] New algorithms [203] shown promise in being able to strongly reduce the computation and storage costs associated with Jacobians, and show comparable performance to EFC at 10^{-7} to 10^{-8} contrasts in laboratory testing[204]. Computational costs for next level of tentpoles is not presently evaluated. Other options for addressing the mismatch could include hardware acceleration and offboarding computation; the Roman Coronagraph Instrument uses a ground-in-the-loop (GITL) implementation of HOWFSC. Purely CPU-based onboard computation was infeasible for Roman Coronagraph.	The goal is 1) to select a mission computing architecture which is capable of supplying the end-to-end algorithmic needs of a flagship-class direct-imaging telescope, 2) create relevant performance metrics for evaluation, such as "overhead time per HOWFSC iteration", along with targets for these metrics, and 3) demonstrate that the relevant architecture is capable of meeting these targets for a large Habitable Worlds Observatory telescope. There is a strong preference for this validation to be done under flight-like conditions (relevant flight software, hardware, and logicware, rather than simply algorithmic agreement on commercial hardware), as the low-level details of the computing architecture can play a outsize role in determining final performance, one which can be difficult to capture on paper without demonstration.

Table A.3: Subgaps of **Coronagraph Stability**.

Subgap Name and Description	Current-State-of-the-Art	Performance Goals and Objectives
Ultra-stable Telescope High contrast imaging with a coronagraph requires wavefront stability of picometers in certain modes and thus optical system stability at the same level. The highest sensitivity regimes are "mid-temporal" (0.01–10 Hz) and "mid spatial" (segment rigid body or monolith mid-frequency)	WFSC in the coronagraph (using LOWFS/Zernike Wavefront Sensor (ZWFS)/HOWFSC) at the required temporal frequency requires either very bright stars (mag ~0) or an external laser guide star to provide sufficient signal for corrections. Another option for segmented architectures is direct metrology of the primary mirror using picometer-capable edge sensors (either capactive or optical). Compensation of perturbations can be done directly at the mirror segments using picometer-capable actuators or offloaded to the deformable mirrors in the coronagraph. Active thermal sensing and control will minimize deformations and passive technologies like low-distortion mirror mounts, stable composite structures, and integrated structural damping will minimize perturbations. The ULTRA-TM program recently demonstrated closed loop gap stability of a capacitive sensor and 3 ultra-fine actuators to <2.5 pm RMS in gap (0.01-10 Hz) [205].	Demonstrate an ultra-stable telescope (focus on actively controlled primary and secondary mirrors) using sub-scale but flight traceable optomechanics and active sensing and control systems.
Integrated Modeling of Telescope/-Coronagraph System The proposed UVOIR flagship astrophysics architectures fundamentally challenge the current test-like-you-fly approach to space systems, because of their physical scale, multiple stages of on-orbit deployment, and extremely stringent optical performance requirements unique to visible-light coronagraph. The inability to exhaustively test, or in some cases test at all, in the laboratory necessitates system design verification and validation that relies on integrated modeling. Current modeling paradigms follow an outdated "bucket-brigade" approach, where models are treated independently, even though their model physics are inherently coupled in the observatory: optics, structural dynamics, thermal deformation, sensing, actuation and control. New integrated modeling tools and processes are needed to break down modeling-by-discipline barriers, so that integrated modeling can be solidly relied on at all phases of observatory design, integration, and test.	Integrated control, structural and optical modeling has been deployed to predict the quasi-static and dynamic wavefront error and line-of-sight of large astrophysics observatories (Terrestrial Planet Finder (TPF): [206], NGST/JWST: [207], Roman Space Telescope (RST) : K.-C. Liu et al (2017)). It has generally been restricted to quantifying telescope dynamic stability from disturbances, and trading vibration isolation approaches (TPF-C [208], LUVOIR [62]). Existing modeling tools (such as IMOS (JPL) and DOCS) do not directly model science instrument performance (e.g., contrast in a coronagraph), nor include higher-order nonlinearities in optical sensitivities and kinematics that may drive science performance output where errors are measured in picometers of displacement and fractions of a milli-arcsecond of Line-of-Sight (LOS) error. Recent advances in reimagining the engineering and testing process using Digital Twins for terrestrial large-scale systems have yet to be applied to large-scale space systems.	► Develop integrated modeling environments from Digital Twin constructs that integrate component and subsystem test data over the engineering lifecycle, and that support a model-based assurance case for the full-scale non-testable system ► Fundamental research into the validity of Finite Element Methods for predicting structural deformation at the picometer level ► Incorporate multiple modeling fidelity levels (first-order linear vs. higher-order nonlinear) and multiple analysis modalities (time-domain, temporal/spatial frequency domain) in a multi-disciplinary modeling environment ► Develop and integrate anchored mathematical models of UV, IR and Optical instruments that directly produce performance metrics that otherwise would be only measured in end-to-end testing

Continued on next page

Table A.3: Subgaps of **Coronagraph Stability**.

Subgap Name and Description	Current-State-of-the-Art	Performance Goals and Objectives
Disturbance Reduction and Observatory Stability From the current Coronagraph Contrast Stability gap, "The capability to maintain the deep starlight suppression provided by a coronagraph for a time period long enough to detect light from an exo-Earth." From the HabEx study report, this drives the requirement for an overall LOS pointing requirement of $\leq$ 2.0 mas RMS with a stability of $\leq$4 mas RMS. For future time-domain astrometry and gravity wave missions, $\leq$ 5 mas attitude stability and $\leq$ 10 nm/Hz$^{1/2}$ positional (drag-free) with $\leq$10 nrad/Hz$^{1/2}$ ($\sim$2 mas precision pointing) observatory stability requirements have been established for GAIA and LISA, respectively, and should still apply to any similar future concept. Multiple spacecraft constellations for interferometric observations have positional stability requirements on the order of a fraction of the wavelength of light being observed and combined.	Disturbance reduction systems include spacecraft Attitude Determination and Control Systems (ADCS) (i.e. reaction wheels, thrusters and control algorithms) as well as the observatory structure, mirror control, and any vibration isolation subsystems. While still challenging, Hubble-class pointing (7-10 mas) represents the TRL 9 state-of-the-art in the US along with 5 mas performance on ESA's GAIA mission. The US Space Technology 7 Disturbance Reduction System (ST7-DRS) provided a space-based demonstration of precision position control and drag-free operation ($\leq$10 nm/Hz$^{1/2}$) [209] ; however, the lifetime required of the single-string colloid microthrusters was only 90 days and improving that to multiple years reduces the overall system TRL to 4/5 with components / assemblies completing environmental testing under the previous LISA program. An independent NASA Engineering and Safety Center report, "Application of Micro-Thruster Technology for Space Observatory Pointing Stability" [210] showed that <1 mas precision and stability performance for both HabEx and LUVOIR-like observatories was possible using a microthruster-based approach without reaction wheels or vibration isolation with a TRL depending on the thrust level required and ultimately the solar pressure induce torque on the observatory.	Disturbance reduction systems include spacecraft Attitude Determination and Control Systems (ADCS) (i.e. reaction wheels, thrusters and control algorithms) as well as the observatory structure, mirror control, and any vibration isolation subsystems. System level performance requirements for the observatory: ► $\leq$2 mas RMS pointing accuracy and stability (goal of $\leq$1 mas RMS) ► $\leq$10 nm/Hz$^{1/2}$ spacecraft position stability (goal of 5 nm/Hz$^{1/2}$) ► $\geq$5 year lifetime with $\geq$10 years of expendables (i.e. propellant)
Wavefront Sensing (Low-order and Out-of-band) LOWFS is capable of tracking pointing errors, as well as slow drifts in low-order aberrations (global focus, astigmatism, coma, etc.). LOWFS systems are limited in the speed at which they can sense aberrations, and the spatial frequency of the sensed aberrations. Out-of-band Wavefront Sensing (OBWFS) uses light that is out-of-band (either spatially or spectrally) to determine wavefront drifts within the science band. It is possible to use the information from the OBWFS to monitor DM actuator drift, and even primary-mirror segment level aberrations. Furthermore, since the OBWFS would use broadband light outside of the 10–20% science band, or could use an off-axis bright guide star or even an internal light source, OBWFS would generally be able to sense the full range of wavefront drifts much faster than LOWFS. One approach to improving the speed of the wavefront sensing system is use an Artificial Guide Star (AGS). Early studies have evaluated the use of a laser source on a cubeSat or smallSat platform, flying in formation with the telescope at a distance of 40,000–80,000 km. Such a source, coupled with an out-of-band Zernike wavefront sensor can improve sensing loop rates from < 1 Hz to > 10 Hz.	Current LOWFS technology has benefitted from years of investment as part of the Roman Coronagraph technology development effort, and will continue to be developed as that instrument matures. While OBWFS techniques are explored as a new technology, it is recommended that the Roman LOWFS system be adapted to LUVOIR as well – both to complement an OBWFS system, but also to serve as a fallback solution should OBWFS prove unviable. Roman: Low-order wavefront sensing has been demonstrated on a 10^{-8} contrast coronagraph testbed with realistic disturbances input to the coronagraph optics. The LOWFS demonstrated <0.5 mas RMS per axis line-of-site residual error and was sensitive to $\sim$100 pm of focus error . Out-of-band wavefront sensing has been simulated with a LUVOIR like aperture and preliminary results show picometer-level sensitivity can be achieved for low and high-order terms with sufficient integration time. A smallSat / cubeSat artificial guide star study has defined the necessary performance requirements of the guide star platform to provide a sufficiently bright out-of-band source. Additional study is needed to continue refining the concept in conjunction with the out-of-band wavefront sensor. References B. Roman Space Telescope Coronagraph: project status reports and review documentation, D. SCDA: reports and white papers available at https://exoplanets.nasa.gov/exep/technology/SCDA/, G. Multiple technology gap submissions from the ULTRA-TM team (Ball Aerospace, Northrop Grumman, L3Harris): submitted to Program Offices in response to current call for input.	Wavefront Stability: $\sim$10 pm RMS Control Bandwidth: $\sim$1 Hz with Mv=9 or brighter source

Continued on next page

Table A.3: Subgaps of **Coronagraph Stability**.

Subgap Name and Description	Current-State-of-the-Art	Performance Goals and Objectives
Vibration Isolation and Pointing System Technology Future space telescopes must achieve unprecedented levels of dynamics stability to maintain coronagraph contrasts of 10^{-10} necessary to image exoplanets by blocking the light of the parent star. Preliminary studies[62] indicate vibration reduction in excess of 40 dB above 1 Hz are required to isolate the optical telescope from likely vibration (control moment gyroscopes, appendages dynamics, thruster impulses, etc) originating from the parent spacecraft. Vibration isolation systems possibly combined with means to reduce or eliminate shunt path such as harnesses used for data and electrical power transfer are needed.	(a) 5-DOF Disturbance Free Payload (DFP) laboratory demonstrations on subscale spacecraft and telescope payload test-bed achieved 40 dB to 60 dB of vibration isolation down to DC [211] (b) Impact of harnesses on vibration isolation system performance evaluated on prior mission such as (1) GOES-R Earth Pointing Platform but with isolation corner frequency (~8 Hz) much higher than required (0.01 Hz) (Chapel et al, 2014), (2) International Space Station Microgravity Vibration Isolation Subsystem (MVIS) (`https://www.asc-csa.gc.ca/eng/sciences/mvis.asp`) but not at scale, (3) Lockheed 2-D DFP (unpublished) (c) Technology for wireless Data/Communication as in Free Space optical communication exist but simplifications/packaging required for communication across non-contact isolation system (d) Multiple means of wireless power transfer (Wireless Power Transfer, Wikipedia) exist but maturation required for use across non-contact vibration isolation system taking into consideration range, impact on transmissibility, power coupling efficiency, reliability, etc	► Perform space flight demonstration of Vibration Isolation and Precision Pointing System ► Advance additional vibration mitigation measures: Advance wireless data transfer and possibly wireless power transfer as well to reduce number of cables required at interface between optical telescope and parent spacecraft ► Reduce knowledge gap: Characterize regime between position-dependent and rate-dependent damping mechanism in representative harnesses in subscale demonstration–rate damping being most detrimental to transmissibility at high-frequencies. Project measuring transmissibility between two rigid bodies connected by representative harness would close that gap and provide data needed to validate harness models and/or bound harness impact. LUVOIR concept had requirements of Transmissability Isolation: >40 dB at frequencies > 1 Hz.
Laser Gauges for Metrology Future space telescopes must achieve unprecedented levels of wavefront control of the large segmented primary in order to maintain coronagraph contrasts of 10^{-10} necessary to image exoplanets by blocking the light of the parent star. Preliminary studies[212] indicate that a laser metrology truss from secondary to primary segments can achieve adequate wavefront control but levy requirements on individual laser gauges to have ~10 pm RMS errors over the long integration times scales (10 min–1 hour) required. Additionally, the metrology components will need to be very volume-constrained in order to fit on the structure without obscuring the aperture.	(a) Zero-path Photonic Integrated Circuit (PIC) metrology gauges demonstrated 21.0 pm rms over 100 seconds (Nordt, TechMAST 2021) [213]. Imperfections in the PIC fabrication likely are the current limitation. (b) Laser metrology for the JPL Space Interferometer Mission demonstrated 10's of pm cyclic error[214]. However, these were large metrology gauges, which may not be compact enough. (c) PIC gauges for an LM program (unpublished) demonstrated 200-pm amplitude cyclic error. Cyclic error in PICs is not well understood. (d) Laser frequency stabilization of <1 Hz over 1000 seconds has been demonstrated[215] and <10 Hz is sufficient for 6-m-diameter-aperture-telescope secondary mirror truss structure. (e) The desired PIC material (silicon nitride) for compact gauges has not flown in space. (f) Laser metrology gauges demonstrated on GRACE Follow-on at nm class, free space optics [215]	► Advance Si_3N_4 fabrication capabilities to minimize waveguide loss into cladding modes ► Develop and perform waveguide modeling to understand sources of cyclic error in PICs ► Demonstrate <10 pm cyclic error with optimized design ► Demonstrate PIC bonding in mounting structure with fraction of 10 pm drift over integration time scales ► Develop calibrated test equipment capable of validated pm-class actuation to verify metrology gauge precision ► Demonstrate multi-gauge (≥3 gauges) performance in a sub-scale truss consistent with analytical error accumulation based on single gauge performance. ► Demonstrate thermal stability over required time scales. LUVOIR concept had requirements of Wavefront Stability: ~10 pm RMS, and Control Bandwidth: ~1 Hz with Mv=9 or brighter source

Continued on next page

Table A.3: Subgaps of **Coronagraph Stability**.

Subgap Name and Description	Current-State-of-the-Art	Performance Goals and Objectives
Segment Relative Pose Sensing and Control Future space telescopes must achieve unprecedented levels of wavefront control and stability to maintain coronagraph contrasts of 10^{-10} necessary to image exoplanets by blocking the light of the parent star. An active sensing and control system robust to dynamics excitation including fine positioning actuators with picometer-resolution, low-drift, linear continuous operation, low-power dissipation in hold mode is required to position the primary mirror segments and realize the required wavefront quality while not impacting optical system thermal stability.	Sensing: Capacitive: 5 pm in gap dimension, 0–60 Hz Inductive: 1 nm/$Hz^{1/2}$ for 1–100 Hz in shear; 100 nm/$Hz^{1/2}$ for 1–10 Hz in gap Optical: 20 pm/$Hz^{1/2}$ up to 100 Hz High-speed Speckle Interferometry: < 5 pm RMS at kHz rates; requires center of curvature location and high-speed computing Prior high precision actuation experience is primarily in 100 pm to 1-nm resolution regime. Picometer actuation is a nascent technology. (a) JWST coarse-fine primary mirror segment positioning actuators[216] provide example space qualified system for 6-DOF positioning of mirrors in segmented primary mirror but not traceable in resolution (10-nm), repeatability (2-nm), or operation (set-and-forget instead of continuous). Gear stepper-motor design is unsuitable as point of departure for fine stage due to inherent limitation in resolution and micro-dynamics stability. (b) Piezoelectric, electrostrictive, and voice-coil actuators all offer high-bandwidth and positioning resolution limited only by drive electronics with applications including linear stages (P753 `https://www.pi-usa.us` being representative), deformable mirrors (Xinetics), and mirror nanopositioning (Thirty Meter Telescope (TMT)), respectively, operating in the 100-pm to 1-nm resolution regime. Electrostrictive stacks offer high-stiffness and are likely preferred over piezoelectric due to lower hysteresis, and over voice-coil due to near-zero power dissipation under hold force. (c) European Nano-Trace project aiming for 10-pm "accuracy" metrology [217]	Advance coarse-fine actuation system for relative pose-control of primary mirror segments in optical telescope assembly. Expect coarse stage to emphasize stability but otherwise be conventional. Expect innovation is in fine flexure-stage with following characteristics: picometer-level resolution, high-linearity, continuous operation, low-drift, near-zero power dissipation under hold force, and high-stiffness for reduced optical system susceptibility to dynamics excitation. Requirements from LUVOIR concept[5]: Sensitivity: < 4 pm at 50–100 Hz loop rate (5–10 Hz control bandwidth)

Continued on next page

Table A.3: Subgaps of **Coronagraph Stability**.

Subgap Name and Description	Current-State-of-the-Art	Performance Goals and Objectives
Thermal Sensing and Control Future space telescopes must achieve unprecedented levels of wavefront control and stability projected at (10-pm)/(10-minutes) or longer integration times to maintain coronagraph contrasts of 10^{-10} necessary to image exoplanets by blocking the light of the parent star. As a measure of the difficulty in achieving such levels of wavefront stability, Crill[1] indicates "JWST is predicted to have a 31-nm rms WFE response to a worst-case thermal slew of 0.22 K and take 14 days to passively achieve < 10-pm per 10-min stability" . Such thermal sensitivities are consistent with optical pathlength displacements observed on prototype all-zerodur-structure interferometer test-bed for Space Interferometer Mission of 7.7pm/mK at 0.5-meter scale. Advances in passively thermally stable telescope architectures, thermal sensing and active thermal control technologies operating in mK stability regime over 10 minutes or longer are needed to supplement active wavefront control—feasibility of wavefront stability objective in open telescope not established.	Experimental evidence in thermal stabilization at mK-level is limited and lacks traceability at scale and in open telescope architectures (a) Technology maturation on Space Interferometer Mission provides valuable experience, highlights thermal modeling challenges, and achieved (10 mK)/hour control of thermal boundary on TOM-3 interferometer test-bed in vacuum chamber (Gouilloud, 2006) (b) mK thermal stabilization at small scale achieved in refractometry apparatus at NIST [218] (c) Study indicates <10mK temperature stability required to bound uncorrected wavefront errors due to higher spatial frequency mirror surface figure errors to <6 pm rms [194] (d) Ultra-stable mirror demonstrator achieved <0.4mK/(80 hour) stabilization and 50 μK peak-valley sensing at small scale (Park, 2019) (e) Thermal sensing at submilliKelvin demonstrated in concept photonic thermometer (Zhang, 2020) (f) HabEx study projects (10 pm)/(10 min) wavefront stability achievable in closed telescope architecture by controlling shroud temperature [219]	► System engineering, problem understanding, and open-telescope-architecture feasibility given low control over thermal boundary (a) Quantify thermal-induced wavefront errors (on both temporal and spatial scales) in purely passive segmented open telescope architectures in expected operational thermal environment and quantify residual errors after active wavefront control (b) Advance telescope design achieving best trade-off in wavefront stability performance and system complexity between active wavefront control and thermal stabilization (c) Evaluate benefits of designing for constant dissipated electrical power throughout individual components to eliminate thermal transients during operation (d) Validate thermal modeling tools predictions (numerical analyses must remain accurate over large dynamic range covering both absolute temperatures to capture T^4 radiative dependencies and submilliKelvin temperature differences throughout optical system) since we cannot accurately test in laboratory (e) Goal is to arrive at simplest telescope architecture (close to being thermally passive) and avoid active mirror-segment surface figure control in particular ► Advance thermal sensing (resolution and stability) and active thermal control (logic strategies and actuation implementation) technologies for operation in mK stability regime over 10 minutes or longer ► Demonstrate active thermal control system first on prototypes and next on subscale test-bed in thermal-vacuum chamber in representative thermal operational environment

Continued on next page

Table A.3: Subgaps of **Coronagraph Stability**.

Subgap Name and Description	Current-State-of-the-Art	Performance Goals and Objectives
Wavefront Sensing and Control Algorithms Directly imaging Earth-like exoplanets relies on the ability of the coronagraphs to reach a contrast of 10^{-10} and maintain it throughout observations. This will be achieved by several wavefront sensing and control loops working in tandem. To achieve the best performance, the fundamental limits of the instrument need to be analyzed. Current algorithms can maintain a contrast at least a factor of 10 worse than the fundamental limits. The algorithms need to be improved to fully exploit all available sources of information in the photon-limited observation including priors on wavefront evolution, model uncertainties, and interaction between control loops. After development, these advanced algorithms need to be tested at 10^{-10} contrast (which is difficult even for standard algorithms). Algorithms that operate at the fundamental limits will significantly improve detection threshold and science yield.	The Roman Coronagraph has two wavefront control loops. The high-order wavefront control relies on decade-old algorithms that can only be used to achieve the desired contrast on a bright star. They can be substantially improved before they reach theoretical efficiency limits. Roman's strategy of switching to bright reference stars several times a day will be infeasible on the Habitable Worlds Observatory telescope due to the much faster control cadence of seconds to minutes [198]. The low-order wavefront control loop will operate continuously on Roman, but its influence on the high-order control loop has not been studied in-depth. Recent theory [220] offers bounds on the performance of the multiple wavefront control loops. Advanced algorithms that come close to these bounds are in an early stage of development and achieve 10 times better closed-loop contrast than existing algorithms [220].	Achieve closed-loop wavefront stability that is within a factor of 4 of the photon-noise limit for each wavefront sensor.
Observatory Pointing Control High contrast imaging with a coronagraph requires wavefront stability of picometers in certain modes and thus optical system stability at the same level. Precision pointing stability is important because line-of-sight deviations will cause beam walk on the optics, which will couple into high spatial frequency errors that are difficult to correct. While a fine steering mirror can correct the line-of-sight and is a necessary part of the architecture, it does not address beam walk in the telescope or the instrument. Preliminary analysis suggests ~1 milliarcsecond pointing stability is needed to keep this WFE contribution small. Development of larger area, highly stable fine steering mirrors is also needed, since they are part of the optical train and small changes to the pointing angle will add WFE.	Pointing stability primarly requires minimizing dynamic perturbations of the observatory. This can be achieved by isolating the payload from the spacecraft or having a "quiet" spacecraft. Active isolation approaches include active struts or voice coil-based isolation systems. Quiet spacecrafts can use micro-thrusters during science operations and reaction wheels for slews[205].	Demonstrate a combined payload (including fine steering mirror)/spacecraft with sub-milliarcsecond pointing stability (likely simulation, potentially cubesat demo).

Table A.4: Subgaps of **Vis/NIR Detection Sensitivity**.

Subgap Name and Description	Current-State-of-the-Art	Performance Goals and Objectives
NIR Low-noise Detector Low-noise, large-format detectors with high quantum efficiency between 1000 —2000 nm enable high-contrast exoplanet spectroscopy in the NIR. For LUVOIR, operating temperatures above ~70 K are necessary to be consistent with currently anticipated thermal architecture.	HgCdTe photodiode arrays are high-TRL, high-performance NIR detectors. Teledyne H4RG-10 detectors have direct heritage to the H4RG detectors baselined on Roman, and H2RG detectors used in JWST. However, for use in a high-contrast coronagraph, it is desirable to reduce read noise and dark current further, if possible. Roman: H4RG detectors developed for Roman already exhibit exceptionally good noise performance (single-digit read noise, 10^{-3} dark current), as well as large-format tileable arrays. SAPHIRA linear mode avalanche HgCdTe photodiode sensors have demonstrated 0.1 e- rms read noise, 0.02 e-/pix/s dark current, 320× 255 pixel format. Reference A. Roman Space Telescope WFI: project status reports and review documentation	Array Format: 4k × 4k Read Noise: < 3 e- Dark Current: $< 1 \times 10^{-3}$ e-/pix/s Quantum Efficiency: > 90% over band Operating Temperature: > 70 K Explore two engineering paths that have been identified to potentially achieve H4RG noise reduction goals: reducing the pixel size (to smaller than 10 μm), and optimizing the readout electronics for lower-noise performance. Invest in the development of a 1k × 1k HgCdTe APD array and evaluate its noise and sensitivity performance relative to the H4RG. Select a single candidate technology for continued development. Following selection of a NIR detector candidate, continue investment in optimizing detector performance for use with a high-contrast imaging system. Specific attention should be made to the operational thermal environment that is required to achieve the best performance, and how that thermal environment might be enabled in the context of the overall LUVOIR system. (see [5] for more detailed plan, schedule, and cost)

Continued on next page

Table A.4: Subgaps of **Vis/NIR Detection Sensitivity**.

Subgap Name and Description	Current-State-of-the-Art	Performance Goals and Objectives
UV/VIS Low-noise Detector Low-noise, large-format detectors with high quantum efficiency between the bands 200-525 nm and 500–1030 nm enable high-contrast imaging and spectroscopy. For the LUVOIR visible band (500–1030 nm), emphasis on improved quantum efficiency between 800 and 1000 nm is desired to maximize exoEarth yields.	EMCCDs are being developed for Roman Coronagraph, and can achieve the low read- and dark-noise requirements for high-contrast imaging (Nemati 2014). However, radiation exposure reduces the long-term performance of these devices (Nemati et al. 2016). An improvement in quantum efficiency at the red end of the visible spectrum (800 — 1000 nm) may be needed to enhance exoEarth detection yields. HMCCD should also be developed as a potential alternative. HMCCDs are inherently radiation hard, and do not suffer long-term degradation under continuous exposure. Furthermore, this radiation hardness allows thicker substrates to be used in the devices, improving long-wavelength quantum efficiency.	Array Format: 4k × 4k (or buttable 1k × 1k) Read Noise: $\ll 1$ e- Dark Current: $< 3 \times 10^{-5}$ e-/pix/s Quantum Efficiency: >80% at all detection wavelengths EMCCD development should be continued in the context of a LUVOIR coronagraph system. Focus on improving radiation tolerance through shielding design and readout electronics optimization, and on improved red-end quantum efficiency via substrate thickness and optical coatings. Building off current development activities that are already funded, design and fabricate a 1k × 1k pixel HMCCD device and evaluate its noise and sensitivity performance relative to the existing EMCCDs. Select a single candidate technology for continued development. Incorporate this 1k × 1k candidate into coronagraph testbeds for validation at the system level. Following the candidate down-select, design and fabricate a 4k × 4k device, including all necessary readout electronics. Complete functional, performance, radiation, and environmental qualification testing to achieve a component-level TRL 6. (see [5] for more detailed plan, schedule, and cost)
Rad-Hard, High-QE, Energy Resolving, Noiseless Single Photon Detector Arrays for the NIR, VIS, and UV The search for life on exoplanets via direct imaging is fundamentally photon starved. For context, the median observation time to collect a single exoEarth twin spectra shown in Astro2020 Fig 7.5, (for Signal-to-Noise Ratio (SNR)=8.5, 6.5 m aperture LUVOIR-B) from the biased catalog of exoEarth candidates is ~12 years. Collecting the lowest hanging fruit, the bottom 25% (2.5%) of biased catalog distribution still takes 2.5 (0.26) years. Additionally, most of the mission is spent finding planets and not collecting spectra (2–2.5 years vs 0.5 year). An efficient spectroscopy detection solution is needed to collect spectra during all phases of the mission without penalty and increased spectra collection rate. This calls for rad-hard, ultra-high QE, energy-resolving, noiseless single photon detector arrays to provide the increased throughput to find and spectrally characterize rocky Earth-like exoplanets. Such an approach dramatically increases science yield and the chance of finding, recognizing, and quantifying life—enabling the required statistical significance with a smaller aperture.	Photoconducting detectors are not noiseless (falsely report photons: dark counts, read noise, spurious charge, charge transfer inefficiency, charge trapping, after pulsing), not energy resolving thus requiring dispersive optics to provide spectroscopy. EMCCDs needs improved radiation hardness, reduced susceptiblity to cosmic ray events. TESs, MKIDs, and Superconducting Tunnel Junction (STJ) detectors are cryogenic energy resolving detectors (up to the Fano noise limit). STJs are difficult to read-out larger arrays whereas TESs and MKIDs use similar multiplexing techniques. TESs have achieved >99% QE narrowband and averaging 97% broadband for VIS and NIR. MKID efficiencies of 70%/40% at 0.4/1 μm. [221]	Need arrayable rad-hard (no performance degradation in 5+ year mission with margin), high-QE detectors (QE >90% across the whole bandpass), operating in the NIR, VIS, and UV that spectrally resolve targeted life-identifying biosignatures for the specific mission bandpass(es). NIR (1000–2000 nm), R>200 or fundamental limits, VIS (515–1030 nm), R>140, UV (200–500 nm), R>10.

Table A.5: Subgaps of **Stellar Reflex Motion Sensitivity: Extreme-Precision Radial Velocity**.

Subgap Name and Description	Current-State-of-the-Art	Performance Goals and Objectives
Detectors for High-resolution, Cross-dispersed Spectrographs Ground-based EPRV spectrographs require large-format, deep-well, precisely-ruled, uniformly-efficient, well-characterized 2D detectors[222]. Though industry and other scientific applications has driven detector development, the particular requirements for EPRV of exquisite uniformity have not been advanced. RV precision achievable with current detectors is hindered by numerous effects including saturation, limited full well capacity, fringing, pixel size variations, "tree rings," cross-talk, cosmic rays, "brighter/fatter" effect, stitching errors, persistence, imperfect Charge Transfer Efficiency (CTE), intra-pixel structure, readout time lost, readout noise, pixel-to-pixel variations, flat-fielding, long- and short-term thermal stabilization, and deformation during readout. The corresponding RV error is estimated to be up to ~40 cm/s on Habitable Zone Planet Finder (HPF; [223, 224]) for its H2RG detectors, and 8.1 cm/s for NEID [159] from its CCD detectors. Further, with changing commercial demands and a decrease in the manufacturing base for the current generation of CCD detectors, there is concern that availability of these detectors may become challenging.	Current visible-light spectrographs use 9k by 9k CCDs with 10 micron pitch. Next generation IR spectrographs are baselining 4k by 4k H4RGs. CCD pixel-positioning non-uniformity (PPNU) in commercial CCDs is typically around 0.02 pixels. Charge Transfer Inefficiency (CTI) may result in charge being read out from a pixel other than the one it originated in, producing asymmetries in line profiles that can manifest as spurious Doppler shifts. CTI is a function of S/N that can change over time. CTI may be the largest uncertainty among detector-related radial velocity errors. Spectral orders are curved in 2D and project across the detector resulting in pixels on one side of an order readout with different detector amplifiers that contribute to line asymmetry[225]. Mosaicking of detectors, in an attempt to achieve larger formats introduces gabs, edges, and seams, causing significant systematic irregularities, and is to be avoided. TRL details: Though CCD technology is quite mature (high TRL), the uniformity requirements needed by EPRV are not met. CMOS architectures have yet to achieve the large formats (9k × 9k) required by EPRV without mosaicking.	1. Develop a detailed characterization program of existing detectors/detector technologies to identify the underlying physical detector characteristics which limit performance. Assessment should also include technologies which currently have limited use in the context of EPRV, for example CMOS, but may be needed in future programs. 2. Work with industry partners, work to develop and demonstrate new detector designs and fabrication processes which may overcome current limitations. Current detector architectures, while well suited for imaging, may benefit from alternative designs (for example electronics architecture) or fabrication processes for EPRV applications. 3. Extend the format size (> 8k × 8k) of CMOS detectors without mosaicking. 4. Use a combination of laboratory and on-sky testing to verify findings and demonstrate improved detector performance.
High-Precision, High-Throughput, High-Spectral Resolution Dispersive Optics Ground-based EPRV spectrographs require echelle gratings with low wavefront error and high efficiency to maximize spectral stability, throughput, resolution, and bandwidth. EPRV instrumentation require high efficiency, steep blaze angle echelle gratings to achieve high spectral resolutions of R > 100,000 for both seeing-limited and diffraction-limited systems.	Currently available echelle gratings with steep blaze angles (~76 deg.) reach a limiting size of only 190×400 mm with absolute peak efficiency around 50%. In ground-based seeing-limited EPRV spectrographs, the grating dimensions scale with the size of the telescope aperture for a fixed spectral resolution. It has been necessary to stitch gratings together in order to achieve the total required diffraction aperture for R~100,000, even for moderately-sized telescopes (D > 2.5 m). The NEID spectrograph (3.5 m) uses a 2x1 grating mosaic while ESPRESSO (8 m) uses 3 separate gratings. The registration of these stitched gratings introduces significant wavefront error, and greatly complicates the fabrication process. For decades, echelle gratings have been fabricated by diamond ruling, but it is difficult to achieve all aspects of the performance required for EPRV instruments with this technique. Newer grating fabrication techniques using lithographic methods to form the grooves may be a promising approach. TRL details: Lithographic fabricated grooves are at TRL 3 with respect to current requirements. Initial experiments have shown success in experimental proof-of-concept, but performance in a spectrograph and scaling has yet to be demonstrated.	Develop grating fabrication techniques as alternatives to the traditional diamond-ruled process to achieve large-format, high-efficiency, steep blaze angle, low wavefront error echelle gratings for both seeing-limited and diffraction-limited spectrographs. These are required to achieve high spectral resolutions of R > 100,000 with high throughput and high image quality. ► Size (seeing-limited): ~200 × 1200 mm (width × length for the clear aperture at the blaze angle) ► Size (diffraction-limited): ~50 × 200 mm (width × length) ► Steep blaze angles (>76° or >R4) for achieving higher spectral resolutions >100,000 (e.g., R6 for a 150,000 resolution). ► Higher efficiency, both by reducing diffraction effects and improving coatings. The state of the art is ~50–60% at peak, while >70% is sought. ► Better wavefront error ($< \lambda/8$) across the aperture. This is important for diffraction-limited, adaptive optics-fed systems where maintaining the PSF profile is required to achieve high resolutions [226], as well as seeing-limited instruments that strive to achieve sharp image quality to mitigate the effects of variable pupil illumination. ► Lower line density echelles < 13 lines per mm to be more compatible with detector array widths in diffraction limited spectrographs.

Continued on next page

Table A.5: Subgaps of **Stellar Reflex Motion Sensitivity: Extreme-Precision Radial Velocity**.

Subgap Name and Description	Current-State-of-the-Art	Performance Goals and Objectives
Advanced Photonics for Extreme-precision Radial Velocity Spectroscopy Current ground-based RV instruments use large, cross-dispersed echelle gratings and prisms fed by multi-mode fibers to achieve high resolution (R>100,000). However, these systems are large, complex, expensive and have been only able to achieve RV precision of 20–30 cm/s about an order of magnitude above the precision needed to detect Earth-mass planets around sun-like stars.	The recent generation of cross-dispersed, multi-mode fiber, RV spectrographs, EXPRES, NEID and ESPRESSO are demonstrating intrinsic instrument resolution between 20 and 30 cm/s. They are limited by the environmental stability due to their size proscribed by multi-mode fiber, the optical stability limitations of multi-mode fiber, and the manufacturing precision limitations of the gratings and detectors, among others. The objectives are for spectrographs that are capable of, higher resolution (RV precision), higher bandwidths, smaller size (more easily stabilized), and lower cost.	► Develop photonic spectrographs based on lithographically formed arrayed waveguide gratings [227], "spectrograph on a chip". Such monolithic devices would occupy a small fraction of the volume of existing RV spectrographs and potentially offer lower cost and greater stability. ► Develop the use of photonic lanterns to convert a multimode fiber input into separate Single Mode Fiber (SMF) outputs by sampling multiple positions centered on the near-diffraction limited input. By using the SMF outputs from such a system, these can illuminate separate traces of a diffraction-limited spectrometer [228, 229]. Photonic lanterns are an attractive technology that can provide an interface between single-mode and multimode optical fibers. This allows a potential pathway to increase diffraction-limited EPRV capabilities into the blue visible. ► Develop externally dispersed spectrograph designs (e.g., Vacuum Extreme Radial Velocity Experiment (VERVE) [230]) integrating interferometry with spectroscopy thereby relaxing the calibration requirements. ► Develop an on-chip photonic spectral flattener to take Laser Frequency Comb (LFC) output with its wide range (10s of dB) of brightness across the wavelength band and produce an output which is spectrally uniform at the level of <5 dB. ► Develop the ability to do integrated, end-to-end modeling of electro-mechanical system designs.

Continued on next page

Table A.5: Subgaps of **Stellar Reflex Motion Sensitivity: Extreme-Precision Radial Velocity**.

Subgap Name and Description	Current-State-of-the-Art	Performance Goals and Objectives
Ground-based Visible-light Adaptive Optics Visible-light adaptive optics (Visible AO) systems capable of achieving diffraction-limited seeing, would enable the use of SMF for feeding EPRV spectrographs. This approach would break the telescope aperture-to-spectrograph beam scaling relation between the size of spectrograph and the size of the telescope aperture, permitting much smaller, lower cost, and more easily stabilized RV spectrographs. This design family would allow spectrographs to be designed independently of the intended aperture, allowing for a standardized spectrograph design that could enable further cost savings.	High Strehl Adaptive Optics (AO) in the near-infrared has been demonstrated at numerous telescopes including the Keck 10 m telescope and the Palomar 5 m telescope with peak K-band Strehl ratios of ~0.65–0.85. Strehls of 0.60 have been demonstrated in the Y-band at the LBT 8.4 m telescope on bright targets. Reaching comparable Strehls at visible wavelengths has yet to be demonstrated routinely, but significant efforts are underway at a number of observatories, including at the Magellan 6 m telescope [231, 232]where the MagAO-X system (new extreme AO system for the Magellan Clay 6.5 m telescope) has achieved Strehls of ~50% at 900 nm in initial commissioning with an eventual expected performance of 70% at Hα (656 nm) in median seeing conditions[233]. Gemini Planet Finder (GPI)/Sphere/SCExAO can achieve >90% Strehl at H-band under good conditions on bright stars. Additional 'extreme-AO' systems include SCExAO, which is on-sky at the Subaru Telescope in Hawaii [234], and Single Conjugated Adaptive Optics Upgrade (SOUL) , which is undergoing commissioning at the LBT in Arizona[235]. TRL details: Demonstration of visible-light AO has been achieved in a laboratory environment, but at wavelengths only into the red and at lower Strehl numbers. Work is on-going to assess, demonstrate and optimize on-sky performance at large ground-based telescope facilities.	► Developing optics (i.e., PIAA lenses) for reshaping the beam into a Gaussian shape with minimal loss of light, allowing for theoretical coupling efficiencies close to 100% (see, e.g., [227]); ► Removing non-common path aberrations; and ► Identifying the optimal method for maintaining fiber coupling and positioning (e.g., with tip/tilt, nodding, or other methods); ► Development of high throughput, broad wavelength coverage Atmospheric Dispersion Correction optics; ► Optimization of performance of fiber optics for broad wavelength operation in single mode; ► Optimization of low loss fiber optics switchyards and automated attenuators for Laser Frequency comb control; ► Development of advanced photonic lanterns, multi-core fibers, few mode fibers (with appropriate DM-based scrambling techniques) to improve light capture efficiency in low Strehl regimes, while conserving single-mode output properties (or equivalent). Strehl ratio improvements can be accomplished by: ► Reducing the fitting error of the wavefront with a high number of actuators and more stroke in deformable mirrors; ► Wavefront sensor choice/development for reduced noise characteristics; ► Latency reduction through judicious choice of real-time controllers (both firmware and processors). Up to 2 kHz is a reasonable present-day assumption; ► Automated parameter correction for adaptive/predictive control (for large apertures); ► High-precision Non Common Path Aberrations (NCPA) compensation algorithms using single-mode fiber output; ► High-precision high-speed acquisition and tracking methods for drift compensation and tip-tilt jitter control. Single-mode fiber polarization improvements: An advantage of using single-mode fibers for illumination is their spatial stability in illumination, which overcomes the 'modal-noise' that must be suppressed in the multimode fibers. However, two polarization states in SMF remain and must be controlled in order to avoid polarization noise in an EPRV system [236, 237]. Therefore, polarization mitigation in SMF needs to be developed. May need technology to enable required sky coverage.

Continued on next page

Table A.5: Subgaps of **Stellar Reflex Motion Sensitivity: Extreme-Precision Radial Velocity**.

Subgap Name and Description	Current-State-of-the-Art	Performance Goals and Objectives
Precision Calibration for Extreme-precision Radial Velocity Spectroscopy EPRV spectrographs require accurate and precise calibration in order to achieve the ability to detect and measure the mass of Earth-mass planets around sun-like stars. And, the calibration must be traced to an absolute standard.	Classically, RV spectrograph calibration has relied on atomic Hollow Cathode Lamp (HCL)s, molecular absorption cells (e.g., I_2) and etalons with wavelength reference for precise wavelength determination. However, these methods have a variety of shortcomings when pushing towards the highest precisions, and have usually been limited at the ∼1 m/s RV precision level on-sky. More recently, broadband optical LFC have been developed for the highest-precision RV applications. LFCs intrinsically produce a uniformly spaced, dense grid of laser lines, each with a frequency known to better than 10–12 fractional accuracy. LFCs represent the pinnacle of RV calibration systems, providing wide bandwidth calibration at levels of precision far better than those set by other instrument systematics. Commercial designs (e.g., Menlo Systems) employ mode filtering of amplified, low repetition rate (∼100-–200 MHz) fiber combs through a series of 3 Fabry-Pérot (FP) filter cavities, thus eliminating (∼99% of the comb lines to achieve the sparse line spacing (10-–30 GHz) needed to match typical EPRV spectrograph resolutions (R > 100,000). But these Astrocombs are highly complex devices that require significant engineering efforts to make them 'turn-key' and suffer from several drawbacks. These devices are relatively expensive (∼$1M), and have yet to demonstrate both long-term operability at the observatory and reasonable performance at wavelengths blueward of 500 nm. Furthermore, these systems require periodic maintenance to replace consumable components, such as the Photonic Crystal Fiber (PCF) that enables spectral broadening of the combs, compounding the high costs. NIR astrocombs have been implemented[238] and operating nearly continuously for years (Frederick et al. 2020). However, broadening NIR combs into the visible range with 10–30 GHz line spacing is challenging because at these high pulse repetition rates, it is difficult to achieve the threshold pulse energies needed to realize the non-linear optical effects without substantial pulse amplification. Broadening well into the blue-visible has been demonstrated with low repetition rate combs. Thus, exploring methods for reducing the line density of such combs using, for example, pulse rate multiplication[239] is an interesting avenue. Fabry-Perot etalons are also being used as spectrograph calibration sources for on-sky observations, HPF [240], ESPRESSO [241], HARPS [242], CARMENES [243], and MAROON-X [244]. TRL details: Other methods of achieving reliable visible band, 10-–30 GHz repetition rate LFCs for EPRV applications are being investigated by multiple groups; most of these approaches involve nonlinear spectral broadening and second harmonic generation of NIR frequency combs generated through either Electro-optic modulation (EOM) of a CW laser, or in high-Q disk or ring microresonators through nonlinear optical processes – so-called Kerr microcombs [245, 246], or a combination of both, i.e., pulse-pumped microcombs.	► EPRV spectrograph calibration source must have spectral coverage from 380 nm through 930 nm, with line spacing in the 10-–30 GHz range, and uniform intensity across the full bandpass that can be matched to the intensity of the stellar target. Wavelength coverage further into the infrared can further stellar variability mitigation. ► Fractional frequency stability should be better than $\sim 3\times10^{-11}$ over ∼100 s integration times or longer, corresponding to an RV accuracy of 1 cm/s. ► The power per mode variation across the comb spectrum must be spectrally "flattened." Flattening is typically achieved using SLM technology. Develop arrayed photonic waveguide devices to flatten the spectrum at reduced volume. ► Develop etalon technologies that leverage fully single-mode operation, have broad wavelength coverage that extends into the blue (<500 nm), are contained in a compact design that is easily thermally stabilized, provide high line brightness and good uniformity, and are referenced to a proven frequency standard. ► Develop advanced hybrid comb-etalon concept based on crystalline CaF_2 and MgF_2 Whispering Gallery Mode (WGM) resonators that may overcome some of the challenges of traditional FP etalons. ► Calibration sources must be robust, long-lived, stable over years, and fiber-coupled for instrument interface.

B Exoplanet Exploration Program Facilities

The ExEP manages several facilities located at JPL and makes them available to technology developers to assist in their technology demonstration goals The available resources, if appropriate for the proposer's needs, may help more efficiently meet milestone goals and reduce proposal costs and schedule. The facilities are normally offered to researchers funded through SAT awards.

B.1 High Contrast Imaging Testbed

The HCIT facility is a set of vacuum and in-air optical testbeds, located at JPL and managed by ExEP. Three optical benches are available:

- The Decadal Survey Testbed (DST) [15, 247]
- The Decadal Survey Testbed 2 (DST 2) [248].
- The In-Air Coronagraph Testbed (IACT) [249].

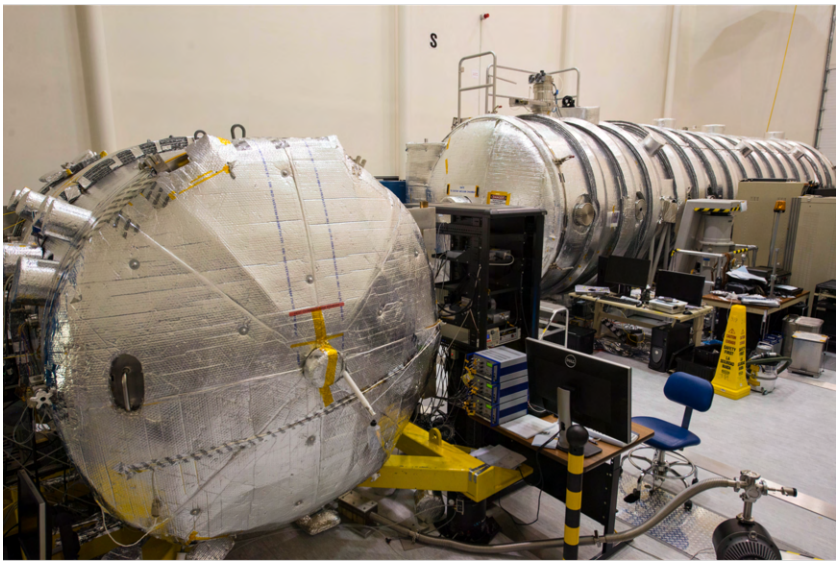

Figure B.1: ExEP's HCIT facility located at JPL. On the left is a chamber historically dedicated to Roman Coronagraph testing. On the right is a larger vacuum chamber that holds both the DST and DST 2.

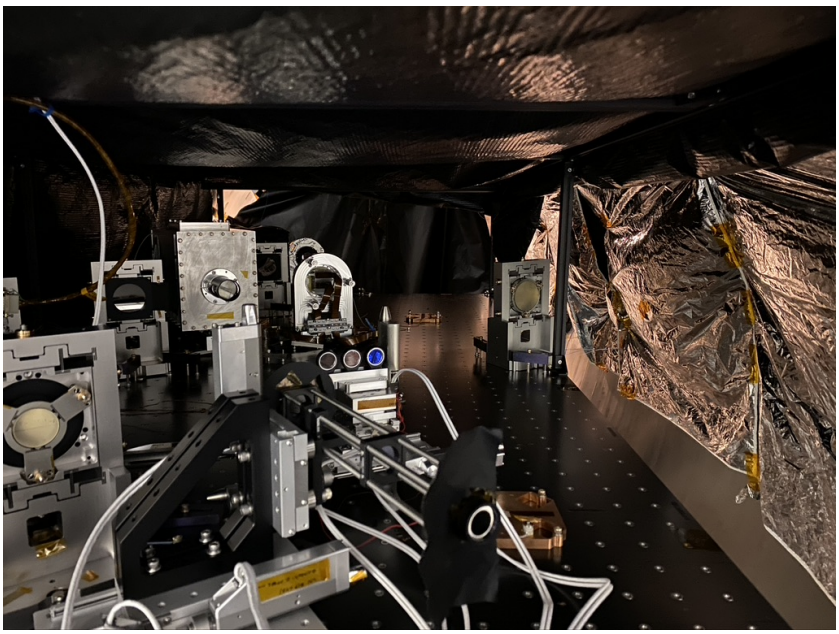

Figure B.2: The DST – an ultrastable coronagraph testbed bench running in vacuum as part of the HCIT facility.

Figure B.3: The DST 2 – a second ultra-stable vacuum coronagraph testbed bench being installed in a vacuum chamber at the HCIT facility. The testbed is being comissioned in late 2022 and will be available to investigations in 2023.

B.2 Starshade Facilities

As the starshade technology development transitions to a competed rather than a directed program, facilities developed under S5 are available to proposers to SAT. These include:

- A scatterometer for measuring petal edge scatter [124]. This facility enables investigators to compare measurements of custom materials or coatings for starshade edges directly with measurements carried out during the S5 program (see Fig. 3.7).
- Support for the Starshade Imaging Simulation Toolkit for Exoplanet Reconnaissance (SISTER) Starshade simulation package[1] [250].

1: http://sister.caltech.edu

Figure B.4: The starshade laboratory at JPL.

B.3 Gaining Access to ExEP Facilities

In order to facilitate access to ExEP-managed resources, please submit answers to the following questionnaire to ExEP's deputy Program Chief Technologist. ExEP personnel will review the responses and schedule a follow-up telecon meeting if needed. The deputy Program Chief Technologist will then supply the investigator a Letter of Committment to attach to the proposal.

Questionnaire for gaining access to ExEP facilities

1. Brief description of the proposed SAT investigation
2. What resources are requested?
3. Milestone(s) to be accomplished and performance goals
4. Brief description of how the work will be conducted
5. Period(s) and preferred dates, if any, over which the resource is requested, stating whether in vacuum or air for testbeds. Include any time required for preparatory work.
6. A list of the personnel, expertise, and level of effort (if any) who will assist in the use of the resource.
7. Any anticipated changes to the resource needed to accommodate your demonstrations.
8. List of items needed for all testbed modifications. Identify items you will be procuring within your proposal's budget and provide approximate cost of needed items.
    a) Otherwise, state that no additional procurements will be necessary for the use of the infrastructure under consideration.
9. Provide any other relevant information or constraints.

References

References in citation order.

[1] Brendan Crill and Nick Siegler. *Exoplanet Exploration Program Technology Plan Appendix*. JPL Document D-102506 https://exoplanets.nasa.gov/exep/technology/technology-overview/. Mar. 2019 (cited on pages 1, 70).

[2] Engineering National Academies of Sciences and Medicine. *Pathways to Discovery in Astronomy and Astrophysics for the 2020s*. 2021 (cited on pages 1, 2).

[3] National Research Council. *New Worlds, New Horizons in Astronomy and Astrophysics*. http://science.nasa.gov/astrophysics/special-events/10-astronomy-and-astrophysics-decadal-survey/. Washington, DC, 2010 (cited on page 1).

[4] SMD Astrophysics Division. *Astrophysics Biennial Technology Report 2022*. https://apd440.gsfc.nasa.gov/images/tech/2022_ABTR.pdf. June 2022 (cited on page 2).

[5] The LUVOIR Team. "The LUVOIR Mission Concept Study Final Report". In: *arXiv e-prints*, arXiv:1912.06219 (Dec. 2019), arXiv:1912.06219 (cited on pages 3, 16, 17, 22, 30, 49, 63, 65, 69, 71, 72).

[6] B. Scott Gaudi et al. "The Habitable Exoplanet Observatory (HabEx) Mission Concept Study Final Report". In: *arXiv e-prints*, arXiv:2001.06683 (Jan. 2020), arXiv:2001.06683 (cited on pages 3, 16, 17, 22, 28, 49, 65).

[7] *NASA Procedural Requirements 7123.1C: NASA Systems Engineering Processes and Requirements*. https://nodis3.gsfc.nasa.gov/displayDir.cfm?Internal_ID=N_PR_7123_001C_&page_name=AppendixE. Mar. 2020 (cited on page 3).

[8] Patricia M. Beauchamp et al. *Technology Readiness Assessment Best Practices Guide*. https://ntrs.nasa.gov/citations/20205003605. June 2020 (cited on page 3).

[9] S. Ertel et al. "The HOSTS Survey for Exozodiacal Dust: Observational Results from the Complete Survey". In: *The Astronomical Journal* 159.4 (Mar. 2020), p. 177. DOI: 10.3847/1538-3881/ab7817 (cited on page 4).

[10] Thai Pham et al. "A decade of NASA strategic astrophysics technology investments: technology maturation, infusion, and other benefits". In: *Advances in Optical and Mechanical Technologies for Telescopes and Instrumentation IV*. Ed. by Roland Geyl and Ramón Navarro. SPIE, Dec. 2020. DOI: 10.1117/12.2562705 (cited on page 6).

[11] Opher Ganel et al. "NASA strategic astrophysics technology investments: a decade of benefits, outlook informed by the 2020 Decadal Survey". In: *Advances in Optical and Mechanical Technologies for Telescopes and Instrumentation V*. Ed. by Roland Geyl and Ramón Navarro. SPIE, Aug. 2022. DOI: 10.1117/12.2630293 (cited on page 6).

[12] John H. Debes, Bin Ren, and Glenn Schneider. "Pushing the limits of the coronagraphic occulters on Hubble Space Telescope/Space Telescope Imaging Spectrograph". In: *Journal of Astronomical Telescopes, Instruments, and Systems* 5.03 (June 2019), p. 1. DOI: 10.1117/1.jatis.5.3.035003 (cited on page 11).

[13] Jens Kammerer et al. "Performance of near-infrared high-contrast imaging methods with JWST from commissioning". In: *Space Telescopes and Instrumentation 2022: Optical, Infrared, and Millimeter Wave*. Ed. by Laura E. Coyle, Marshall D. Perrin, and Shuji Matsuura. SPIE, Aug. 2022. DOI: 10.1117/12.2628865 (cited on page 11).

[14] John Trauger et al. "A hybrid Lyot coronagraph for the direct imaging and spectroscopy of exoplanet systems: recent results and prospects". In: *SPIE Proceedings*. Ed. by Stuart Shaklan. SPIE, Sept. 2011. DOI: 10.1117/12.895032 (cited on page 11).

[15] Byoung-Joon Seo et al. "Testbed demonstration of high-contrast coronagraph imaging in search for Earth-like exoplanets". In: *Techniques and Instrumentation for Detection of Exoplanets IX*. Ed. by Stuart B. Shaklan. SPIE, Sept. 2019. DOI: 10.1117/12.2530033 (cited on pages 11, 14, 66, 77).

[16] Margaret C. Turnbull et al. "Community exoplanet imaging data challenge for Roman CGI and starshade rendezvous". In: *Journal of Astronomical Telescopes, Instruments, and Systems* 7.02 (May 2021). DOI: 10.1117/1.jatis.7.2.021218 (cited on page 11).

[17] Rémi Soummer et al. "High-contrast imager for complex aperture telescopes (HiCAT): 8. Dark zone demonstration with simultaneous closed loop low-order wavefront sensing and control". In: *Space Telescopes and Instrumentation 2022: Optical, Infrared, and Millimeter Wave*. Ed. by Laura E. Coyle, Marshall D. Perrin, and Shuji Matsuura. SPIE, Aug. 2022. DOI: 10.1117/12.2630444 (cited on pages 11, 14, 22).

[18] A. J. Eldorado Riggs et al. "High-contrast demonstration of a vector vortex coronagraph with a segmented, off-axis aperture". In: *Space Telescopes and Instrumentation 2022: Optical, Infrared, and Millimeter Wave*. Ed. by Laura E. Coyle, Marshall D. Perrin, and Shuji Matsuura. SPIE, Aug. 2022. DOI: 10.1117/12.2630130 (cited on pages 12, 13, 28).

[19] Bertrand Mennesson et al. "The Roman space telescope coronagraph technology demonstration: current status and relevance to future missions". In: *Techniques and Instrumentation for Detection of Exoplanets X*. Ed. by Stuart B. Shaklan and Garreth J. Ruane. SPIE, Sept. 2021. DOI: 10.1117/12.2603343 (cited on pages 12, 24).

[20] Garreth Ruane et al. "Wavefront sensing and control in space-based coronagraph instruments using Zernike's phase-contrast method". In: *Journal of Astronomical Telescopes, Instruments, and Systems* 6.04 (Nov. 2020). DOI: 10.1117/1.jatis.6.4.045005 (cited on pages 12, 22).

[21] A.J. Eldorado Riggs et al. "Flight mask designs of the Roman Space Telescope coronagraph instrument". In: *Techniques and Instrumentation for Detection of Exoplanets X*. Ed. by Stuart B. Shaklan and Garreth J. Ruane. SPIE, Sept. 2021. DOI: 10.1117/12.2598599 (cited on page 12).

[22] Byoung-Joon Seo et al. *Milestone 4 Final Report: Narrowband Contrast Testbed Demonstration of Hybrid Lyot Coronagraph for WFIRST-AFTA*. https://exoplanets.nasa.gov/exep/resources/documents/ (cited on page 14).

[23] Eric Cady et al. *Milestone 5 Final Report: Hybrid Lyot and Shaped Pupil Broadband Contrast Testbed Demonstration for WFIRST-AFTA*. https://exoplanets.nasa.gov/exep/resources/documents/ (cited on page 14).

[24] WFIRST Coronagraph Testbed and Modeling Teams. *WFIRST CGI Milestone 9 Dynamic Contrast Demonstration Status Update*. https://exoplanets.nasa.gov/exep/resources/documents/ (cited on pages 14, 21).

[25] Tyler D. Groff et al. "Wavefront control methods for high-contrast integral field spectroscopy". In: *Techniques and Instrumentation for Detection of Exoplanets VIII*. Ed. by Stuart Shaklan. SPIE, Sept. 2017. DOI: 10.1117/12.2274709 (cited on page 14).

[26] David S. Marx et al. "Shaped pupil coronagraph: disk science mask experimental verification and testing". In: *Space Telescopes and Instrumentation 2018: Optical, Infrared, and Millimeter Wave*. Ed. by Howard A. MacEwen et al. SPIE, July 2018. DOI: 10.1117/12.2312602 (cited on page 14).

[27] James Breckinridge et al. *Threshold Raw Retrieved Contrast in Coronagraphs Is Limited by Internal Polarization*. https://exoplanets.nasa.gov/internal_resources/1686/. Aug. 2020 (cited on page 13).

[28] Garreth J. Ruane et al. "Broadband vector vortex coronagraph testing at NASA's high contrast imaging testbed facility". In: *Space Telescopes and Instrumentation 2022: Optical, Infrared, and Millimeter Wave*. Ed. by Laura E. Coyle, Marshall D. Perrin, and Shuji Matsuura. SPIE, Aug. 2022. DOI: 10.1117/12.2628972 (cited on pages 13, 19).

[29] John Trauger et al. *Super Lyot ExoEarth Coronagraph (SLEEC)*. https://exoplanets.nasa.gov/internal_resources/842/. Mar. 2018 (cited on page 13).

[30] Mamadou N'Diaye et al. "High-contrast imager for complex aperture telescopes (HiCAT): 1. testbed design". In: *SPIE Proceedings*. Ed. by Stuart Shaklan. SPIE, Sept. 2013. DOI: 10.1117/12.2023718 (cited on page 14).

[31] Mamadou N'Diaye et al. "High-contrast Imager for Complex Aperture Telescopes (HICAT): II. Design overview and first light results". In: *SPIE Proceedings*. Ed. by Jacobus M. Oschmann et al. SPIE, Aug. 2014. DOI: 10.1117/12.2056694 (cited on page 14).

[32] Mamadou N'Diaye et al. "High-contrast imager for complex aperture telescopes (HiCAT): 3. first lab results with wavefront control". In: *SPIE Proceedings*. Ed. by Stuart Shaklan. SPIE, Sept. 2015. DOI: 10.1117/12.2188497 (cited on page 14).

[33] Lucie Leboulleux et al. "High-contrast imager for Complex Aperture Telescopes (HiCAT). 4. Status and wavefront control development". In: *SPIE Proceedings*. Ed. by Howard A. MacEwen et al. SPIE, July 2016. DOI: 10.1117/12.2233640 (cited on page 14).

[34] Rémi Soummer et al. "High-contrast imager for complex aperture telescopes (HiCAT): 5. first results with segmented-aperture coronagraph and wavefront control". In: *Space Telescopes and Instrumentation 2018: Optical, Infrared, and Millimeter Wave*. Ed. by Howard A. MacEwen et al. SPIE, Aug. 2018. DOI: 10.1117/12.2314110 (cited on page 14).

[35] Christopher Moriarty et al. "High-contrast imager for complex aperture telescopes (HiCAT): 6. software control infrastructure and calibration". In: *Space Telescopes and Instrumentation 2018: Optical, Infrared, and Millimeter Wave*. Ed. by Howard A. MacEwen et al. SPIE, Aug. 2018. DOI: 10.1117/12.2314058 (cited on page 14).

[36] Rémi Soummer et al. "High-contrast imager for complex aperture telescopes (HiCAT): 6. Two deformable mirror wavefront control (Conference Presentation)". In: *Techniques and Instrumentation for Detection of Exoplanets IX*. Ed. by Stuart B. Shaklan. SPIE, Sept. 2019. DOI: 10.1117/12.2530299 (cited on page 14).

[37] Rémi Soummer et al. "High-contrast imager for complex aperture telescopes (HiCAT): 7. Dark zone demonstration with fully segmented aperture coronagraph". In: *Techniques and Instrumentation for Detection of Exoplanets X*. Ed. by Stuart B. Shaklan and Garreth J. Ruane. SPIE, Aug. 2021. DOI: 10.1117/12.2594684 (cited on page 14).

[38] Ruslan Belikov et al. "High contrast imaging in multi-star systems: technology development and first lab results". In: *SPIE Proceedings*. Ed. by Howard A. MacEwen et al. SPIE, July 2016. DOI: 10.1117/12.2233914 (cited on page 15).

[39] Dan Sirbu et al. "Demonstration of multi-star wavefront control for WFIRST, Habex, and LUVOIR". In: *Techniques and Instrumentation for Detection of Exoplanets IX*. Ed. by Stuart B. Shaklan. SPIE, Sept. 2019. DOI: 10.1117/12.2529622 (cited on page 15).

[40] Eugene E. Pluzhnik et al. "Multi-star wavefront control with SCExAO instrument: demonstration with an internal source". In: *Techniques and Instrumentation for Detection of Exoplanets X*. Ed. by Stuart B. Shaklan and Garreth J. Ruane. SPIE, Sept. 2021. DOI: 10.1117/12.2594942 (cited on page 15).

[41] A. J. Eldorado Riggs et al. "Initial super-Nyquist wavefront control experiments in the Decadal Survey Testbed". In: *Techniques and Instrumentation for Detection of Exoplanets X*. Ed. by Stuart B. Shaklan and Garreth J. Ruane. SPIE, Sept. 2021. DOI: 10.1117/12.2594800 (cited on page 15).

[42] Dan Sirbu et al. "Initial laboratory demonstration of multi-star wavefront control at the occulting mask coronagraph testbed". In: *Space Telescopes and Instrumentation 2022: Optical, Infrared, and Millimeter Wave*. Ed. by Laura E. Coyle, Marshall D. Perrin, and Shuji Matsuura. SPIE, Aug. 2022. DOI: 10.1117/12.2630639 (cited on page 15).

[43] Eduardo Bendek et al. "Enabling high-contrast imaging of binary stars with the Roman Space Telescope coronagraph instrument". In: *Techniques and Instrumentation for Detection of Exoplanets X*. Ed. by Stuart B. Shaklan and Garreth J. Ruane. SPIE, Sept. 2021. DOI: 10.1117/12.2594992 (cited on page 15).

[44] Garreth Ruane et al. "Scalar vortex coronagraph mask design and predicted performance". In: *Techniques and Instrumentation for Detection of Exoplanets IX*. Ed. by Stuart B. Shaklan. SPIE, Sept. 2019. DOI: 10.1117/12.2528625 (cited on page 16).

[45] Niyati Desai et al. "High contrast demonstrations of novel scalar vortex coronagraph designs at the high contrast spectroscopy testbed". In: *Techniques and Instrumentation for Detection of Exoplanets X*. Ed. by Stuart B. Shaklan and Garreth J. Ruane. SPIE, Sept. 2021. DOI: 10.1117/12.2603953 (cited on page 16).

[46] Kevin W. Fogarty et al. "The PIAA-vortex coronagraph: a new coronagraph technology to maximize exo-Earth yields in the Astro2020 era". In: *Space Telescopes and Instrumentation 2022: Optical, Infrared, and Millimeter Wave*. Ed. by Laura E. Coyle, Marshall D. Perrin, and Shuji Matsuura. SPIE, Aug. 2022. DOI: 10.1117/12.2630638 (cited on page 16).

[47] Scott D. Will and James R. Fienup. "Effects and mitigation of polarization aberrations in LUVOIR coronagraph". In: *Techniques and Instrumentation for Detection of Exoplanets IX*. Ed. by Stuart B. Shaklan. SPIE, Sept. 2019. DOI: 10.1117/12.2525377 (cited on page 16).

[48] Susan M. Redmond et al. "Dark zone maintenance results for segmented aperture wavefront error drift in a high contrast space coronagraph". In: *Techniques and Instrumentation for Detection of Exoplanets X*. Ed. by Stuart B. Shaklan and Garreth J. Ruane. SPIE, Sept. 2021. DOI: 10.1117/12.2594647 (cited on pages 16, 22).

[49] Rachel Morgan et al. "Optical calibration and first light for the deformable mirror demonstration mission CubeSat (DeMi)". In: *Journal of Astronomical Telescopes, Instruments, and Systems* 7.02 (June 2021). DOI: 10.1117/1.jatis.7.2.024002 (cited on page 18).

[50] Christopher B. Mendillo et al. "The PICTURE-C exoplanetary imaging balloon mission: laboratory coronagraph demonstrations of high-contrast imaging and low-order wavefront control". In: *Space Telescopes and Instrumentation 2022: Optical, Infrared, and Millimeter Wave*. Ed. by Laura E. Coyle, Marshall D. Perrin, and Shuji Matsuura. SPIE, Aug. 2022. DOI: 10.1117/12.2630237 (cited on page 18).

[51] Paul Bierden. *MEMS Deformable Mirror Technology Development for Space-Based Exoplanet Detection*. https://exoplanets.nasa.gov/internal_resources/2236/. Apr. 2022 (cited on page 18).

[52] Axel Potier et al. "Update on the survivability of high-actuator-count MEMS deformable mirror to rocket launch." In: *Space Telescopes and Instrumentation 2022: Optical, Infrared, and Millimeter Wave*. Ed. by Laura E. Coyle, Marshall D. Perrin, and Shuji Matsuura. SPIE, Aug. 2022. DOI: 10.1117/12.2629915 (cited on page 18).

[53] M. Laslandes. "Towards the spatialization of ALPAO DMs". In: *International Conference on Space Optics — ICSO 2020*. Ed. by Zoran Sodnik, Bruno Cugny, and Nikos Karafolas. SPIE, June 2021. DOI: 10.1117/12.2599663 (cited on page 18).

[54] Eduardo A. Bendek et al. "Microelectromechanical deformable mirror development for high-contrast imaging, part 1: miniaturized, flight-capable control electronics". In: *Journal of Astronomical Telescopes, Instruments, and Systems* 6.4 (2020), pp. 1–20. DOI: 10.1117/1.JATIS.6.4.045001 (cited on pages 18, 19).

[55] Garreth J. Ruane et al. "Microelectromechanical deformable mirror development for high-contrast imaging, part 2: the impact of quantization errors on coronagraph image contrast". In: *Journal of Astronomical Telescopes, Instruments, and Systems* 6.04 (Oct. 2020). DOI: 10.1117/1.jatis.6.4.045002 (cited on page 19).

[56] Hari B. Subedi et al. "Parabolic deformable mirror testbed for the ExoSpec project". In: *Space Telescopes and Instrumentation 2020: Optical, Infrared, and Millimeter Wave*. Ed. by Makenzie Lystrup et al. SPIE, Jan. 2021. DOI: 10.1117/12.2562642 (cited on page 19).

[57] Laurent Pueyo et al. "Amplitude and phase control of pupil coronagraph for exoplanet detection using spatial light modulators". In: *SPIE Proceedings*. Ed. by Daniel R. Coulter. SPIE, Nov. 2003. DOI: 10.1117/12.505612 (cited on page 19).

[58] S. G. Leon-Saval et al. "Multimode fiber devices with single-mode performance". In: *Optics Letters* 30.19 (Oct. 2005), p. 2545. DOI: 10.1364/ol.30.002545 (cited on page 19).

[59] Jane Rigby et al. *Characterization of JWST science performance from commissioning*. Tech. rep. NASA, 2022 (cited on pages 21, 26, 58).

[60] Milan Mandic, Oscar S. Alvarez-Salazar, and Alina Kiessling. "HabEx: A high-precision pointing architecture using microthrusters and a fine steering mirror". In: *Space Telescopes and Instrumentation 2018: Optical, Infrared, and Millimeter Wave*. Ed. by Howard A. MacEwen et al. SPIE, July 2018. DOI: 10.1117/12.2315545 (cited on page 21).

[61] Benjamin M. Cromey et al. "Picometer-scale edge sensing and actuation for ultra-stable mission concepts". In: *Space Telescopes and Instrumentation 2022: Optical, Infrared, and Millimeter Wave*. Ed. by Laura E. Coyle, Marshall D. Perrin, and Shuji Matsuura. SPIE, Aug. 2022. DOI: 10.1117/12.2628183 (cited on pages 21, 23).

[62] Larry D. Dewell et al. "Dynamic wavefront error and line-of-sight performance predictions for the 15-meter segmented Large Ultraviolet/Optical/Infrared Surveyor (LUVOIR) with non-contact vibration isolation". In: *UV/Optical/IR Space Telescopes and Instruments: Innovative Technologies and Concepts IX*. Ed. by James B. Breckinridge, H. Philip Stahl, and Allison A. Barto. SPIE, Sept. 2019. DOI: 10.1117/12.2528190 (cited on pages 22, 62, 66, 68).

[63] Thomas E. Brooks and H. Philip Stahl. "Precision thermal control technology to enable thermally stable telescopes". In: *Journal of Astronomical Telescopes, Instruments, and Systems* 8.02 (Apr. 2022). DOI: 10.1117/1.jatis.8.2.024001 (cited on page 22).

[64] John Steeves et al. "Picometer wavefront sensing using the phase-contrast technique". In: *Optica* 7.10 (Sept. 2020), p. 1267. DOI: 10.1364/optica.398768 (cited on page 22).

[65] Thayne Currie et al. "Laboratory Demonstration of Spatial Linear Dark Field Control For Imaging Extrasolar Planets in Reflected Light". In: *Publications of the Astronomical Society of the Pacific* 132.1016 (Sept. 2020), p. 104502. DOI: 10.1088/1538-3873/aba9ad (cited on page 22).

[66] K. L. Miller et al. "Spatial linear dark field control on Subaru/SCExAO". In: *Astronomy and Astrophysics* 646 (Feb. 2021), A145. DOI: 10.1051/0004-6361/202039583 (cited on page 22).

[67] Olivier Guyon et al. "High contrast imaging at the photon noise limit with self-calibrating WFS/C systems". In: *Techniques and Instrumentation for Detection of Exoplanets X*. Ed. by Stuart B. Shaklan and Garreth J. Ruane. SPIE, Sept. 2021. DOI: 10.1117/12.2594885 (cited on page 22).

[68] Olivier Guyon et al. *Linear Dark Field Control Milestones White Paper)*. https://exoplanets.nasa.gov/internal_resources/2240/. Apr. 2022 (cited on page 23).

[69] Laura E. Coyle et al. "Achieved technology maturation of key component-level technologies for ultra-stable optical systems". In: *Space Telescopes and Instrumentation 2022: Optical, Infrared, and Millimeter Wave*. Ed. by Laura E. Coyle, Marshall D. Perrin, and Shuji Matsuura. SPIE, Aug. 2022. DOI: 10.1117/12.2627057 (cited on page 23).

[70] Laura E. Coyle and J. S. Knight. "Integrated modeling of large, segmented telescopes with ultra-stable wavefronts". In: *Space Telescopes and Instrumentation 2022: Optical, Infrared, and Millimeter Wave*. Ed. by Laura E. Coyle, Marshall D. Perrin, and Shuji Matsuura. SPIE, Aug. 2022. DOI: 10.1117/12.2629079 (cited on page 23).

[71] Kevin Weed et al. “Mechanisms for large IR/O/UV space telescope thermal efficiency”. In: *Space Telescopes and Instrumentation 2022: Optical, Infrared, and Millimeter Wave*. Ed. by Laura E. Coyle, Marshall D. Perrin, and Shuji Matsuura. SPIE, Aug. 2022. DOI: 10.1117/12.2629468 (cited on page 23).

[72] Laurent Pueyo et al. “Coronagraphic detection of Earth-like planets with large, actively controlled space telescopes”. In: *Journal of Astronomical Telescopes, Instruments, and Systems* 8.04 (Oct. 2022). DOI: 10.1117/1.jatis.8.4.049002 (cited on page 23).

[73] Alison A. Nordt et al. “Non-contact vibration isolation technology demonstration on a CubeSat”. In: *Space Telescopes and Instrumentation 2020: Optical, Infrared, and Millimeter Wave*. Ed. by Makenzie Lystrup et al. SPIE, Dec. 2020. DOI: 10.1117/12.2563019 (cited on page 23).

[74] Jacob H. Wirth, James E. Mason, and Alison A. Nordt. “Progress in demonstrating picometer class laser metrology using photonics integrated gauges”. In: *Space Telescopes and Instrumentation 2022: Optical, Infrared, and Millimeter Wave*. Ed. by Laura E. Coyle, Marshall D. Perrin, and Shuji Matsuura. SPIE, Aug. 2022. DOI: 10.1117/12.2630776 (cited on page 23).

[75] Kiarash Tajdaran et al. “Line-of-sight and wavefront error dynamic stability during coronagraphic imaging for a 6.7-meter inscribed diameter UVOIR segmented telescope with non-contact pointing and vibration isolation”. In: *Space Telescopes and Instrumentation 2022: Optical, Infrared, and Millimeter Wave*. Ed. by Laura E. Coyle, Marshall D. Perrin, and Shuji Matsuura. SPIE, Aug. 2022. DOI: 10.1117/12.2630343 (cited on page 23).

[76] Lee D. Feinberg et al. “Ultra-stable telescope testbed: results and implications”. In: *Space Telescopes and Instrumentation 2022: Optical, Infrared, and Millimeter Wave*. Ed. by Laura E. Coyle, Marshall D. Perrin, and Shuji Matsuura. SPIE, Aug. 2022. DOI: 10.1117/12.2626490 (cited on page 23).

[77] Roser Juanola-Parramon et al. “Modeling and performance analysis of the LUVOIR coronagraph instrument”. In: *Journal of Astronomical Telescopes, Instruments, and Systems* 8.03 (July 2022). DOI: 10.1117/1.jatis.8.3.034001 (cited on page 23).

[78] A.J. Eldorado Riggs et al. “Fast linearized coronagraph optimizer (FALCO) I: a software toolbox for rapid coronagraphic design and wavefront correction”. In: *Space Telescopes and Instrumentation 2018: Optical, Infrared, and Millimeter Wave*. Ed. by Howard A. MacEwen et al. SPIE, Aug. 2018. DOI: 10.1117/12.2313812 (cited on page 24).

[79] Dwight Moody et al. “Fast linearized coronagraph optimizer (FALCO) II: optical model validation and time savings over other methods”. In: *Space Telescopes and Instrumentation 2018: Optical, Infrared, and Millimeter Wave*. Ed. by Howard A. MacEwen et al. SPIE, July 2018. DOI: 10.1117/12.2312950 (cited on page 24).

[80] Carl T. Coker et al. "Fast linearized coronagraph optimizer (FALCO) III: optimization of key coronagraph design parameters". In: *Space Telescopes and Instrumentation 2018: Optical, Infrared, and Millimeter Wave*. Ed. by Howard A. MacEwen et al. SPIE, Aug. 2018. DOI: 10.1117/12.2313788 (cited on page 24).

[81] A.J. Eldorado Riggs et al. "Fast linearized coronagraph optimizer (FALCO) IV: coronagraph design survey for obstructed and segmented apertures". In: *Space Telescopes and Instrumentation 2018: Optical, Infrared, and Millimeter Wave*. Ed. by Howard A. MacEwen et al. SPIE, Aug. 2018. DOI: 10.1117/12.2312973 (cited on page 24).

[82] Axel Potier et al. "Adaptive optics performance of a simulated coronagraph instrument on a large, segmented space telescope in steady state". In: *Journal of Astronomical Telescopes, Instruments, and Systems* 8.03 (Sept. 2022). DOI: 10.1117/1.jatis.8.3.035002 (cited on page 24).

[83] Dmitry Savransky and Daniel Garrett. "WFIRST-AFTA coronagraph science yield modeling with EXOSIMS". In: *Journal of Astronomical Telescopes, Instruments, and Systems* 2.1 (Dec. 2015), p. 011006. DOI: 10.1117/1.jatis.2.1.011006 (cited on page 25).

[84] Christopher C. Stark et al. "Maximizing the ExoEarth Candidate Yield from a Future Direct Imaging Mission". In: *The Astrophysical Journal* 795.2 (Oct. 2014), p. 122. DOI: 10.1088/0004-637x/795/2/122 (cited on page 25).

[85] B. Scott Gaudi, Michael Meyer, and Jessie Christiansen. "The Demographics of Exoplanets". In: *ExoFrontiers*. IOP Publishing, Oct. 2021. DOI: 10.1088/2514-3433/abfa8fch2 (cited on page 25).

[86] Steve Bryson et al. "The Occurrence of Rocky Habitable-zone Planets around Solar-like Stars from Kepler Data". In: *The Astronomical Journal* 161.1 (Dec. 2020), p. 36. DOI: 10.3847/1538-3881/abc418 (cited on page 25).

[87] Danley C. Hsu et al. "Occurrence Rates of Planets Orbiting FGK Stars: Combining Kepler, Gaia DR2, and Bayesian Inference". In: *The Astronomical Journal* 158.3 (Aug. 2019), p. 109. DOI: 10.3847/1538-3881/ab31ab (cited on page 25).

[88] Galen J. Bergsten et al. "The Demographics of Kepler's Earths and Super-Earths into the Habitable Zone". In: *The Astronomical Journal* 164.5 (Oct. 2022), p. 190. DOI: 10.3847/1538-3881/ac8fea (cited on page 25).

[89] Kunjithapatham Balasubramanian et al. "Coatings for large-aperture UV optical infrared space telescope mirrors". In: *UV/Optical/IR Space Telescopes and Instruments: Innovative Technologies and Concepts VIII*. Ed. by Howard A. MacEwen and James B. Breckinridge. SPIE, Sept. 2017. DOI: 10.1117/12.2274794 (cited on page 26).

[90] Manuel A. Quijada et al. "Advanced Al mirrors protected with LiF overcoat to realize stable mirror coatings for astronomical telescopes". In: *Advances in Optical and Mechanical Technologies for Telescopes and Instrumentation V*. Ed. by Roland Geyl and Ramón Navarro. SPIE, Aug. 2022. DOI: 10.1117/12.2630585 (cited on page 26).

[91] D. A. Sheikh, S. J. Connell, and R. S. Dummer. "Durable silver coating for Kepler Space Telescope primary mirror". In: *Space Telescopes and Instrumentation 2008: Optical, Infrared, and Millimeter*. Ed. by Jr. Jacobus M. Oschmann, Mattheus W. M. de Graauw, and Howard A. MacEwen. SPIE, July 2008. DOI: 10.1117/12.789996 (cited on page 26).

[92] Lee D. Feinberg et al. "Commissioning the James Webb Space Telescope optical telescope element". In: *Space Telescopes and Instrumentation 2022: Optical, Infrared, and Millimeter Wave*. Ed. by Laura E. Coyle, Marshall D. Perrin, and Shuji Matsuura. SPIE, Aug. 2022. DOI: 10.1117/12.2628626 (cited on page 29).

[93] J. Scott Knight and Paul A. Lightsey. "Webb Telescope imaging performance". In: *Space Telescopes and Instrumentation 2022: Optical, Infrared, and Millimeter Wave*. Ed. by Laura E. Coyle, Marshall D. Perrin, and Shuji Matsuura. SPIE, Aug. 2022. DOI: 10.1117/12.2632186 (cited on page 29).

[94] Gary Matthews et al. "Kodak AMSD mirror program: overview and cryo test results". In: *SPIE Proceedings*. Ed. by H. Philip Stahl. SPIE, Jan. 2004. DOI: 10.1117/12.505181 (cited on page 29).

[95] Michael J. Eisenhower et al. "ATLAST ULE mirror segment performance analytical predictions based on thermally induced distortions". In: *SPIE Proceedings*. Ed. by Howard A. MacEwen and James B. Breckinridge. SPIE, Sept. 2015. DOI: 10.1117/12.2188008 (cited on page 29).

[96] Rudranarayan Mukherjee, Nicholas Siegler, and Harley Thronson. "The Future of Space Astronomy will be Built: Results from the NASA-Chartered In-Space Assembled Telescope (iSAT) Study". In: *70th International Astronautical Congress (IAC)*. https://iafastro.directory/iac/archive/browse/IAC-19/A7/1/49711/. International Astronautical Federation. Oct. 2019 (cited on page 29).

[97] Gerard L. Rafanelli et al. "Revolutionary astrophysics using an incoherent synthetic optical aperture". In: *UV/Optical/IR Space Telescopes and Instruments: Innovative Technologies and Concepts VIII*. Ed. by Howard A. MacEwen and James B. Breckinridge. SPIE, Sept. 2017. DOI: 10.1117/12.2272782 (cited on page 30).

[98] Dániel Apai et al. "A Thousand Earths: A Very Large Aperture, Ultralight Space Telescope Array for Atmospheric Biosignature Surveys". In: *The Astronomical Journal* 158.2 (July 2019), p. 83. DOI: 10.3847/1538-3881/ab2631 (cited on page 30).

[99] Joseph J. Green et al. "Architecture for space-based exoplanet spectroscopy in the mid-infrared". In: *Space Telescopes and Instrumentation 2018: Optical, Infrared, and Millimeter Wave*. Ed. by Howard A. MacEwen et al. SPIE, July 2018. DOI: 10.1117/12.2314338 (cited on page 30).

[100] James B. Breckinridge et al. "Stealth telescopes for space and ground astronomy". In: *UV/Optical/IR Space Telescopes and Instruments: Innovative Technologies and Concepts IX*. Ed. by James B. Breckinridge, H. Philip Stahl, and Allison A. Barto. SPIE, Sept. 2019. DOI: 10.1117/12.2528825 (cited on page 30).

[101] Sara Seager et al. "The Exo-S probe class starshade mission". In: *SPIE Proceedings*. Ed. by Stuart Shaklan. SPIE, Sept. 2015. DOI: 10.1117/12.2190378 (cited on page 31).

[102] David C. Redding et al. "A Habitable Exoplanet Observatory (HabEx) starshade-only architectures". In: *UV/Optical/IR Space Telescopes and Instruments: Innovative Technologies and Concepts IX*. Ed. by James B. Breckinridge, H. Philip Stahl, and Allison A. Barto. SPIE, Sept. 2019. DOI: 10.1117/12.2529646 (cited on pages 31, 63).

[103] Phil Willems and Doug Lisman. "NASA's starshade technology development activity". In: *Journal of Astronomical Telescopes, Instruments, and Systems* 7.02 (Jan. 2021). DOI: 10.1117/1.jatis.7.2.021203 (cited on pages 32, 39).

[104] Phil Willems. *Starshade to TRL5 (S5) Technology Development Plan*. https://exoplanets.nasa.gov/exep/technology/starshade/. Dec. 2018 (cited on page 32).

[105] Eliad Peretz et al. "Mapping the observable sky for a Remote Occulter working with ground-based telescopes". In: *Journal of Astronomical Telescopes, Instruments, and Systems* 7.02 (Jan. 2021). DOI: 10.1117/1.jatis.7.2.021212 (cited on page 32).

[106] Markus Janson et al. "Occulter to earth: prospects for studying earth-like planets with the E-ELT and a space-based occulter". In: *Experimental Astronomy* (Aug. 2021). DOI: 10.1007/s10686-021-09792-y (cited on page 32).

[107] Renyu Hu et al. "Overview and reassessment of noise budget of starshade exoplanet imaging". In: *Journal of Astronomical Telescopes, Instruments, and Systems* 7.02 (Jan. 2021). DOI: 10.1117/1.jatis.7.2.021205 (cited on page 33).

[108] Anthony Harness et al. "Optical verification experiments of subscale starshades". In: *Journal of Astronomical Telescopes, Instruments, and Systems* 7.02 (Jan. 2021). DOI: 10.1117/1.jatis.7.2.021207 (cited on pages 34, 35).

[109] E. Schindhelm et al. "Laboratory studies of petal-shaped occulters". In: *SPIE Proceedings*. Ed. by Daniel R. Coulter. SPIE, Sept. 2007. DOI: 10.1117/12.734480 (cited on page 34).

[110] Douglas B. Leviton et al. "White-light demonstration of one hundred parts per billion irradiance suppression in air by new starshade occulters". In: *SPIE Proceedings*. Ed. by Howard A. MacEwen and James B. Breckinridge. SPIE, Sept. 2007. DOI: 10.1117/12.742927 (cited on page 34).

[111] Amy S. Lo et al. "New Worlds Probe". In: *SPIE Proceedings*. Ed. by Jr. Jacobus M. Oschmann, Mark C. Clampin, and Howard A. MacEwen. SPIE, July 2010. DOI: 10.1117/12.856270 (cited on page 34).

[112] Rocco Samuele et al. "Progress at the starshade testbed at Northrop Grumman Aerospace Systems: comparisons with computer simulations". In: *SPIE Proceedings*. Ed. by Jr. Jacobus M. Oschmann, Mark C. Clampin, and Howard A. MacEwen. SPIE, July 2010. DOI: 10.1117/12.856334 (cited on page 34).

[113] Anthony Harness et al. "Ground-based testing and demonstrations of starshades". In: *SPIE Proceedings*. Ed. by Howard A. MacEwen et al. SPIE, July 2016. DOI: 10.1117/12.2231916 (cited on page 34).

[114] Daniel Smith et al. "Measurements of high-contrast starshade performance in the field". In: *SPIE Proceedings*. Ed. by Howard A. MacEwen et al. SPIE, July 2016. DOI: 10.1117/12.2232841 (cited on page 34).

[115] Eric Cady et al. "Broadband suppression and occulter position sensing at the Princeton occulter testbed". In: *SPIE Proceedings*. Ed. by Jr. Jacobus M. Oschmann, Mark C. Clampin, and Howard A. MacEwen. SPIE, July 2010. DOI: 10.1117/12.857133 (cited on page 34).

[116] Anthony Harness et al. *Starshade Technology Development Activity Milestone 1A:Demonstration of High Contrast in Monochromatic Light at a Flight-like Fresnel Number*. https://exoplanets.nasa.gov/internal_resources/1210/. Jan. 2019 (cited on page 35).

[117] Anthony Harness et al. *Starshade Technology Development Activity Milestone 1B: Demonstration of High Contrast in Broadband Light at a Flight-like Fresnel Number*. https://exoplanets.nasa.gov/internal_resources/1211/. Mar. 2019 (cited on page 35).

[118] Anthony Harness et al. *Starshade Technology Development Activity Milestone 2: Optical Model Validation*. https://exoplanets.nasa.gov/internal_resources/2526/. Oct. 2022 (cited on page 35).

[119] Stuart Shaklan et al. "Completion of model validation experiments at the Princeton starshade testbed". In: *Space Telescopes and Instrumentation 2022: Optical, Infrared, and Millimeter Wave*. Ed. by Laura E. Coyle, Marshall D. Perrin, and Shuji Matsuura. SPIE, Aug. 2022. DOI: 10.1117/12.2629445 (cited on page 35).

[120] Stefan R. Martin et al. "Starshade optical edge modeling, requirements, and laboratory tests". In: *SPIE Proceedings*. Ed. by Stuart Shaklan. SPIE, Sept. 2013. DOI: 10.1117/12.2024188 (cited on page 36).

[121] John Steeves et al. "Development of low-scatter optical edges for starshades". In: *Advances in Optical and Mechanical Technologies for Telescopes and Instrumentation III*. Ed. by Roland Geyl and Ramón Navarro. SPIE, July 2018. DOI: 10.1117/12.2312694 (cited on page 36).

[122] Evan W. Hilgemann et al. "Advancements in precision edges for a starshade external occulter". In: *Techniques and Instrumentation for Detection of Exoplanets IX*. Ed. by Stuart B. Shaklan. SPIE, Sept. 2019. DOI: 10.1117/12.2530160 (cited on page 36).

[123] Evan Hilgemann et al. *Starshade Technology Development Activity Milestone 3: Demonstration of Solar Glint Lobe Scatter Performance*. https://exoplanets.nasa.gov/internal_resources/1544/. Nov. 2019 (cited on page 36).

[124] Stuart Shaklan et al. "Solar glint from uncoated starshade optical edges". In: *Journal of Astronomical Telescopes, Instruments, and Systems* 7.02 (Jan. 2021). DOI: 10.1117/1.jatis.7.2.021204 (cited on pages 37, 80).

[125] Dylan McKeithen et al. "Antireflection coatings on starshade optical edges for solar glint suppression". In: *Journal of Astronomical Telescopes, Instruments, and Systems* 7.02 (Jan. 2021). DOI: 10.1117/1.jatis.7.2.021208 (cited on page 37).

[126] Michael Bottom et al. "Starshade formation flying I: optical sensing". In: *Journal of Astronomical Telescopes, Instruments, and Systems* 6.01 (Feb. 2020), p. 1. DOI: 10.1117/1.jatis.6.1.015003 (cited on page 38).

[127] Thibault L. B. Flinois et al. "Efficient starshade retargeting architecture using chemical propulsion". In: *Journal of Astronomical Telescopes, Instruments, and Systems* 7.02 (Jan. 2021). DOI: 10.1117/1.jatis.7.2.021206 (cited on page 38).

[128] Leonel Palacios, Anthony Harness, and N. Jeremy Kasdin. "Hardware demonstration of starshade formation flying sensing and control algorithms". In: *Techniques and Instrumentation for Detection of Exoplanets IX*. Ed. by Stuart B. Shaklan. SPIE, Sept. 2019. DOI: 10.1117/12.2528437 (cited on page 38).

[129] Thibault Flinois et al. *S5: Starshade Technology to TRL5 Milestone 4 Report: Lateral Formation Sensing and Control*. https://exoplanets.nasa.gov/internal_resources/1077/. Nov. 2018 (cited on page 38).

[130] Stefan R. Martin and Thibault L. B. Flinois. "Simultaneous sensing of telescope pointing and starshade position". In: *Journal of Astronomical Telescopes, Instruments, and Systems* 8.01 (Mar. 2022). DOI: 10.1117/1.jatis.8.1.014010 (cited on page 38).

[131] Manan Arya et al. "Demonstration of deployment repeatability of key subsystems of a furled starshade architecture". In: *Journal of Astronomical Telescopes, Instruments, and Systems* 7.02 (Jan. 2021). DOI: 10.1117/1.jatis.7.2.021202 (cited on pages 38–40).

[132] M.W. Thomson. "The AstroMesh deployable reflector". In: *IEEE Antennas and Propagation Society International Symposium. 1999 Digest. Held in conjunction with: USNC/URSI National Radio Science Meeting (Cat. No.99CH37010)*. Vol. 3. 1999, pp. 1516–1519. DOI: 10.1109/APS.1999.838231 (cited on page 39).

[133] Flora Mechentel et al. *Starshade Technology Development Activity Milestone 5A: Verify Petal Pre-launch Accuracy*. https://exoplanets.nasa.gov/internal_resources/1683/. Aug. 2020 (cited on page 40).

[134] David Webb et al. *Starshade Technology Development Activity Milestone 6A: Verify Petal Shape on-Orbit Stability*. https://exoplanets.nasa.gov/internal_resources/2008/. Aug. 2021 (cited on page 40).

[135] Manan Arya et al. *Starshade Technology Development Activity Milestone 7A:Demonstration of Dimensional Stability of Perimeter Truss Bay Longeron and Node*. https://exoplanets.nasa.gov/internal_resources/1677/. July 2020 (cited on page 42).

[136] David Webb et al. *Starshade Technology Development Activity Milestone 8A: Verify Petal Position On-Orbit Stability*. https://exoplanets.nasa.gov/internal_resources/1696/. Feb. 2020 (cited on page 42).

[137] Manan Arya et al. *Starshade Technology Development Activity Milestone 7C: Demonstration of Deployment Accuracy of the Starshade Inner Disk Subsystem*. https://exoplanets.nasa.gov/internal_resources/1676/. July 2020 (cited on page 42).

[138] Bernard J. Rauscher et al. "Radiation tolerant, photon counting, visible, and near-IR detectors for space coronagraphs". In: *Space Telescopes and Instrumentation 2022: Optical, Infrared, and Millimeter Wave*. Ed. by Laura E. Coyle, Marshall D. Perrin, and Shuji Matsuura. SPIE, Aug. 2022. DOI: 10.1117/12.2628961 (cited on pages 45, 47).

[139] C.J. Bebek et al. "Status of the CCD development for the Dark Energy Spectroscopic Instrument". In: *Journal of Instrumentation* 12.04 (Apr. 2017), pp. C04018–C04018. DOI: 10.1088/1748-0221/12/04/c04018 (cited on page 45).

[140] Javier Tiffenberg et al. "Single-Electron and Single-Photon Sensitivity with a Silicon Skipper CCD". In: *Physical Review Letters* 119.13 (Sept. 2017), p. 131802. DOI: 10.1103/physrevlett.119.131802 (cited on page 45).

[141] Peter W. A. Roming et al. "The Swift Ultra-Violet/Optical Telescope". In: *Space Science Reviews* 120.3-4 (Oct. 2005), pp. 95–142. DOI: 10.1007/s11214-005-5095-4 (cited on page 45).

[142] Gert Finger et al. "Development of high-speed, low-noise NIR HgCdTe avalanche photodiode arrays for adaptive optics and interferometry". In: *SPIE Proceedings*. Ed. by Andrew D. Holland and David A. Dorn. SPIE, July 2010. DOI: 10.1117/12.857316 (cited on page 45).

[143] B. A. Mazin et al. "ARCONS: A 2024 Pixel Optical through Near-IR Cryogenic Imaging Spectrophotometer". In: *Publications of the Astronomical Society of the Pacific* 125.933 (Nov. 2013), pp. 1348–1361. DOI: 10.1086/674013 (cited on page 45).

[144] M. S. Allman et al. "A near-infrared 64-pixel superconducting nanowire single photon detector array with integrated multiplexed readout". In: *Applied Physics Letters* 106.19 (May 2015), p. 192601. DOI: 10.1063/1.4921318 (cited on page 45).

[145] Leon K. Harding et al. "Technology advancement of the CCD201-20 EMCCD for the WFIRST coronagraph instrument: sensor characterization and radiation damage". In: *Journal of Astronomical Telescopes, Instruments, and Systems* 2.1 (Dec. 2015), p. 011007. DOI: 10.1117/1.jatis.2.1.011007 (cited on page 46).

[146] Charles-Antoine Claveau et al. "First tests of a 1 megapixel near-infrared avalanche photodiode array for ultra-low background space astronomy". In: *X-Ray, Optical, and Infrared Detectors for Astronomy X*. Ed. by Andrew D. Holland and James Beletic. SPIE, Aug. 2022. DOI: 10.1117/12.2627285 (cited on pages 46, 47).

[147] Jiaju Ma et al. "Ultra-high-resolution quanta image sensor with reliable photon-number-resolving and high dynamic range capabilities". In: *Scientific Reports* 12.1 (Aug. 2022). DOI: 10.1038/s41598-022-17952-z (cited on page 47).

[148] Justin P. Gallagher et al. "Characterization of single-photon sensing and photon-number resolving CMOS image sensors". In: *X-Ray, Optical, and Infrared Detectors for Astronomy X*. Ed. by Andrew D. Holland and James Beletic. SPIE, Aug. 2022. DOI: 10.1117/12.2629006 (cited on page 47).

[149] Saad Ahmed et al. "Understanding the evolution of radiation damage on the Gaia CCDs after 72 months at L2". In: *Journal of Astronomical Telescopes, Instruments, and Systems* 8.01 (Feb. 2022). DOI: 10.1117/1.jatis.8.1.016003 (cited on page 47).

[150] Markus Loose et al. "The ACADIA ASIC - detector control and digitization for the Wide-Field Infrared Survey Telescope (WFIRST)". In: *High Energy, Optical, and Infrared Detectors for Astronomy VIII*. Ed. by Andrew D. Holland and James Beletic. SPIE, July 2018. DOI: 10.1117/12.2313067 (cited on page 47).

[151] Noah J. Swimmer et al. "The PICTURE-C MKID camera". In: *Ground-based and Airborne Instrumentation for Astronomy VIII*. Ed. by Christopher J. Evans, Julia J. Bryant, and Kentaro Motohara. SPIE, Dec. 2020. DOI: 10.1117/12.2561770 (cited on page 48).

[152] Michael E. Hoenk et al. "2D-doped silicon detectors for UV/optical/NIR and x-ray astronomy". In: *X-Ray, Optical, and Infrared Detectors for Astronomy X*. Ed. by Andrew D. Holland and James Beletic. SPIE, Aug. 2022. DOI: 10.1117/12.2631542 (cited on page 49).

[153] Timothee Greffe et al. "Characterization of low light performance of a complementary metal-oxide semiconductor sensor for ultraviolet astronomical applications". In: *Journal of Astronomical Telescopes, Instruments, and Systems* 8.02 (Apr. 2022). DOI: 10.1117/1.jatis.8.2.026004 (cited on page 49).

[154] Guillem Anglada-Escudé et al. "A terrestrial planet candidate in a temperate orbit around Proxima Centauri". In: *Nature* 536.7617 (Aug. 2016), pp. 437–440. DOI: 10.1038/nature19106 (cited on page 50).

[155] Rhonda Morgan et al. "Faster Exo-Earth yield for HabEx and LUVOIR via extreme precision radial velocity prior knowledge". In: *Journal of Astronomical Telescopes, Instruments, and Systems* 7.02 (June 2021). DOI: 10.1117/1.jatis.7.2.021220 (cited on page 50).

[156] Debra A. Fischer et al. "State of the Field: Extreme Precision Radial Velocities". In: *Publications of the Astronomical Society of the Pacific* 128.964 (May 2016), p. 066001. DOI: 10.1088/1538-3873/128/964/066001 (cited on page 51).

[157] Peter Plavchan et al. *EarthFinder: A Precise Radial Velocity Probe Mission Concept For the Detection of Earth-Mass Planets Orbiting Sun-like Stars*. 2018. DOI: 10.48550/ARXIV.1803.03960 (cited on page 51).

[158] Jonathan Crass et al. "Extreme Precision Radial Velocity Working Group Final Report". In: *arXiv e-prints*, arXiv:2107.14291 (July 2021), arXiv:2107.14291 (cited on pages 51, 53).

[159] Samuel Halverson et al. "A comprehensive radial velocity error budget for next generation Doppler spectrometers". In: *SPIE Proceedings*. Ed. by Christopher J. Evans, Luc Simard, and Hideki Takami. SPIE, Aug. 2016. DOI: 10.1117/12.2232761 (cited on pages 51, 73).

[160] Francesco A. Pepe et al. "ESPRESSO: the Echelle spectrograph for rocky exoplanets and stable spectroscopic observations". In: *SPIE Proceedings*. Ed. by Ian S. McLean, Suzanne K. Ramsay, and Hideki Takami. SPIE, July 2010. DOI: 10.1117/12.857122 (cited on page 53).

[161] C. Jurgenson et al. "EXPRES: a next generation RV spectrograph in the search for earth-like worlds". In: *SPIE Proceedings*. Ed. by Christopher J. Evans, Luc Simard, and Hideki Takami. SPIE, Aug. 2016. DOI: 10.1117/12.2233002 (cited on page 53).

[162] Andreas Seifahrt et al. "MAROON-X: a radial velocity spectrograph for the Gemini Observatory". In: *Ground-based and Airborne Instrumentation for Astronomy VII*. Ed. by Hideki Takami, Christopher J. Evans, and Luc Simard. SPIE, July 2018. DOI: 10.1117/12.2312936 (cited on page 53).

[163] C. Schwab et al. "Design of NEID, an extreme precision Doppler spectrograph for WIYN". In: *SPIE Proceedings*. Ed. by Christopher J. Evans, Luc Simard, and Hideki Takami. SPIE, Aug. 2016. DOI: 10.1117/12.2234411 (cited on page 53).

[164] Andrea S. J. Lin et al. "Observing the Sun as a Star: Design and Early Results from the NEID Solar Feed". In: *The Astronomical Journal* 163.4 (Mar. 2022), p. 184. DOI: 10.3847/1538-3881/ac5622 (cited on page 53).

[165] Stephanie Leifer et al. "A microresonator-based etalon for visible light precision radial velocity measurements". In: *Ground-based and Airborne Instrumentation for Astronomy VIII*. Ed. by Christopher J. Evans, Julia J. Bryant, and Kentaro Motohara. SPIE, Dec. 2020. DOI: 10.1117/12.2562369 (cited on page 53).

[166] Steven R. Gibson et al. "Keck Planet Finder: design updates". In: *Ground-based and Airborne Instrumentation for Astronomy VIII*. Ed. by Christopher J. Evans, Julia J. Bryant, and Kentaro Motohara. SPIE, Dec. 2020. DOI: 10.1117/12.2561783 (cited on page 53).

[167] Committee on Exoplanet Science Strategy. *Exoplanet Science Strategy*. https://nap.nationalacademies.org/catalog/25187/exoplanet-science-strategy. 2018 (cited on page 54).

[168] S. Hinkley et al. *Direct Discovery of the Inner Exoplanet in the HD206893 System*. 2022. DOI: 10.48550/ARXIV.2208.04867 (cited on page 54).

[169] Peter Melchior, David Spergel, and Arianna Lanz. "In the Crosshair: Astrometric Exoplanet Detection with WFIRST's Diffraction Spikes". In: *The Astronomical Journal* 155.2 (Feb. 2018), p. 102. DOI: 10.3847/1538-3881/aaa422 (cited on page 54).

[170] Fabien Malbet et al. "Faint objects in motion: the new frontier of high precision astrometry". In: *Experimental Astronomy* 51.3 (June 2021), pp. 845–886. DOI: 10.1007/s10686-021-09781-1 (cited on page 54).

[171] Eduardo A. Bendek et al. "Precision astrometry mission for exoplanet detection around binary stars". In: *Space Telescopes and Instrumentation 2018: Optical, Infrared, and Millimeter Wave*. Ed. by Howard A. MacEwen et al. SPIE, Aug. 2018. DOI: 10.1117/12.2313919 (cited on pages 54, 55).

[172] Bijan Nemati et al. "The Micro-arcsecond Astrometry Small Satellite: MASS". In: *Space Telescopes and Instrumentation 2020: Optical, Infrared, and Millimeter Wave*. Ed. by Makenzie Lystrup et al. SPIE, Dec. 2020. DOI: 10.1117/12.2574986 (cited on pages 54, 55).

[173] Gaia Collaboration et al. "Gaia Early Data Release 3. Summary of the contents and survey properties". In: *Astronomy & Astrophysics* (Dec. 2020). DOI: 10.1051/0004-6361/202039657 (cited on page 55).

[174] and R. Abuter et al. "Improved GRAVITY astrometric accuracy from modeling optical aberrations". In: *Astronomy and Astrophysics* 647 (Mar. 2021), A59. DOI: 10.1051/0004-6361/202040208 (cited on page 55).

[175] S. Lacour et al. "First direct detection of an exoplanet by optical interferometry". In: *Astronomy and Astrophysics* 623 (Mar. 2019), p. L11. DOI: 10.1051/0004-6361/201935253 (cited on pages 55, 60).

[176] A. Crouzier et al. "A detector interferometric calibration experiment for high precision astrometry". In: *Astronomy and Astrophysics* 595 (Nov. 2016), A108. DOI: 10.1051/0004-6361/201526321 (cited on page 55).

[177] Eduardo A. Bendek et al. "Status of NASA's stellar astrometry testbeds for exoplanet detection: Science and technology overview". In: *Space Telescopes and Instrumentation 2020: Optical, Infrared, and Millimeter Wave*. Ed. by Makenzie Lystrup et al. SPIE, Jan. 2021. DOI: 10.1117/12.2562994 (cited on page 55).

[178] Alessandro Sozzetti. "Gaia and exoplanets: a revolution in the making". In: *Techniques and Instrumentation for Detection of Exoplanets VIII*. Ed. by Stuart Shaklan. SPIE, Sept. 2017. DOI: 10.1117/12.2276987 (cited on page 56).

[179] A.-M. Lagrange et al. "Using the Sun to estimate Earth-like planets detection capabilities". In: *Astronomy and Astrophysics* 528 (Feb. 2011), p. L9. DOI: 10.1051/0004-6361/201016354 (cited on page 56).

[180] Thomas P. Greene et al. "Characterizing Transiting Exoplanet Atmospheres with JWST". In: *The Astrophysical Journal* 817.1 (Jan. 2016), p. 17. DOI: 10.3847/0004-637x/817/1/17 (cited on page 57).

[181] Thomas L. Roellig et al. "Mid-infrared detector development for the Origins Space Telescope". In: *Journal of Astronomical Telescopes, Instruments, and Systems* 6.04 (Dec. 2020). DOI: 10.1117/1.jatis.6.4.041503 (cited on page 57).

[182] Johannes G. Staguhn et al. "Development of an ultra-stable mid-infrared detector array for space-based exoplanet transit and phase curve spectroscopy". In: *Space Telescopes and Instrumentation 2022: Optical, Infrared, and Millimeter Wave*. Ed. by Laura E. Coyle, Marshall D. Perrin, and Shuji Matsuura. SPIE, Aug. 2022. DOI: 10.1117/12.2630424 (cited on page 58).

[183] Meghan Dorn et al. "A monolithic 2k x 2k LWIR HgCdTe detector array for passively cooled space missions". In: *High Energy, Optical, and Infrared Detectors for Astronomy VIII*. Ed. by Andrew D. Holland and James Beletic. SPIE, July 2018. DOI: 10.1117/12.2313521 (cited on page 58).

[184] Brittany E. Miles et al. "Testing a 10 micron HgCdTe detector for ground-based exoplanet science". In: *Techniques and Instrumentation for Detection of Exoplanets X*. Ed. by Stuart B. Shaklan and Garreth J. Ruane. SPIE, Sept. 2021. DOI: 10.1117/12.2594915 (cited on page 58).

[185] Planck Collaboration. "Planck early results. II. The thermal performance of Planck". In: *Astronomy and Astrophysics* 536 (Dec. 2011), A2. DOI: 10.1051/0004-6361/201116486 (cited on page 59).

[186] Bernard J. Rauscher et al. "Detectors and cooling technology for direct spectroscopic biosignature characterization". In: *Journal of Astronomical Telescopes, Instruments, and Systems* 2.4 (Aug. 2016), p. 041212. DOI: 10.1117/1.jatis.2.4.041212 (cited on page 59).

[187] A. Boccaletti et al. “The Mid-Infrared Instrument for the James Webb Space Telescope, V: Predicted Performance of the MIRI Coronagraphs”. In: *Publications of the Astronomical Society of the Pacific* 127.953 (July 2015), pp. 633–645. DOI: 10.1086/682256 (cited on page 60).

[188] Aoi Takahashi et al. “Laboratory demonstration of a cryogenic deformable mirror for wavefront correction of space-borne infrared telescopes”. In: *Applied Optics* 56.23 (Aug. 2017), p. 6694. DOI: 10.1364/ao.56.006694 (cited on page 60).

[189] D. Defrère et al. “Nulling Data Reduction and On-sky Performance of the Large Binocular Telescope Interferometer”. In: *The Astrophysical Journal* 824.2 (June 2016), p. 66. DOI: 10.3847/0004-637x/824/2/66 (cited on page 60).

[190] Gravity Collaboration. “First Light for GRAVITY: A New Era for Optical Interferometry”. In: *The Messenger* 170 (Dec. 2017), pp. 10–15. DOI: 10.18727/0722-6691/5048 (cited on page 60).

[191] R. N. Bracewell. “Detecting nonsolar planets by spinning infrared interferometer”. In: *Nature* 274.5673 (Aug. 1978), pp. 780–781. DOI: 10.1038/274780a0 (cited on page 60).

[192] S. P. Quanz et al. “Large Interferometer For Exoplanets (LIFE)”. In: *Astronomy and Astrophysics* 664 (Aug. 2022), A21. DOI: 10.1051/0004-6361/202140366 (cited on page 61).

[193] Daniel Echeverri et al. “Detecting and characterizing close-in exoplanets with vortex fiber nulling”. In: *Optical and Infrared Interferometry and Imaging VII*. Ed. by Antoine Mérand, Stephanie Sallum, and Peter G. Tuthill. SPIE, Dec. 2020. DOI: 10.1117/12.2563142 (cited on page 61).

[194] H. Philip Stahl et al. “Habitable-Zone Exoplanet Observatory baseline 4-m telescope: systems-engineering design process and predicted structural thermal optical performance”. In: *Journal of Astronomical Telescopes, Instruments, and Systems* 6.03 (Aug. 2020). DOI: 10.1117/1.jatis.6.3.034004 (cited on pages 62, 63, 70).

[195] Alain C. Carrier et al. “Development and demonstration of a precision latch for deployable optical systems”. In: *SPIE Proceedings*. Ed. by John C. Mather. SPIE, Mar. 2003. DOI: 10.1117/12.461549 (cited on page 62).

[196] Babak N. Saif et al. “Picometer level spatial metrology for next generation telescopes”. In: *UV/Optical/IR Space Telescopes and Instruments: Innovative Technologies and Concepts IX*. Ed. by James B. Breckinridge, H. Philip Stahl, and Allison A. Barto. SPIE, Sept. 2019. DOI: 10.1117/12.2543034 (cited on page 63).

[197] Stefan Martin et al. “HabEx Lite: a starshade-only habitable exoplanet imager alternative”. In: *Space Telescopes and Instrumentation 2018: Optical, Infrared, and Millimeter Wave*. Ed. by Howard A. MacEwen et al. SPIE, July 2018. DOI: 10.1117/12.2310058 (cited on page 63).

[198] Laurent Pueyo et al. "Fundamental limits of high contrast imaging with continuous WFS&C control in space." In: *Techniques and Instrumentation for Detection of Exoplanets X*. Ed. by Stuart B. Shaklan and Garreth J. Ruane. SPIE, Aug. 2021. DOI: 10.1117/12.2594955 (cited on pages 65, 71).

[199] Nicholas Belsten et al. "Strategies for high order wavefront sensing and control (HOWFSC) computation on future space telescopes". In: *Techniques and Instrumentation for Detection of Exoplanets X*. Ed. by Stuart B. Shaklan and Garreth J. Ruane. SPIE, Sept. 2021. DOI: 10.1117/12.2594695 (cited on pages 65, 66).

[200] Ruslan Belikov et al. "Theoretical performance limits for coronagraphs on obstructed and unobstructed apertures: how much can current designs be improved?" In: *Techniques and Instrumentation for Detection of Exoplanets X*. Ed. by Stuart B. Shaklan and Garreth J. Ruane. SPIE, Sept. 2021. DOI: 10.1117/12.2594855 (cited on page 65).

[201] Amir Give'on, Brian D. Kern, and Stuart Shaklan. "Pair-wise, deformable mirror, image plane-based diversity electric field estimation for high contrast coronagraphy". In: *SPIE Proceedings*. Ed. by Stuart Shaklan. SPIE, Sept. 2011. DOI: 10.1117/12.895117 (cited on page 66).

[202] Tyler D. Groff et al. "Methods and limitations of focal plane sensing, estimation, and control in high-contrast imaging". In: *Journal of Astronomical Telescopes, Instruments, and Systems* 2.1 (Dec. 2015), p. 011009. DOI: 10.1117/1.jatis.2.1.011009 (cited on page 66).

[203] Scott D. Will, Tyler D. Groff, and James R. Fienup. "Jacobian-free coronagraphic wavefront control using nonlinear optimization". In: *Journal of Astronomical Telescopes, Instruments, and Systems* 7.01 (Feb. 2021). DOI: 10.1117/1.jatis.7.1.019002 (cited on page 66).

[204] Scott D. Will et al. "Wavefront control with algorithmic differentiation on the HiCAT testbed". In: *Techniques and Instrumentation for Detection of Exoplanets X*. Ed. by Stuart B. Shaklan and Garreth J. Ruane. SPIE, Sept. 2021. DOI: 10.1117/12.2594283 (cited on page 66).

[205] Laura E. Coyle et al. "Technology maturation of key component-level technologies for ultra-stable optical systems". In: *Astronomical Optics: Design, Manufacture, and Test of Space and Ground Systems III*. Ed. by Pascal Hallibert et al. SPIE, Aug. 2021. DOI: 10.1117/12.2594643 (cited on pages 66, 71).

[206] David M. LoBosco et al. "Integrated modeling of optical performance for the Terrestrial Planet Finder structurally connected interferometer". In: *SPIE Proceedings*. Ed. by Simon C. Craig and Martin J. Cullum. SPIE, Sept. 2004. DOI: 10.1117/12.550929 (cited on page 66).

[207] Olivier L. de Weck et al. "Integrated modeling and dynamics simulation for the Next Generation Space Telescope (NGST)". In: *SPIE Proceedings*. Ed. by James B. Breckinridge and Peter Jakobsen. SPIE, July 2000. DOI: 10.1117/12.393964 (cited on page 66).

[208] Larry Dewell et al. “Precision telescope pointing and spacecraft vibration isolation for the Terrestrial Planet Finder Coronagraph”. In: *UV/Optical/IR Space Telescopes: Innovative Technologies and Concepts II*. Ed. by Howard A. MacEwen. SPIE, Aug. 2005. DOI: 10.1117/12.618939 (cited on page 66).

[209] G. Anderson et al. “Experimental results from the ST7 mission on LISA Pathfinder”. In: *Physical Review D* 98.10 (Nov. 2018), p. 102005. DOI: 10.1103/physrevd.98.102005 (cited on page 67).

[210] Conrhelius J. Dennehy et al. *Application of Micro-Thruster Technology for Space Observatory Pointing Stability*. NESC-RP-18-01375 https://ntrs.nasa.gov/citations/20205011556/. Dec. 2020 (cited on page 67).

[211] Nelson Pedreiro et al. “Disturbance-Free Payload Concept Demonstration”. In: *AIAA Guidance, Navigation, and Control Conference and Exhibit*. American Institute of Aeronautics and Astronautics, June 2002. DOI: 10.2514/6.2002-5027 (cited on page 68).

[212] John Z. Lou et al. “LUVOIR primary mirror segment alignment control with joint laser metrology and segment edge sensing”. In: *Space Telescopes and Instrumentation 2018: Optical, Infrared, and Millimeter Wave*. Ed. by Howard A. MacEwen et al. SPIE, July 2018. DOI: 10.1117/12.2311495 (cited on page 68).

[213] Luke Horowitz et al. “A picometer-class displacement metrology system using photonic integrated circuit”. In: *Optomechanics and Optical Alignment*. Ed. by Keith B. Doyle et al. SPIE, Aug. 2021. DOI: 10.1117/12.2594874 (cited on page 68).

[214] Xin An et al. “Laser metrology in the micro-arcsecond metrology testbed”. In: *SPIE Proceedings*. Ed. by Yun-Jiang Rao, Osuk Y. Kwon, and Gang-Ding Peng. SPIE, Feb. 2005. DOI: 10.1117/12.580030 (cited on page 68).

[215] Klaus Abich et al. “In-Orbit Performance of the GRACE Follow-on Laser Ranging Interferometer”. In: *Physical Review Letters* 123.3 (July 2019), p. 031101. DOI: 10.1103/physrevlett.123.031101 (cited on page 68).

[216] Robert M. Warden. “Cryogenic Nano-Actuator for JWST”. In: *38th Aerospace Mechanisms Symposium*. NASA CP-2006-214290 https://www.esmats.eu/amspapers/completelist.php?whichYear=2006. 2006 (cited on page 69).

[217] Marco Pisani and Andrea Giugni. “A portable picometer reference actuator with 100 μm range, picometer resolution, subnanometer accuracy and submicroradian tip-tilt error for the characterization of measuring instruments at the nanoscale”. In: *Metrologia* 55.4 (June 2018), pp. 541–557. DOI: 10.1088/1681-7575/aaca6f (cited on page 69).

[218] Patrick Egan and Jack Stone. “Temperature Stabilization System with Millikelvin Gradients for Air Refractometry Measurements Below the $10^{-}8$ Level”. en. In: 6 (Mar. 2011). https://tsapps.nist.gov/publication/get_pdf.cfm?pub_id=907214 (cited on page 70).

[219] Thomas Brooks et al. "Modeling the Extremely Lightweight Zerodur Mirror (ELZM) thermal soak test". In: *Optical Modeling and Performance Predictions IX*. Ed. by Marie B. Levine-West and Mark A. Kahan. SPIE, Sept. 2017. DOI: 10.1117/12.2274084 (cited on page 70).

[220] Leonid Pogorelyuk et al. "Information-theoretical Limits of Recursive Estimation and Closed-loop Control in High-contrast Imaging". In: *The Astrophysical Journal Supplement Series* 256.2 (Oct. 2021), p. 39. DOI: 10.3847/1538-4365/ac126d (cited on page 71).

[221] P. Szypryt et al. "Direct detection of SDSS J0926+3624 orbital expansion with ARCONS". In: *Monthly Notices of the Royal Astronomical Society* 439.3 (Feb. 2014), pp. 2765–2770. DOI: 10.1093/mnras/stu137 (cited on page 72).

[222] Jonathan Crass et al. *Extreme Precision Radial Velocity Working Group Final Report*. https://arxiv.org/abs/2107.14291. 2021. DOI: 10.48550/ARXIV.2107.14291 (cited on page 73).

[223] Joe P. Ninan et al. "Impact of crosshatch patterns in H2RGs on high-precision radial velocity measurements: exploration of measurement and mitigation paths with the Habitable-Zone Planet Finder". In: *Journal of Astronomical Telescopes, Instruments, and Systems* 5.04 (Oct. 2019), p. 1. DOI: 10.1117/1.jatis.5.4.041511 (cited on page 73).

[224] Eric B. Bechter et al. "Assessing the suitability of H4RG near-infrared detectors for precise Doppler radial velocity measurements". In: *Journal of Astronomical Telescopes, Instruments, and Systems* 5.03 (Aug. 2019), p. 1. DOI: 10.1117/1.jatis.5.3.038004 (cited on page 73).

[225] Ryan T. Blackman et al. "Performance Verification of the EXtreme PREcision Spectrograph". In: *The Astronomical Journal* 159.5 (Apr. 2020), p. 238. DOI: 10.3847/1538-3881/ab811d (cited on page 73).

[226] Eric B. Bechter et al. "Studying the impact of optical aberrations on diffraction-limited radial velocity instruments". In: *Journal of Astronomical Telescopes, Instruments, and Systems* 7.03 (Sept. 2021). DOI: 10.1117/1.jatis.7.3.035008 (cited on page 73).

[227] N. Jovanovic et al. "Efficient injection from large telescopes into single-mode fibres: Enabling the era of ultra-precision astronomy". In: *Astronomy & Astrophysics* 604 (Aug. 2017), A122. DOI: 10.1051/0004-6361/201630351 (cited on pages 74, 75).

[228] Christian Schwab et al. "Single Mode, Extreme Precision Doppler Spectrographs". In: *Proceedings of the International Astronomical Union* 8.S293 (Aug. 2012), pp. 403–406. DOI: 10.1017/s1743921313013264 (cited on page 74).

[229] Dimitri Mawet et al. "High-resolution Infrared Spectrograph for Exoplanet Characterization with the Keck and Thirty Meter Telescopes". In: *Bulletin of the American Astronomical Society*. Vol. 51. Sept. 2019, 134, p. 134 (cited on page 74).

[230] Judah Van Zandt et al. "The Spectral Calibration of VERVE". In: *2019 IEEE Aerospace Conference*. IEEE, Mar. 2019. DOI: 10.1109/aero.2019.8741644 (cited on page 74).

[231] Laird M. Close. "A review of astronomical science with visible light adaptive optics". In: *Adaptive Optics Systems V*. Ed. by Enrico Marchetti, Laird M. Close, and Jean-Pierre Véran. SPIE, July 2016. DOI: 10.1117/12.2234024 (cited on page 75).

[232] Laird M. Close et al. "Status of MagAO and review of astronomical science with visible light adaptive optics". In: *Adaptive Optics Systems VI*. Ed. by Dirk Schmidt, Laura Schreiber, and Laird M. Close. SPIE, July 2018. DOI: 10.1117/12.2313107 (cited on page 75).

[233] Laird M. Close et al. "Prediction of the planet yield of the MagAO-X ProtoPlanetS high-contrast survey for H-alpha protoplanets with MagAO-X based on first light contrasts". In: *Adaptive Optics Systems VII*. Ed. by Dirk Schmidt, Laura Schreiber, and Elise Vernet. SPIE, Dec. 2020. DOI: 10.1117/12.2561677 (cited on page 75).

[234] Julien Lozi et al. "Status of the SCExAO instrument: recent technology upgrades and path to a system-level demonstrator for PSI". In: *Adaptive Optics Systems VII*. Ed. by Dirk Schmidt, Laura Schreiber, and Elise Vernet. SPIE, Dec. 2020. DOI: 10.1117/12.2562832 (cited on page 75).

[235] E. Pinna et al. "SOUL: the Single conjugated adaptive Optics Upgrade for LBT". In: *Adaptive Optics Systems V*. Ed. by Enrico Marchetti, Laird M. Close, and Jean-Pierre Véran. SPIE, July 2016. DOI: 10.1117/12.2234444 (cited on page 75).

[236] Samuel Halverson et al. "Modal Noise in Single-mode Fibers: A Cautionary Note for High Precision Radial Velocity Instruments". In: *The Astrophysical Journal* 814.2 (Nov. 2015), p. L22. DOI: 10.1088/2041-8205/814/2/l22 (cited on page 75).

[237] Andrew J. Bechter et al. "Mitigation of Polarization Effects in Single-mode Fiber Spectrographs". In: *Publications of the Astronomical Society of the Pacific* 132.1015 (July 2020), p. 095001. DOI: 10.1088/1538-3873/ab9cc6 (cited on page 75).

[238] Andrew J. Metcalf et al. "30 GHz electro-optic frequency comb spanning 300 THz in the near infrared and visible". In: *Optics Letters* 44.11 (May 2019), p. 2673. DOI: 10.1364/ol.44.002673 (cited on page 76).

[239] A. Haboucha et al. "Optical-fiber pulse rate multiplier for ultralow phase-noise signal generation". In: *Optics Letters* 36.18 (Sept. 2011), p. 3654. DOI: 10.1364/ol.36.003654 (cited on page 76).

[240] Ryan C. Terrien et al. "Broadband Stability of the Habitable Zone Planet Finder Fabry–Pérot Etalon Calibration System: Evidence for Chromatic Variation". In: *The Astronomical Journal* 161.6 (May 2021), p. 252. DOI: 10.3847/1538-3881/abef68 (cited on page 76).

[241] Tobias M. Schmidt et al. "Fundamental physics with ESPRESSO: Towards an accurate wavelength calibration for a precision test of the fine-structure constant". In: *Astronomy & Astrophysics* 646 (Feb. 2021), A144. DOI: 10.1051/0004-6361/202039345 (cited on page 76).

[242] Françcis Wildi, Bruno Chazelas, and Francesco Pepe. "A passive cost-effective solution for the high accuracy wavelength calibration of radial velocity spectrographs". In: *SPIE Proceedings*. Ed. by Ian S. McLean, Suzanne K. Ramsay, and Hideki Takami. SPIE, Sept. 2012. DOI: 10.1117/12.926841 (cited on page 76).

[243] F. F. Bauer, M. Zechmeister, and A. Reiners. "Calibrating echelle spectrographs with Fabry-Pérot etalons". In: *Astronomy & Astrophysics* 581 (Sept. 2015), A117. DOI: 10.1051/0004-6361/201526462 (cited on page 76).

[244] Julian Stürmer et al. "A rubidium traced white-light etalon calibrator for MAROON-X". In: *SPIE Proceedings*. Ed. by Ramón Navarro and James H. Burge. SPIE, July 2016. DOI: 10.1117/12.2232865 (cited on page 76).

[245] P. Del'Haye et al. "A chip-scale microwave repetition rate frequency comb". In: *SPIE Proceedings*. Ed. by Manijeh Razeghi, Rengarajan Sudharsanan, and Gail J. Brown. SPIE, Jan. 2009. DOI: 10.1117/12.814912 (cited on page 76).

[246] T. J. Kippenberg, R. Holzwarth, and S. A. Diddams. "Microresonator-Based Optical Frequency Combs". In: *Science* 332.6029 (Apr. 2011), pp. 555–559. DOI: 10.1126/science.1193968 (cited on page 76).

[247] Keith Patterson et al. "Design description and commissioning performance of a stable coronagraph technology development testbed for direct imaging of Earth-like exoplanets". In: *Techniques and Instrumentation for Detection of Exoplanets IX*. Ed. by Stuart B. Shaklan. SPIE, Sept. 2019. DOI: 10.1117/12.2530401 (cited on page 77).

[248] Seth R. Meeker et al. "The Twin decadal survey testbeds in the high contrast imaging testbed facility at NASA's jet propulsion laboratory". In: *Techniques and Instrumentation for Detection of Exoplanets X*. Ed. by Stuart B. Shaklan and Garreth J. Ruane. SPIE, Sept. 2021. DOI: 10.1117/12.2594668 (cited on page 77).

[249] Wesley Baxter et al. "Design and commissioning of an in-air coronagraph testbed in the HCIT facility at NASA's Jet Propulsion Laboratory". In: *Techniques and Instrumentation for Detection of Exoplanets X*. Ed. by Stuart B. Shaklan and Garreth J. Ruane. SPIE, Sept. 2021. DOI: 10.1117/12.2601432 (cited on page 77).

[250] Sergi R. Hildebrandt et al. "Starshade Imaging Simulation Toolkit for Exoplanet Reconnaissance". In: *Journal of Astronomical Telescopes, Instruments, and Systems* 7.02 (May 2021). DOI: 10.1117/1.jatis.7.2.021217 (cited on page 80).

List of Acronyms

ABTR	Astrophysics Biennial Technology Report
ACADIA	ASIC for Control And Digitization of Imagers for Astronomy
ADCS	Attitude Determination and Control Systems
ADCS	Attitude Determination and Control Systems
AGS	Artificial Guide Star
AMTD	Advanced Mirror Technology Demonstration
AO	Adaptive Optics
AOX	AOA Xinetics
APD	Astrophysics Division
APD	Avalanche Photodiode
APLC	Apodized Pupil Lyot Coronagraph
APRA	Astrophysics Research and Analysis
ASIC	Application Specific Integrated Circuit
ATLAST	Advanced Technology Large-Aperture Space Telescope
AU	Astronomical Unit
BMC	Boston Micromachines Corporation
BW	Bandwidth
CCD	Charge Coupled Device
CIC	Clock-Induced Charge
CMOS	Complementary Metal Oxide Semiconductor
COR	Cosmic Origins
cpa	Cycles per Aperture
CRR	Capture Range Replication
CTE	Charge Transfer Efficiency
CTE	Coeffient of Thermal Expansion
CTI	Charge Transfer Inefficiency
DAC	Digital-to-Analog Converter
DFP	Disturbance Free Payload
DM	Deformable Mirror
DOE	Department of Energy
DOF	Degrees of Freedom
DRM	Design Reference Mission
DST	Decadal Survey Testbed
DST 2	Decadal Survey Testbed 2
EMCCD	Electron-Multiplying Charge Coupled Device
EOM	Electro-optic modulation
EPRV	Extreme Precision Radial Velocity
ExEP	Exoplanet Exploration Program
ExoTAC	Exoplanet Technology Assessment Committee

FALCO	Fast Linearized Coronagraph Optimizer
FP	Fabry-Pérot
FPGA	Field-Programmable Gate Array
GEO	Geosynchronous Equatorial Orbit
GOMAP	Great Observatories Maturation Program
GPI	Gemini Planet Finder
HabEx	Habitable Exoplanet Observatory
Habitable Worlds Observatory	Infrared/Optical/Ultraviolet Future Great Observatory
HCIT	High Contrast Imaging Testbed
HCL	Hollow Cathode Lamp
HiCAT	High-contrast imager for Complex Aperture Telescope
HLC	Hybrid Lyot Coronagraph
HMCCD	Hole-Multiplying Charge Coupled Device
HOWFSC	High-Order Wavefront Sensing and Control
HST	Hubble Space Telescope
IACT	In-Air Coronagraph Testbed
iSAT	in-Space Assembled Telescope
ISFM	Internal Scientist Funding Model
IWA	Inner Working Angle
JWST	James Webb Space Telescope
L2	Earth-Sun Second Lagrange Point
LBT	Large Binocular Telescope
LC	Lyot Coronagraph
LCRD	Laser Communications Relay Demonstration
LEO	Low Earth Orbit
LFC	Laser Frequency Comb
LLCD	Lunar Laser Communication Demonstration
LMAPD	Linear-Mode Avalache Photodiode
LOS	Line-of-Sight
LOWFS	Low-Order Wavefront Sense and Control
LUVOIR	Large Ultraviolet / Optical / Infrared Surveyor
MASS	Micro-Arcsecond Small Satellite
MCP	Multi-Channel Plate
MEMS	Micro-Elecrical Mechanical Sensor
MIRI	Mid-Infrared Instrument
MKID	Microwave Kinetic Induction Device
MMSD	Multiple Mirror System Demonstrator
MSFC	Marshall Space Flight Center
MVIS	Microgravity Vibration Isolation Subsystem
NC	Nulling Coronagraph
NCPA	Non Common Path Aberrations

NEO	Near Earth Object
NExScI	the NASA Exoplanet Science Institute
NIR	Near Infrared
NN-EXPLORE	NASA-NSF Exoplanet Observational Research
OBWFS	Out-of-band Wavefront Sensing
OWA	Outer Working Angle
PAPLC	Phase-Apodized-Pupil Lyot Coronagraph
PCF	Photonic Crystal Fiber
PhysCOS	Physics of the Cosmos
PIAA	Phase-Induced Amplitude Apodized
PIAACMC	Phase-Induced Amplitude Apodized / Complex Mask Coronagraph
PIC	Photonic Integrated Circuit
PM	Primary Mirror
PMN	lead-magnesium-niobate
PSF	Point-Spread Function
PZT	Piezo-electric
QE	Quantum Efficiency
QIS	Quanta Image Sensors
RMS	Root Mean Square
ROSES	Research Opportunities in Space and Earth Sciences
RST	Roman Space Telescope
RV	Radial Velocity
SAT	Strategic Astrophysics Technology
SBIR	Small Business Innovation Research
SCDA	Segmented Coronagraph Design and Analysis
SCExAO	Subaru Coronagraphic Extreme Adaptive Optics
SFE	Surface Figure Error
SIM	Space Interferometry Mission
SISTER	Starshade Imaging Simulation Toolkit for Exoplanet Reconnaissance
SLEEC	Super Lyot Exo-Earth Coronagraph
SLM	Spatial Light Modulators
SLS	Space Launch System
SMF	Single Mode Fiber
SNR	Signal-to-Noise Ratio
SOTA	State-of-the-Art
SOUL	Single Conjugated Adaptive Optics Upgrade
STIS	Space Telescope Imaging Spectrograph
STJ	Superconducting Tunnel Junction
STOP	Structural Thermal Optical Performance
TBIRD	Terabyte Infrared Delivery
TDEM	Technology Development for Exoplanet Missions
TES	Transition Edge Sensor

TFLOP	Trillions of Floating-Point Operations
TMT	Thirty Meter Telescope
TPF	Terrestrial Planet Finder
TPF-I	Terrestrial Planet Finder Interferometer
TRL	Technology Readiness Level
ULE	Ultra Low Expansion
ULTRA-TM	Ultra-Stable Large Telescope Research and Analysis – Technology Maturation
VC	Vortex Coronagraph
VERVE	Vacuum Extreme Radial Velocity Experiment
VLT	Very Large Telescope
WDM	wavelength division multiplexed
WFE	Wavefront Error
WFI	Wide Field Instrument
WFSC	Wavefront Sense and Control
WGM	Whispering Gallery Mode
ZWFS	Zernike Wavefront Sensor

About the Author

Brendan Crill (JPL/Caltech) has served NASA's Exoplanet Exploration Program (ExEP) as dDeputy Program Chief Technologist since 2016. In this role, he is involved in strategic planning for developing technology to will enable future space-based direct imaging and spectroscopic characterization of Earth-sized rocky exoplanets in the habitable zone of their stars such as the Habitable Worlds Observatory recommended by the 2020 Decadal Survey.

Dr. Crill is an astrophysicist with more than 25 years of experience and an author or co-author of over 200 peer-reviewed publications. Over his career he has participated in multiple projects and missiosn that have revolutionized the understanding of the Universe using new technology. He's worked on the NASA-funded BOOMERANG long duration balloon-borne millimeter-wave telescope that provided the first image of degree-scale CMB anisotropy in 2000 and a precise measurement of the density of the Universe. and was the US lead for the Planck mission's High Frequency Instrument data analysis.

In addition to his duties as Deputy Program Chief Technologist at ExEP, Dr. Crill is a co-investigator and science team member on the SPHEREx Explorer mission, leading the science data pipeline in the role of Data Pipeline Architect.